UNIVERSITY OF CAPE TOWN

DEPARTMENT OF MECHANICAL ENGINEERING

SIMULATION

OF A

SOLAR WATER HEATING SYSTEM

by

H.E. BEHR

A thesis submitted to the Department of Mechanical Engineering in fulfilment of the requirements for the degree of Master of Science in Engineering.

September 1977.

The copyright of this thesis vests in the author. No quotation from it or information derived from it is to be published without full acknowledgement of the source. The thesis is to be used for private study or non-commercial research purposes only.

Published by the University of Cape Town (UCT) in terms of the non-exclusive license granted to UCT by the author.

University of Cape Town

ABSTRACT

A computer simulation model of a domestic solar water heater, using natural circulation, is presented here.

Tests were conducted on an experimental system, using a flat plate collector and solar storage tank, auxilliary to an electric geyser. Temperatures were recorded, solar radiation was measured using a solarimeter and thermosyphon mass flow rates were measured using a thermistor inserted into the flow circuit.

Close correlation was obtained between predicted and experimental results.

Daily efficiencies varied according to the times and quantities of hot water draw offs.

The thermal performance of similarly designed solar water heaters could be predicted using this computer simulation model with the necessary modifications.

ACKNOWLEDGEMENTS

The author wishes to thank :
Professor R.K. Dutkiewicz, the project supervisor, for his guidance and encouragement;
Chris Davis and Malcolm Phillips for their computer assistance;
Peter Kemper for sharing his knowledge on multiple aspects of solar heating;
Mr. J. Busbridge, Mr. D. Finlayson, Mr. W.K. Bettesworth and Mr. R.M. Stegen for their advice and assistance on experimental construction and procedures;
Peter Lewis and Abdullah Janodien for their helping hands building the rig and during experiments;
Mr. T.V. Appleton for photographic assistance;
Tessa Malcolm for patiently typing the script; and
the C.S.I.R. for backing and supporting this research project.

TABLE OF CONTENTS

NOMENCLATURE

Ac	collector surface area
a	a constant
b	a constant
Cp	specific heat of water
E	equation of time
g	gravitational constant
h	head
h_j	height of jth section
h_{dp}	height of the down pipe
h_{up}	height of the upriser pipe
h_{coll}	vertical height of the collector
h_w	wind loss coefficient
$h_{r,c-s}$	cover to sky radiation coefficient
$h_{r,p-c}$	plate to cover radiation coefficient
h_{p-c}	plate to cover convection coefficient
k	thermal conductivity
K	extinction coefficient for the collector cover
ℓ	plate to cover distance
L	latitude of the place
L_{st}, L_{loc}	longitude of the standard time and local time mediants respectively.

$\dot{m}_c$	thermosyphon mass flow rate through the collector
$\dot{m}_L$	draw off mass flow rate
M	Mass
n	reflective index
Nu	Nusselt number
Q	energy
Rad	solar radiation on the collector surface
Re	Reynolds number
s	collector angle of tilt from the horizontal
T	time
Tst	standard time
T	temperature
$\bar{T}$	average temperature between the plate and cover of the collector
t_i	thickness of collector insulation
t_c	thickness of the collector cover
t	thickness of the collector
U	heat loss coefficient
V	volume
V_w	wind velocity
W	thermal capacity
ω	hour angle
α	absorptivity
τ	transmissivity
$(\tau\alpha)$	transmissivity absorptivity product
ϵ	emmisivity
ρ	reflectance

δ	declination
θ	angle of incidence
η	efficiency
σ	Stefan Boltzman constant
$\Delta\tau$	time interval
ΔT	temperature difference
Δp	pressure head difference

subscripts

a	absorbed
amb	ambient
c	cover or collector
co	collector outlet
ci	collector inlet
coll	collector
dp	down pipe
e	effective
Eo	eletric geyser outlet
elec	electrical
in	cold water mains inlet
j	tank section
o	overall
p	collector plate
pi	pipe
s	stored
s	solar tank

GRAPHS NOMENCLATURE

Experimental values are plotted in red

Theoretical predictions are plotted in yellow

The following symbols are used in the graphs :

O	collector outlet temperature	collector temperatures
P	collector mean plate temperature	
I	collector inlet temperature	

1	top section temperature	4 section, tank model temperatures (SOLASIM 4A and 4B)
4	bottom section temperature	

1	top section temperature	5 section, tank model temperatures (SOLASIM 5B)
3	3rd section temperature	
5	bottom section temperature	

M thermosyphon mass flow rate.

CHAPTER 1.

INTRODUCTION

1.1. MAN AND THE EARTH

The history of the earth shows man to be only a recent addition. (The earth is approximately 3 000 million years old, whilst the earliest evidence of humans is 2 million years ago). Of all the living creatures supported by the earth's tenuous surface, he is one of the most fragile. Yet, in the manner of his explosive appearance on the scene and the ways he has profoundly altered his environment, he is the most powerful organism to emerge.

However, since the industrial revolution and the invention of power driven machines, he has consumed vast quantities of resources which the earth has taken millions of years to produce. In so doing he has contaminated his environment and 'wiped out' certain species of life.

As countries develop and 'progress', their material needs increase and the per capita energy consumption increases exponentially. Simultaneously the population increases, resulting in a rapid depletion of resources and a diminishing capability of the earth to handle the waste products.

Nuclear power is now being produced at an increasing rate with plans for many more such supply stations. This is only a temporary solution, as it provides man with similar problems as other fossil fuels. (Limited supplies and poisoning of the environment are unavoidable repercussions).

What is ultimately needed is the production of energy by renewable non-polluting sources. Solar power and its manifestations (wind, tidal wave, ocean-thermal and direct solar powers) provide this more balanced and stable supply. However, these have their

present day/...

present day problems and disadvantages. The two most serious being:

1. the energy density is extremely low compared with present fossil or uranium fuels,
2. the storage of energy is difficult.

Both these problems create extremely high capital costs and, it therefore appears, that alternative forms of energy production will not come into large scale use for the next few decades. However, for small scale energy production these methods could presently be economically feasible.

1.2. A HISTORY OF SOLAR ENERGY UTILIZATION

Experiments using the sun's energy date back many centuries, with stories of Archimedes concentrating sunlight and setting fire to the attacking Roman fleet in 212 B.C.

In about 100 B.C. Aeron of Alexandria built a device for pumping water using air heated in a closed hollow sphere.

History shows no record of much other utilization of energy until the fifteenth century when Leonardo Da Vinci described reflection from a concave mirror, and a water surface, to concentrate heat. In 1615 S. de Caux raised water by expansion of air from solar heat.

The first flat plate collector appeared in 1774 when H.R. de Saussure invented the "hot box". (An insulated, air tight, wooden box, painted black inside, using two layers of glass with air spaces in between.) He produced hot air at 160^{o}C.

During the nineteenth century more interest was directed towards solar energy experiments. Sir John Herschel, in Cape Town 1837, produced "a small mahogany box", with a glass cover, obtaining temperatures of 115^{o}C. Towards the later part of the century solar engines, printing presses and distillation plants were constructed. The collector designs varied. Mouchot used a truncated cone as a reflecting surface and two concentric copper bells as the boilers, while Ericson employed a series of parabolic mirrors concentrating

solar energy/..

solar energy on to metallic tubes, and Adams utilized a hemispherical collector made of plane glass mirrors concentrated on to two copper bells.

Realising the potential of solar energy, experimenters in the early twentieth century were achieving temperatures of up to 180°C, producing effective powers between 700 and 1100 W/m^2.

The basic collector designs were similar to previous designs with detailed improvements. Maier and Remshart in 1913 constructed a collector to follow the path of the sun using two separate axes. (A daily and an hourly axis)

Professor A. Marcuse in 1923 built a great bi-convex lens to concentrate solar radiation through a small opening in a big hollow sphere. A larger sphere was concentric with the first, with a layer of oil between the two, in which was a system of water pipes. 1,3 h.p. was obtained from $1m^2$ of irradiating surface.

Numerous other experimenters worked on various designs, and by 1951 and Italian Company SOMOR produced a portable engine with plane solar collectors without concentration.

In 1954 the Bell Telephone Laboratories announced the production of photovoltaic cells with an overall conversion efficiency of 6%. (Later increased to about 11%).

The conversion of solar into electrical energy introduced a new era in the history of solar energy. The early history of solar energy utilisation was dominated by attempts to convert solar energy to power, despite the large technical problems involved. It is now recognised that the collection of solar energy for low temperature applications is thermodynamically simpler and economically cheaper.

During the past twenty years emphasis has been towards solar water heating and space heating and cooling. Many solar houses have been built employing these systems, as well as solar cookers and ovens.

However/.....

However, research still continues into high temperature applications and solar furnaces are in operation at Mount Louis in France and Odeillo.

Solar drying has been used throughout history and work at the National Physical Laboratory in India is showing how the use of simple mirrors to concentrate heat could speed up the evaporation rate.

The most valuable area of solar energy utilization today appears to be solar water heating, where, with present increasing fuel prices it is an economic proposition. However, a greater economic advantage is required to encourage the use and change over to solar heating. Intensive research into specific areas of solar heating designs is playing an important rôle.

This thesis is directed towards this area and considers only low temperature solar water heating.

1.3. SOLAR WATER HEATERS

The engineering literature indicates that one of the earliest major research developments in solar water heating was in 1942 by Hottel and Woertz (1). Employing collectors consisting of a blackened metal absorbing surface with one to three glass plate covers, under forced-circulation flow and specified weather conditions, an extensive evaluation of the thermal performance was made. Radiation and temperatures were recorded and integrated over hourly periods, and flow rates were calculated from differential pressures across orifices in the water supply line. The rate of useful heat collection in the water was expressed in terms of radiation, air temperature, collector angle of tilt and properties of the collector parts. An analytical model for determining the heat losses and hence the useful heat from the collector was presented, for steady state operation.

This work provided a basis for the research work which was to follow.

Intensive/...

Intensive study only began in the fifties, when several papers were published and work expanded into different areas, focusing on specific factors influencing the performance of the solar water heaters.

Whillier (2) in 1956 made valuable contributions to solar energy work in South Africa, presenting several types of collector designs, performances curves, and an economic feasibility study of solar water heating utilization in this country.

In 1959 Bliss (3) performed similar work to Hottel and Woertz also using forced circulation. Efficiency factors were derived. These are more or less design constants, determined by the plate construction details and can be qualitatively related to the various factors influencing the overall plate performance.

Natural circulation systems were used by Close (4) and De Sa (5). Close (1962) used 'typical flat plate solar heaters'. (These consisted of copper absorber plates with selective black coatings and transparent covers of tedlar and glass connected to storage tanks by one inch diameter copper tubes. The return pipe from the absorber was connected to the tank, one fourth of the tank's height from the top.) He designed an analytical model, assuming sine function expressions for solar radiation and ambient temperature, for clear weather and no draw off during the day.

He obtained close agreement between calculated and measured temperatures in the storage tank for the entire day and at the absorber inlet and outlet only between 10h00 and 14h00.

In the theoretical model he assumed the heat absorbed by the collector water to be only dependant on radiation, and assumed constant maximum values of transmittance of the cover and absorptance of the plate. The thermosyphon flow was determined using the difference in densities of the water in the system, and the temperatures were calculated using a heat balance for the tank and the collector. The mean tank and collector temperatures

were assumed/...

were assumed equal on the basis of experimental observations.

De Sa in 1964 predicted the mean water temperature variation throughout the day. He considered the water heating system as one unit, without taking into account the system geometry and thermosyphon flow. He then equated the sum of the heat losses from it and the heat gained by the water with the incident radiation.

Gupta and Garg (6) in 1968 used a flexible solar water heater design so that the collector type, area, tilt and orientation, syphon parameters and circulation pipe diameters could be changed as required.

They modified Close's model by considering the system capacity and the heat exchanger efficiency of the absorber. The radiation intensity and the ambient air temperature were harmonically analysed using Fourier series expansions. Mean system temperatures were determined by considering a heat balance for the absorber and pipes, considered as one unit, and the storage tank.

Ideal conditions of no draw off during the day were assumed. Predictions were made of the mean system temperature and thermosyphon mass flow rates for clear and cloudy weather.

K.S. Ong (7) in 1973 used an experimental solar water heater with an absorber unit consisting of longitudinally placed copper tubes on a copper sheet. The plate was coated with dull blackboard paint and placed inside an insulated wooden box. The cover was $\frac{1}{8}$ inch thick glass. A 28 gallon storage tank was connected via one inch diameter insulated copper pipes.

The mathematical model he presented employed a finite difference method of solution, enabling more accurate instantaneous performance figures to be predicted for a thermosyphon flow system with no draw off. Whereas Close (5) and Gupta and Garg (6) assumed constant values for plate efficiencies, heat losses, heat transfer coefficients, friction factors and physical properties of water, Ong's finite

difference/...

difference technique allowed these variables to vary with temperature, and water flow rates were evaluated at the instant of time considered. He also employed actual measured ambient temperatures and radiation values.

He predicted the mean temperatures of the collector and tank, the mass flow rate and efficiencies, satisfactorily, during the main insolation period.

In 1975 he presented an improved program (8). His previous assumptions that the mean collector plate temperature, the average water temperature in the storage tank and the mean water temperature in the collector tubes were equal, and the tank temperature distribution was linear, were experimentally proved incorrect. His new model considered the entire system to be divided into a finite number of sections, each individual section having a uniform mean temperature. By considering an energy balance over each section, finite difference equations were employed to evaluate the mean section temperature. The mass flow rate was evaluated from the temperature distribution over the whole system.

Experimentally mass flow rates were measured using a dye injection method and instantaneous total radiations were measured at the angle of the collector. The temperatures were recorded using thermocouples.

Predictions of system temperatures, mass flow rates and efficiencies correlated well with experimental results during the main part of the day. The predictions in the early morning and late afternoon were inaccurate, and one of the reasons suggested was that the effect of the angle of incidence of the sun was not taken into account.

All of the above models assumed zero draw off of hot water during operation. To simulate a solar water heating system hot water draw off should be considered. This complicates the problem of predicting the thermal performance of the system since water at a different

temperature/...

temperature and flow rate is introduced into the system, while hot water is removed.

A technique is presented here, based on the finite-difference method of K.S. Ong (8), to predict the system temperatures and thermosyphon flow rates, during a day's operation. The changing effect of the angle of incidence of the sun was taken into account, and low and high draw-off flows were considered. Actual measured and ambient temperatures and solar radiation values were employed.

The predicted results were compared with experimental values obtained during summer and autumn in Cape Town.

CHAPTER 2.

BACKGROUND THEORY

2.1. THE SUN

The most powerful of all physical forces reaching the earth from the space beyond it's atmosphere comes from the star we call our sun. All life on earth is ultimately dependent on the sun.

Diameter of the sun	$1{,}39 \times 10^6$ km
Average distance from the earth	$1{,}5 \times 10^8$ km
Surface temperature	5762^{o} K
Temperature of the central regions	8×10^6 to 40×10^6 ^{o}K
Density	80 to 100 gms/cc
Mass	$0{,}33 \times 10^6$ times that of the earth

The sun rotates about its own axis, the equator taking approximately 27 earth days and the polar regions 30 days for each rotation.

It belongs to a class of dwarf stars and is, in effect, a continuous fusion reactor. The energy being produced in the interior of the solar sphere, by the conversion of hydrogen to helium in the presence of carbon and nitrogen, is transferred to the outer surface and then radiated into space.

The radiation beginning at the sun's core is gamma and X-ray radiation. The wavelengths increase as the temperature decreases with increasing radial distance from its centre.

The outer surface layer of the sun is called the photosphere, which is the source of most solar radiation. Above this, in ascending order, is the reversing layer (several hundred kilometres thick), the chromosphere (about 10 000 kilometres thick), and the corona.

For engineering/....

For engineering purposes, however, the sun can be adequately considered to be a blackbody radiator at 5760^{o} K.

2.2. THE EARTH

The earth is a distorted sphere, slightly flattened at the poles, resembling a pear shape with a bulge in the Southern Hemisphere.

Average diameter	12 700 km
Distance from the sun	$1,5 \times 10^{8}$ km $\pm$ 3%
Mean density	5,52 gms/cc

The earth rotates about it's own axis once every 24 hours and revolves about the sun once every 365¼ days.

2.3. EARTH-SUN RELATIONSHIP

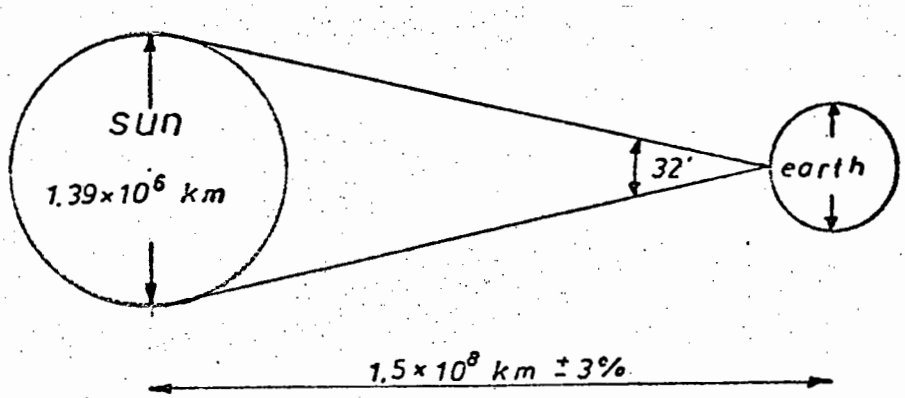

Fig. 2.3.1. Earth-Sun Relationship (not to scale)

The earth's revolution about the sun is almost eliptical with a slight eccentricity such that a variation of approximately 3% occurs in the distance between the sun and the earth. The earth is closest to the sun in January and furthest in July. At the mean earth-sun distance ($1,5 \times 10^{8}$ km), the sun subtends an angle of 32 minutes.

The earth's seasons are caused by a tilt in the earth's rotational axis ($23,5^{o}$ to the vertical) with respect to its orbit around the sun.

This/.....

This accounts for the uneven distribution of solar radiation over the earth's surface and the variation in daylight hours.

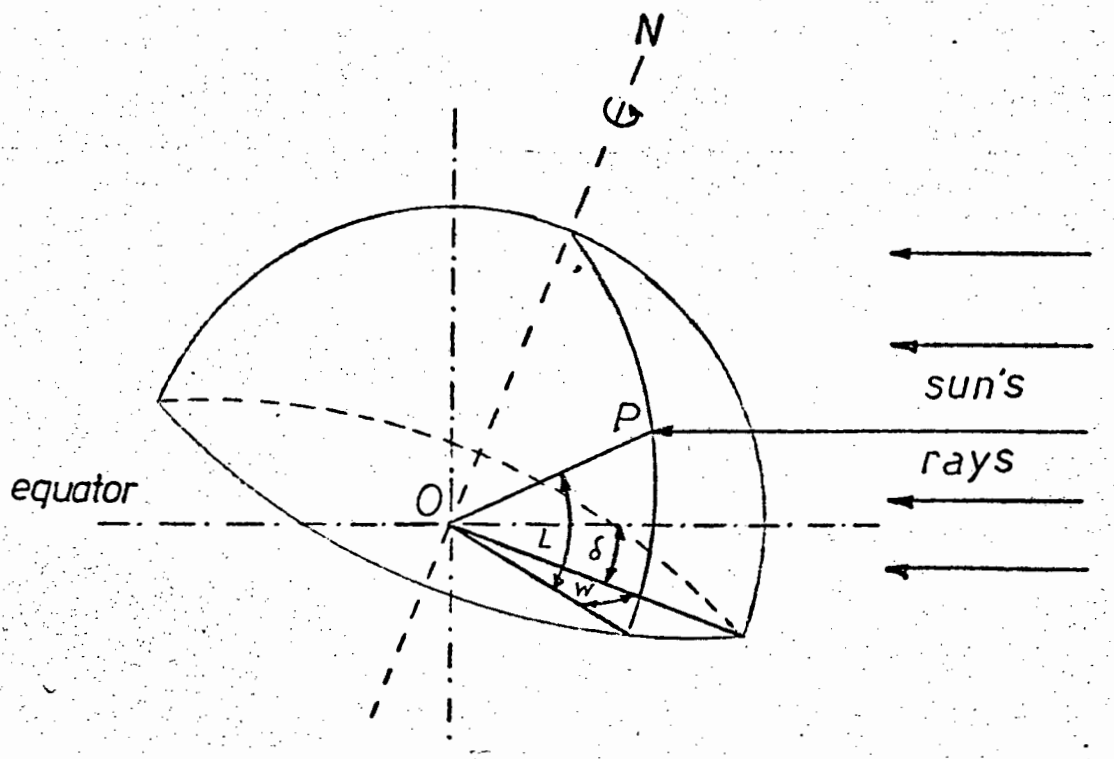

Fig. 2.3.2. Latitude, hour angle and declination

Fig. 2.3.2. shows the three basic earth-sun angles : the latitude angle L is the angular distances of a place P from the equator.

The seasonal variation in the sun's apparent position is represented by the declination δ, the angle between the sun's rays and the equatorial plane.

At noon the sun is due north (in the Southern hemisphere) and at its maximum altitude (solar noon). The sun's hourly motion is measured relative to solar noon by the hour angle ω.

2.4. RADIATION AT THE EARTH'S SURFACE

The earth receives only a minute fraction of the sun's energy. The solar radiation is depleted through the atmosphere, resulting in scattering (Fig. 2.4.1.)

Fig. 2.4.1./.....

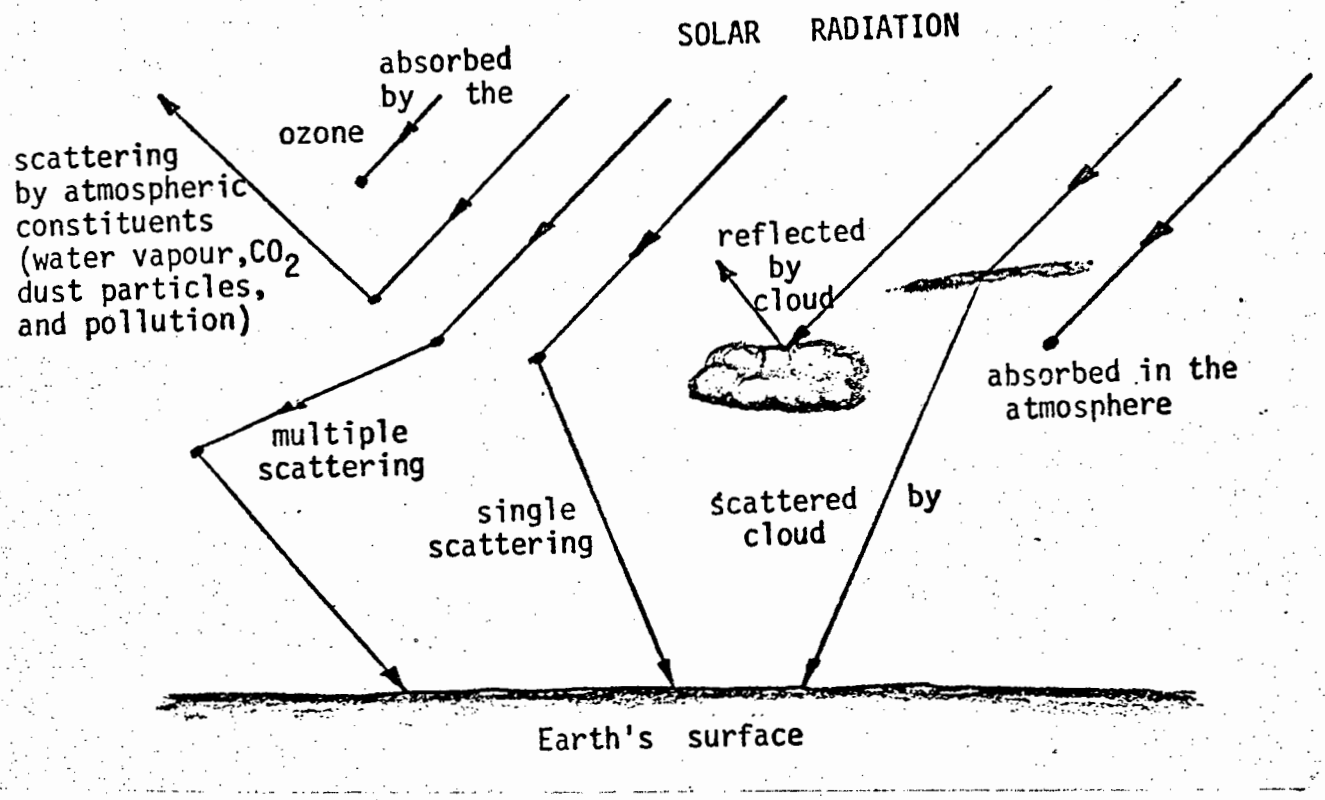

Fig. 2.4.1. Interaction of Solar Radiation with the Atmosphere

The solar constant is the energy received from the sun per unit time on a unit area of outer atmosphere surface perpendicular to the radiation (= 1353 W/m^2).

The solar radiation received on the earth's surface is either beam or diffuse radiation. Beam radiation is that received without change in direction (i.e. direct radiation). Diffuse radiation is that received after its direction has been altered due to reflection and scattering by the atmosphere.

The variation is sun-earth distance results in a variation of extraterrestrial radiation flux of about 3% (Fig.2.4.2.).

Fig. 2.4.2./....

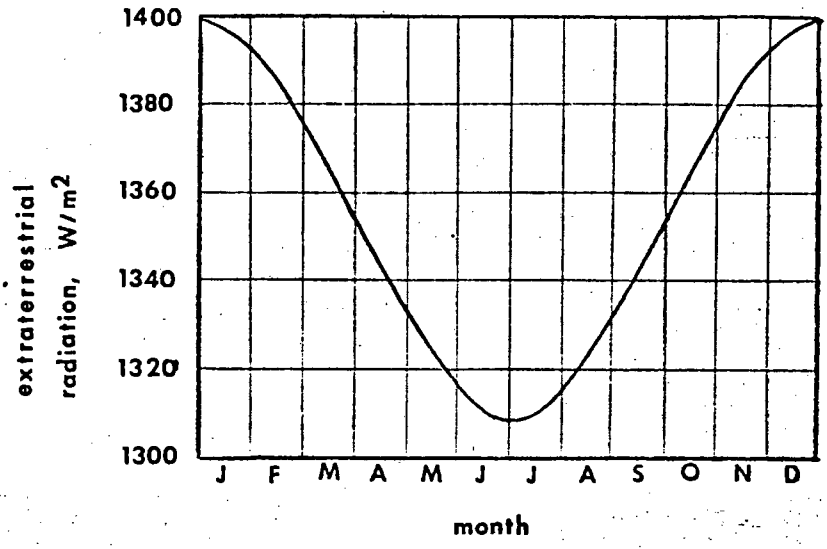

Fig. 2.4.2. Variation of Extraterrestrial Radiation with time of year (9)

The sun's radiation is distributed over a wide range of wavelengths. The spectral distribution of this radiation is shown in Fig. 2.4.3.

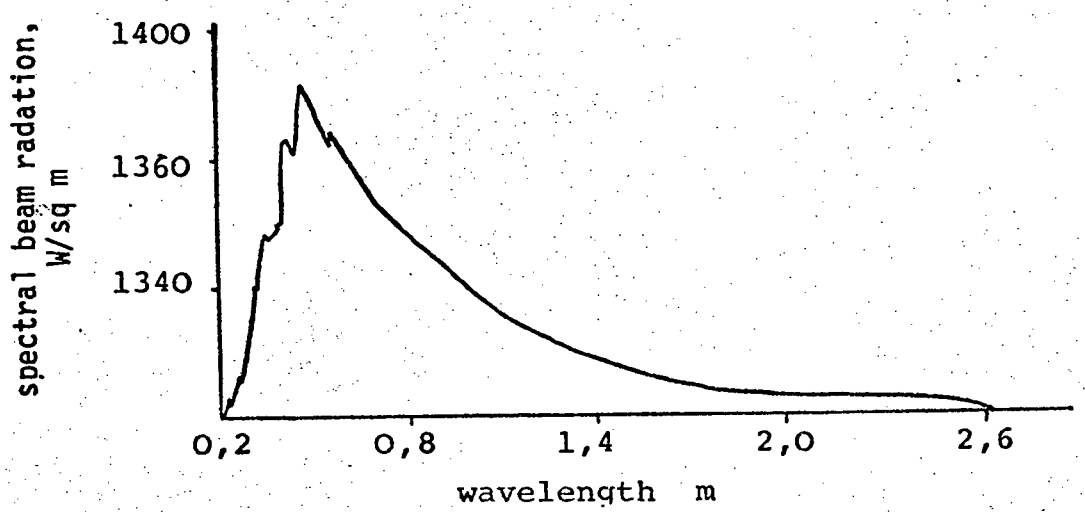

Fig. 2.4.3. The NASA (1971) Standard Spectral Irradiance at the mean sun-earth distance and a solar constant of 1353 W/m^2

2.5./.....

Table 2.5.1

Mean daily total (1), diffuse (2), and standard deviation (S) of solar radiation on a horizontal surface in MJm^{-2}, for 12 stations in Southern Africa

		Alexander Bay	S	Bloemfontein	S	Cape Town (Wingfield and D.F. Malan Airports)	S	Durban (Louis Botha Airport)	S	Keetmanshoop	S	Kimberley	S	Maun	S	Pietersburg	S	Port Elizabeth	S	Pretoria	S	Upington	S	Windhoek	S
Jan.	1	31,397	1,101	26,884	1,737	30,375	0,666	21,237	2,600	30,195	0,904	26,721	1,381	23,104	2,901	26,599	2,235	24,778	–	24,037	2,675	27,629	2,189	26,101	2,022
	2	6,899	0,042	7,305	0,804	6,225	0,435	8,619	0,603	5,438	0,615			8,904	0,787			9,356	–	8,561	1,335			8,008	0,720
Feb.	1	28,140	1,540	24,489	2,796	25,955	1,264	19,826	1,344	27,428	1,344	24,946	1,980	21,216	1,997	24,008	1,005	25,398	–	21,773	1,700	25,184	2,227	23,828	1,775
	2	6,242	–	6,807	0,816	6,095	0,833	7,962	0,628	5,626	0,130			8,984	–			6,786	–	7,895	0,699			7,498	0,812
Mar.	1	23,589	1,047	20,676	2,194	21,856	0,720	17,946	0,896	23,380	1,072	20,789	1,775	20,056	2,633	22,091	0,829	19,278	0,310	20,186	1,118	21,233	2,152	21,500	1,846
	2	4,563	–	5,903	0,477	5,103	0,364	6,196	0,477	4,517	0,448			5,990	0,155			5,706	0,151	6,807	0,783			6,459	0,791
April	1	19,516	1,356	18,164	0,879	15,271	0,203	15,029	0,833	21,061	0,548	17,741	0,942	18,704	2,528	19,541	1,143	14,041	0,339	17,469	1,377	18,168	1,490	20,504	0,825
	2	4,546	0,063	4,057	0,427	4,714	0,435	4,626	0,306	3,102	0,373			4,165	0,682			4,496	0,264	4,768	0,682			4,224	0,469
May	1	15,380	1,917	14,384	0,712	10,905	1,942	12,132	0,540	17,164	0,465	14,208	0,548	17,306	2,474	17,264	1,067	11,294	0,414	15,033	0,829	15,196	1,758	18,620	0,758
	2	4,182	0,360	3,454	0,385	4,015	0,435	3,487	0,460	2,847	0,193			2,608	0,180			3,098	0,205	3,315	0,331			2,951	0,448
June	1	13,287	1,239	13,040	1,063	9,373	0,557	11,303	0,506	15,506	0,573	12,781	0,716	16,004	2,361	15,707	1,093	9,779	0,661	14,124	0,561	14,212	1,540	16,996	0,833
	2	2,914	0,113	2,838	0,490	3,299	0,297	2,884	0,511	2,323	0,297			2,759	0,218			2,780	0,264	2,868	0,331			2,562	0,301
July	1	13,283	1,926	14,020	0,720	9,946	0,917	11,755	0,816	16,389	0,356	13,831	1,310	16,975	0,523	16,577	2,918	10,671	0,243	14,727	0,917	14,170	1,423	18,302	0,523
	2	3,173	0,205	2,968	0,393	3,646	0,490	3,131	0,402	2,478	0,100			3,391	0,561			2,935	0,188	3,119	0,410			2,595	0,234
August	1	16,695	2,118	17,750	1,172	12,772	0,833	13,714	0,896	19,512	0,410	18,089	1,390	20,019	2,055	18,859	3,219	13,517	0,699	18,198	0,502	17,331	1,298	21,052	0,594
	2	4,266	0,025	3,449	0,410	4,576	0,490	4,228	0,481	3,001	0,084			3,487	0,511			3,906	0,427	3,634	0,293			3,315	0,381
Sept.	1	21,814	1,394	21,735	1,273	18,047	0,896	16,142	1,461	23,761	0,791	22,191	2,361	22,614	1,402	21,258	3,575	17,277	0,917	20,400	1,679	20,814	0,728	23,933	1,197
	2	5,270	0,389	4,676	0,527	6,057	0,356	5,957	0,531	4,149	0,163			5,187	0,815			6,221	0,682	4,848	0,444			4,902	0,691
Oct.	1	27,022	2,499	24,418	1,582	22,999	0,980	17,147	1,402	27,391	1,197	26,294	2,491	23,012	2,357	24,456	2,068	20,948	1,000	22,246	1,256	24,247	1,415	25,959	1,474
	2	6,384	0,460	6,212	0,707	7,029	0,678	7,405	0,682	5,078	0,599			7,225	0,603			7,338	0,427	6,773	0,335			6,388	0,712
Nov.	1	30,338	1,808	27,353	2,160	27,591	1,612	19,236	1,955	30,693	0,724	28,965	2,855	23,652	2,491	26,587	2,076	25,854	1,846	23,841	1,469	27,210	1,474	27,575	1,679
	2	6,367	0,686	6,857	0,791	7,460	0,975	8,753	0,762	4,735	0,402			7,598	1,013			8,829	0,607	7,523	0,800			6,455	0,653
Dec.	1	30,932	3,600	27,801	1,432	29,969	1,076	20,885	0,774	31,229	0,933	29,157	3,290	22,639	1,758	26,101	3,604	25,770	0,875	23,267	1,566	27,638	1,105	28,056	2,323
	2	6,970	0,326	7,431	0,628	7,104	0,770	9,624	0,858	5,128	0,636			9,021	1,281			9,213	0,737	8,498	0,703			6,937	0,858
Total for year	1	8 243,837		7 618,371		7 138,762		5965,706		8 621,699		7 770,566		7 459,712		7 840,354		6 633,625		7 153,154		7 688,067		8 284,774	
	2	1 877,633		1 881,799		1 985,169		2 212,289		1 469,902				2 102,259				2 147,893		2 083,165				1 890,523	
2/1 %		22,8		24,7		27,8		37		17,0				28,1				32,3		29,1				22,8	
Approx. latitude		29°S		29°S		34°S		30°S		27°S		29°S		20°S		24°S		34°S		26°S		28°S		23°S	
No. of years		7		7		9		9		4		6		7		7		3		9		4		9	

Table 2.5.2

Mean duration of sunshine for 12 stations in Southern Africa

(a) Mean daily hours of sunshine
(b) Mean daily hours of sunshine expressed as a percentage of the possible hours of sunshine
(c) Average no. of days with $\leq$10 per cent of the possible sunshine, expressed as a percentage of the no. of days in the month
(d) Average no. of days with 11-49 per cent of the possible sunshine, expressed as a percentage of the no. of days in the month
(e) Average no. of days with $\geq$50 per cent of the possible sunshine, expressed as a percentage of the no. of days in the month

	Alexander Bay		Bloemfontein		Cape Town (Wingfield)		Durban (Airport)		Kootmanshoop		Kimberley (Airport)		Maun		Pietersburg (Airport)		Port Elizabeth (Airport)		Pretoria		Upington		Windhoek	
	a	b	a	b	a	b	a	b	a	b	a	b	a	b	a	b	a	b	a	b	a	b	a	b
Jan.	10,24	75	9,79	71	10,94	77	6,49	47	11,44	84	9,69	70	7,98	61	7,99	59	8,55	60	8,35	62	11,52	84	9,26	70
Feb.	9,72	74	9,24	70	10,47	79	6,74	51	10,34	80	9,48	72	7,27	57	7,55	58	8,23	62	8,08	62	10,51	81	8,98	70
Mar.	9,09	73	8,52	70	9,10	74	6,17	50	9,92	81	8,87	72	8,03	67	7,55	62	7,51	61	7,68	63	9,53	78	9,05	74
Apr.	8,94	78	8,80	77	6,92	62	6,83	60	10,15	89	8,96	78	9,25	79	8,06	70	7,57	67	8,69	75	9,67	86	9,09	78
May	8,12	75	8,77	82	5,92	56	7,40	69	9,94	92	8,64	80	9,93	89	8,61	79	6,91	67	9,27	85	9,18	86	10,04	91
June	8,50	82	8,74	85	5,96	60	6,94	68	9,65	93	8,82	85	10,11	93	8,91	84	6,85	69	9,23	87	8,97	87	10,25	95
July	7,51	71	9,02	86	5,72	56	6,87	66	9,84	92	9,05	86	10,34	93	8,63	80	7,15	71	9,36	88	9,10	86	10,50	97
Aug.	8,29	74	9,60	87	6,42	59	6,91	63	10,51	94	9,71	88	10,77	94	8,64	79	7,61	70	9,91	88	10,00	90	11,01	97
Sep.	9,11	77	9,43	79	7,16	60	5,83	49	10,92	93	9,67	81	10,51	88	8,72	73	7,44	63	9,26	78	10,61	89	10,75	90
Oct.	9,55	75	9,66	76	8,87	69	5,24	41	11,32	89	9,70	76	9,15	72	8,73	69	7,67	59	8,90	70	10,92	85	10,30	82
Nov.	10,16	75	10,35	77	9,85	71	5,75	42	11,79	88	10,20	75	8,66	66	8,23	62	8,29	60	9,02	68	11,63	86	9,85	75
Dec.	10,28	74	10,57	76	11,10	77	5,97	43	11,95	87	10,54	76	7,25	54	8,13	60	8,93	62	9,05	66	11,65	84	9,21	69
Year	9,13	75	9,37	78	8,20	67	6,43	54	10,64	88	9,44	78	9,10	76	8,34	70	7,73	64	8,90	74	10,27	85	9,86	82

	c	d	e	c	d	e	c	d	e	c	d	e	c	d	e	c	d	e	c	d	e	c	d	e	c	d	e	c	d	e	c	d	e	c	d	e
Jan.	0,0	12,4	87,6	6,5	9,7	83,8	2,9	7,3	90,0	28,1	20,3	51,4	0,5	6,5	93,1	5,1	15,2	79,9	6,4	26,7	65,9	8,7	29,1	62,4	11,5	19,7	69,0	10,0	18,7	71,3	2,6	5,2	92,3	4,2	15,5	80,1
Feb.	2,3	11,2	86,5	7,8	12,4	79,8	1,6	10,0	88,4	23,0	17,3	59,7	0,5	13,6	85,9	3,3	13,6	83,2	8,5	29,3	62,2	10,0	31,8	58,2	13,4	16,9	69,8	12,0	16,5	72,0	0,6	12,4	87,2	0,0	18,3	81,7
Mar.	1,1	13,4	85,5	13,2	5,8	81,1	3,2	10,7	86,1	25,8	17,4	57,0	2,8	7,8	89,4	5,7	12,2	82,2	5,1	20,3	74,7	7,5	29,8	62,6	17,6	11,1	71,3	12,0	18,7	69,4	3,8	12,4	83,9	1,3	19,4	79,4
Apr.	1,1	9,4	89,4	4,6	10,3	85,0	8,0	25,0	66,9	18,0	15,0	67,1	1,4	3,8	94,8	2,6	12,1	85,2	4,8	8,6	85,7	5,7	19,5	74,7	11,5	11,8	76,7	6,4	7,3	86,4	1,1	5,6	93,3	5,3	6,0	88,6
May	1,6	15,1	83,3	3,2	8,1	88,8	17,4	19,0	63,4	8,9	21,8	69,5	0,0	2,8	97,2	2,2	10,7	87,3	0,5	5,1	94,5	1,7	17,6	80,7	9,4	14,7	75,8	2,6	4,2	93,2	1,6	7,5	90,9	0,0	1,3	98,7
June	1,1	7,8	91,1	3,7	3,0	93,4	17,6	15,6	66,7	12,0	12,7	75,1	0,5	1,4	98,1	1,5	7,2	91,1	0,0	2,3	97,7	2,1	13,6	84,1	6,7	16,0	77,3	3,4	3,7	93,0	0,6	6,1	93,3	0,0	2,0	98,0
July	7,5	13,4	79,0	2,4	5,2	92,6	17,1	24,2	58,7	12,6	13,2	74,1	0,5	0,9	98,6	1,7	5,2	93,0	1,4	0,5	98,2	2,6	15,8	81,8	8,2	12,5	79,1	1,6	5,2	93,3	0,0	5,9	94,1	0,0	1,2	98,9
Aug.	5,4	13,4	81,2	1,9	4,2	94,2	17,3	18,2	64,4	15,8	11,3	73,0	0,0	0,9	99,1	0,7	5,3	94,1	0,0	0,0	100,0	3,2	13,9	82,8	6,5	14,1	79,6	1,0	4,5	94,6	0,0	2,2	97,9	0,0	0,0	100,0
Sep.	1,7	12,8	85,6	5,3	8,3	86,4	11,7	19,7	68,6	32,6	12,7	54,7	0,5	0,5	99,1	3,0	6,9	90,1	1,0	2,4	96,7	7,4	11,5	80,9	12,6	15,9	71,7	5,3	9,7	85,0	1,1	3,3	95,6	1,4	2,0	96,7
Oct.	1,1	12,4	86,6	3,8	13,4	83,0	6,8	14,2	79,0	40,7	15,5	43,9	0,0	5,1	94,9	4,4	10,3	85,5	5,1	13,8	81,1	6,4	21,2	72,5	13,8	17,7	68,6	10,0	12,6	77,6	1,6	6,5	91,9	0,6	11,0	88,5
Nov.	1,1	16,1	82,8	3,3	9,7	87,1	3,2	17,6	79,4	41,4	12,3	46,3	0,5	6,2	93,3	3,3	12,6	84,0	6,2	22,9	71,0	9,6	27,6	62,8	18,9	13,8	67,4	8,2	15,6	76,4	1,7	6,1	92,2	3,3	12,0	84,8
Dec.	2,2	11,3	86,6	3,2	9,4	86,6	1,6	9,4	89,1	35,5	18,1	46,4	0,5	5,5	94,0	2,5	12,9	84,7	12,0	30,4	57,6	8,1	28,8	63,2	10,7	18,1	71,2	6,5	19,0	74,4	1,6	7,0	91,4	3,2	22,0	74,9
Year	2,2	12,4	85,4	5,0	8,3	86,8	9,0	15,8	75,3	24,4	15,7	60,0	0,6	4,6	94,8	3,0	10,2	87,0	4,2	13,5	82,1	6,1	21,6	72,3	11,8	15,2	73,1	6,5	11,3	82,4	1,4	6,7	92,0	1,6	9,2	89,2
No. of years		6			10			10			10			7			14			7			13			10			10			6			5	

2.5. THE POTENTIAL OF SOLAR ENERGY IN SOUTH AFRICA

The utilization and efficiency of any solar heating system is dependent on climatic conditions.

South Africa's climatic conditions are almost ideal. Most parts of the country have summer rainfall with cloudfree winters and thus solar energy is available when it is most required.

Tables 2.5.1. and 2.5.2. (10) show solar radiation and mean duration of sunshine at different parts of South Africa. The tables show that diffuse radiation amounts to a large percentage of the total solar radiation, and it is therefore important that solar collecting devices utilize diffuse as well as direct (beam) radiation. Flat plate collectors fulfill this requirement.

Solar water heating can be effectively used on days which the sunshine hours exceed 50% of the total possible sunshine. Table 2.5.2. reflects that for most stations more than three quarters of the year will be effective for solar heating.

2.6. THE SOLAR WATER HEATER

The heating of water for domestic purposes using solar energy is quite common in Israel, Japan, Australia and the United States of America. With the present escalation in fuel prices, the moderate cost of solar water heating systems, their simplicity and freedom from maintenance have made them competitive with conventional systems and they are now being utilized in many other countries.

Many variations in solar water heater designs exist. However, these can be divided into two types, both of which utilize the flat plate collector principle (whereby solar energy is absorbed on plane surfaces which are in thermal contact with the water being heated). One type consists of separate solar heating and water storage facilities whilst the other is a single unit combining the heating and storage functions.

The most /...

The most commonly used design consists of a blackened metal surface in contact with the water (or water tubes) above which a transparent cover is supported forming an air gap. A box-type frame, with insulation at the sides and back provides a relatively air-tight enclosure. This solar collector is connected via pipes to an insulated storage tank.

If the tank is mounted above the top of the collector natural (thermosyphon) circulation of water occurs, and if it is positioned below the collector, a pump is necessary to create water circulation.

A thermosyphon system operates on the following principle. The water in the collector is heated by solar radiation. Since the density of water decreases with increasing temperature, the difference in relative densities of the water in the system causes circulation to occur. Hot water rises up into the top of the tank, whilst the cold water in the tank descends into the bottom of the collector (see Fig. 2.6.1.). Hot water is drawn off from the top of the tank as cold water enters at the bottom of the storage tank.

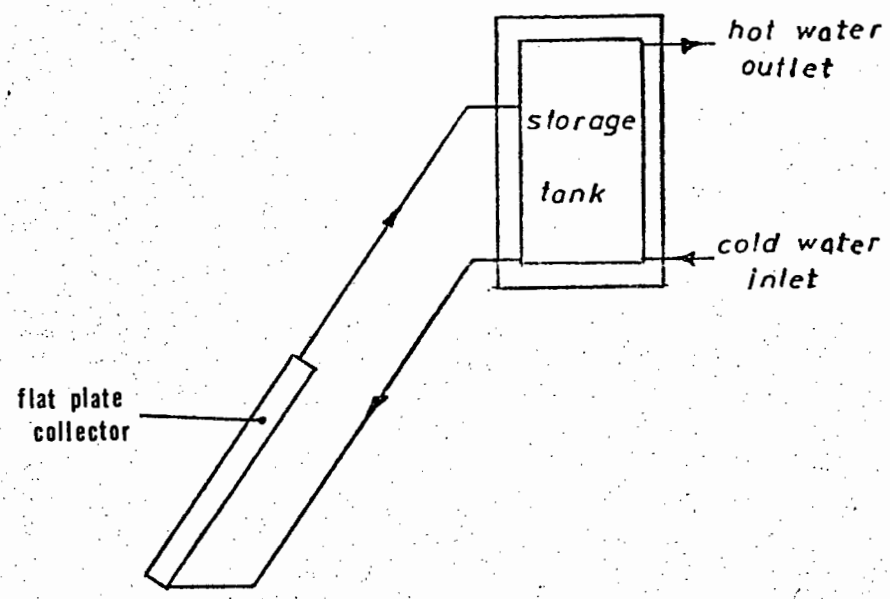

Fig. 2.6.1. Thermosyphon Solar Water Heater

The combined/.....

The combined collector-storage tank solar water heater (Fig. 2.6.2.) comprises of a transparent cover and a blackened surface, below which the water is stored and heated. The operation is not continuous and water is usually drawn off and used in the late afternoon.

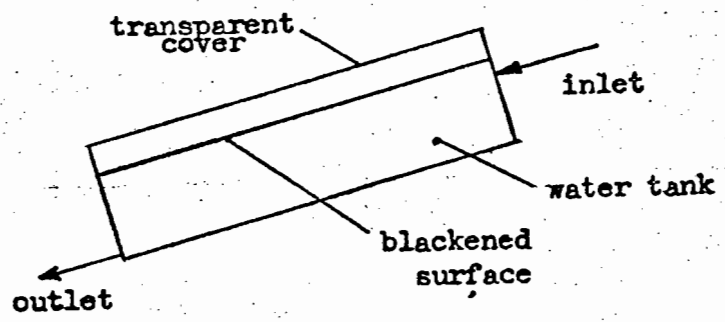

Fig. 2.6.2. Combined Collector-storage type Solar Water Heater

Conventional auxiliary heat is necessary if a completely dependable source of hot water is required. Electricity or fuel can be employed to increase the temperature of the hot water supplied by the solar heated system. Another technique is to use an electrical resistance in the solar storage tank itself to obtain water at a preselected temperature.

2.7. COLLECTION OF SOLAR ENERGY

A solar heat collector incercepts solar radiation, converts it to thermal energy and transfers this heat to a working fluid. Some collectors utilize mirrors or lenses to increase the flux density of solar radiation. The most successful for domestic water heating so far is the flat plate collector.

The flux incident radiation has a maximum value of about 1100 W/m^2 (without optical concentration) and is variable. The wavelength range is from 0,3 to 3,0 μm , being considerably shorter than

the emitted/...

the emitted radiation from most energy absorbing surfaces. Thus problems of low and variable energy fluxes and radiation play a large role in the analysis of solar collectors.

2.7.1. Flat Plate Collectors

Flat plate collectors can be designed for applications requiring moderate temperature delivery (up to 100°C). They use both beam and diffuse solar radiation, not necessarily requiring continual orientation towards the sun, and needing little maintenance. Present applications include water heating, building heating and air conditioning.

A flat plate collector consists of a sheet of flat material constructed such that channels are formed where a fluid medium can circulate.

The surface of the collector should have a high absorptance and therefore a blackened surface is required, and should not emit low temperature radiation. This can be achieved by using selective surface coatings (usually polished metal surfaces coated with thin layers of metal oxides).

Heat losses caused mainly by radiation from the plate, air convection below and above) and conduction losses via direct contact with the outdoor air must be reduced. To the rear of the plate, insulation is used, and above it transparent covers keep out rain and snow, and reduce the cooling effect of outside air movement. An air gap between the plate and cover provides an insulation layer for retaining the heat of the plate. The transparent cover should also possess characteristics of selective transmission of radiation (glass is the most common). This allows short wave solar radiation to pass through the cover while long wave reradiated heat from the plate surface cannot pass through, creating a greenhouse effect in the air gap. The ideal angle of operation is such that the collector is continually perpendicular to the sun's rays. This requires a sun tracking system for which the cost is high. A

stationary/...

stationary system should face due north (in the southern hemisphere) and for year round performance should be inclined at an angle 10^{o} larger than the latitude angle. (This favours heat collection during the winter when heat requirements are greater.

Due to the intermittancy and low flux density of solar radiation, thermal storage is necessary. For solar water heating a well insulated tank is required.

Figure 2.7.1. shows a typical flat plate collector.

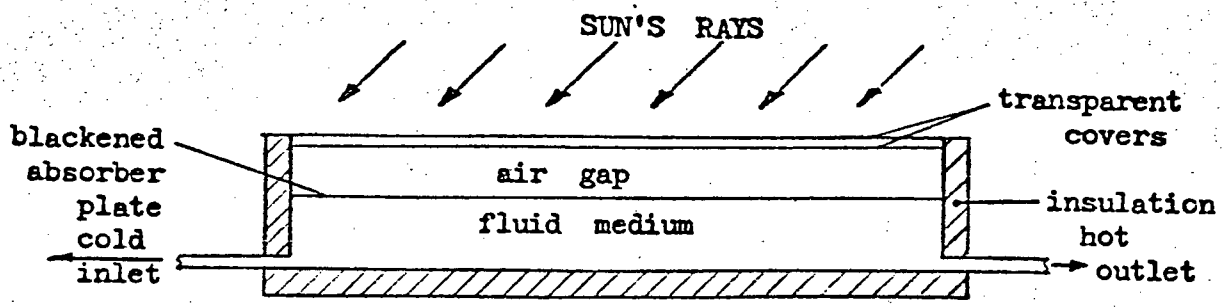

Fig. 2.7.1. A cross-section of a typical flat plate collector.

2.7.2. Concentrating Collectors

The incoming solar rays are refracted or reflected by lenses or mirrors on to a collector or boiler.

These optical systems are utilized to increase the intensity of solar radiation on the energy absorbing surface. Higher energy flux implies a smaller surface area for a given amount of energy, and correspondingly reduced thermal losses. However, most systems operate only on the beam component of solar radiation and the diffuse radiation is lost. Additional optical losses also become significant and sun tracking systems are required.

Due to the extra cost and maintenance required, these types of systems are not commonly used for domestic or commercial purposes and will not be considered in any further detail.

Fig. 2.7.2./...

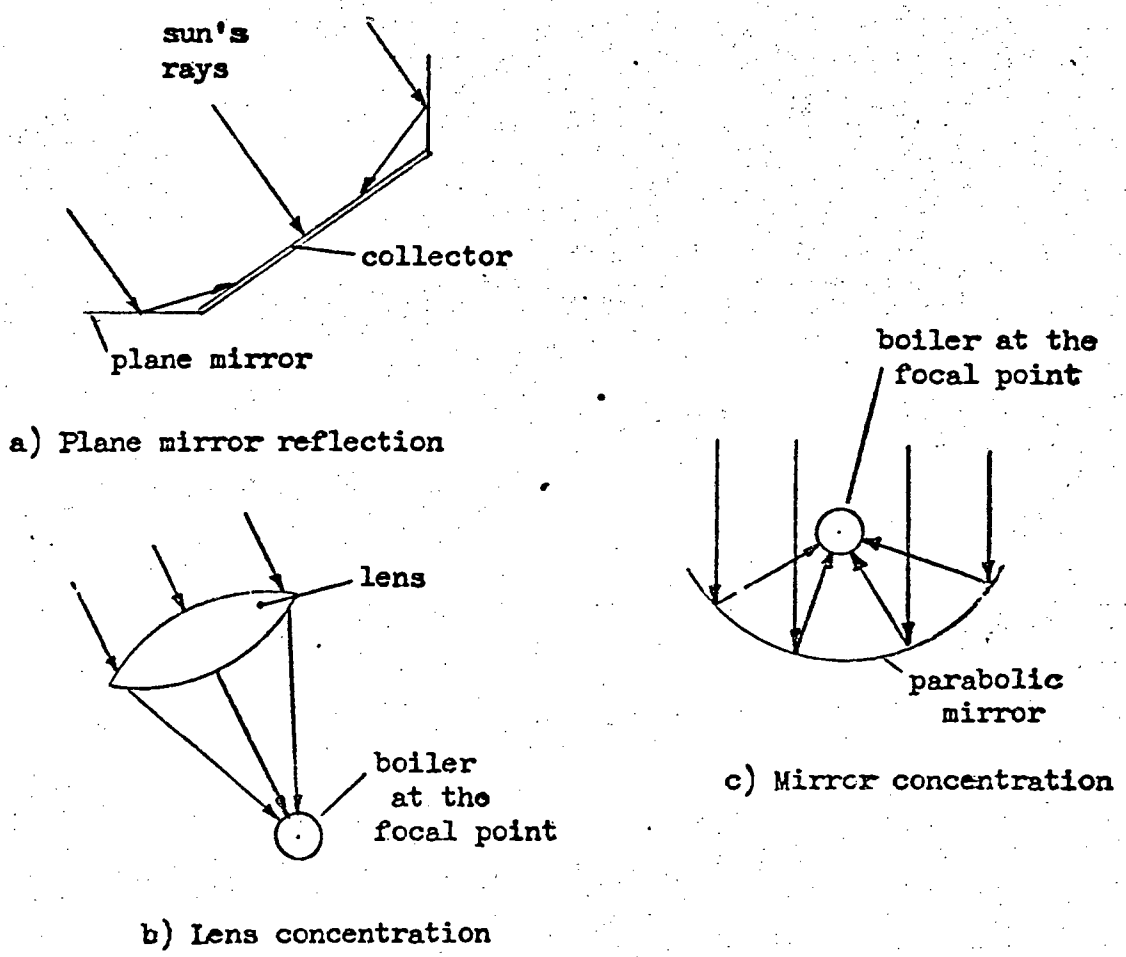

Fig. 2.7.2. Concentrating Collectors.

2.8. ENERGY STORAGE

The radiant energy collected during daylight hours needs to be stored, so that it may be utilized at times when it is required.

Energy storage must be considered with respect to the solar process system. It may be in the form of sensible heat of a solid or liquid medium, as heat of fusion in chemical systems or as chemical energy of products in a reversible chemical reaction. The choice

of the /....

of the storage medium depends on the process.

For solar water heating, it is logical to use water as the energy storage medium. For a thermosyphon flow system the following requirements are necessary to obtain optimum conditions :

(i) The storage tank should be at least 600 mm above the top of the collector.

(ii) The flow pipe from the absorber should be situated at a height of 2/3 that of the tank (see Fig. 2.8.1.).

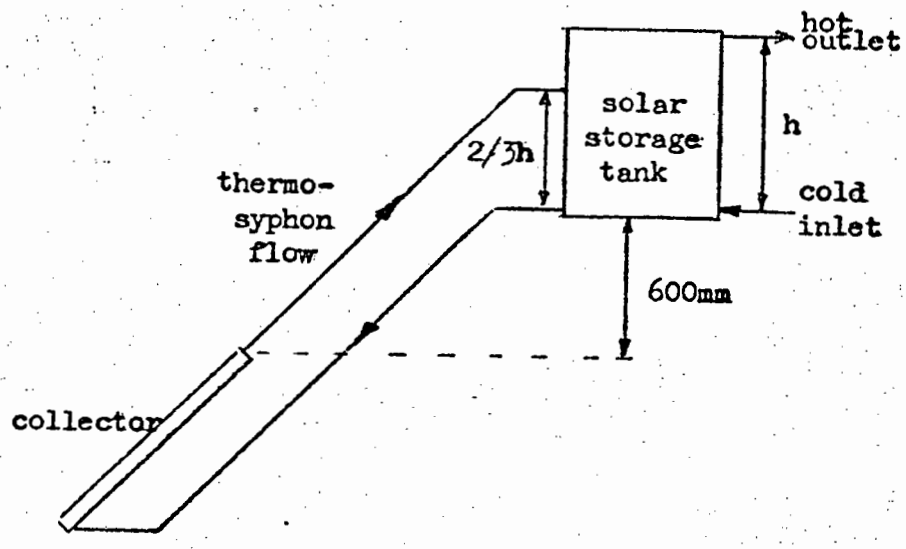

Fig. 2.8.1. Basic Layout of a thermosyphon flow, solar water heating system

CHAPTER 3.

THE MATHEMATICAL MODEL

3.1. INTRODUCTION

The purpose of building a theoretical model of a solar water heating system is to enable the prediction of the thermal performance of an actual system to be designed. Conversely, it can aid in the design of a particular system with certain performance requirements.

In designing the model it is necessary to know how the energy flows through the system. It is therefore essential to simulate each part of the entire system so that heat losses can be calculated accurately.

The incoming solar radiation strikes the transparent cover of the collector at a certain angle (the angle of incidence). This angle changes constantly throughout the day and is different for each day of the year, due to the change in declination of the sun. Part of this radiation is transmitted through the cover, some radiation is reflected back into the atmosphere, and a small quantity is absorbed into the cover. The amount reflected is dependent on the angle of incidence and the reflectivity of the transparent cover. It is therefore essential to know this angle of incidence at any given moment.

To determine the amount of radiation transmitted and absorbed by the cover, it is necessary to analyse in detail how the solar radiation interacts at the two interfaces of the cover.

Radiation heat losses occur from the cover to the atmosphere, which must be considered.

Once the solar radiation has passed through the collector cover it traverses the air gap and strikes the absorber plate. It is necessary to know exactly how : (i) the heat is transferred across

this air/...

this air gap; (ii) the losses occur in this space due to convection and radiation between the plate and the cover.

The heat is then conducted through the plate and stored in the water in the collector. The heat capacity of the water is determined and the amount of energy stored is calculated.

Heat losses from the sides and bottom of the collector by conduction, and convection losses due to the prevailing wind, must be assessed. The overall heat losses in the collector can then be calculated.

Heat losses also occur in the pipes and the storage tank due to conduction through the insulation, and are determined using the thermal conductivity of insulation of the respective components.

To determine the mass flow rate of the water through the system, the temperatures throughout the system must be known. By dividing the system into components and assuming constant water temperatures in these sections, the pressure difference due to the difference in density of the water in the sections, can be calculated at the inlet to the collector.

Using an equation (experimentally determined) of the relationship between this pressure difference and mass flow rate, the thermosyphon mass flow rate can be assessed.

The mathematical equations simulating the heat transfer processes in the solar water heater system are presented in this chapter.

3.2. RADIATION AND ANGLE OF INCIDENCE

Since the sun is constantly changing its position throughout the day, the angle at which the beam radiation strikes the collector is constantly changing. The amount of radiation transmitted through the transparent cover is therefore constantly varying.

The angle between the beam radiation and the normal to the plane of the collector, is known as the angle of incidence θ, and can be

described/...

described in terms of several angles (see Figs. 2.3.2. and 3.2.1.).

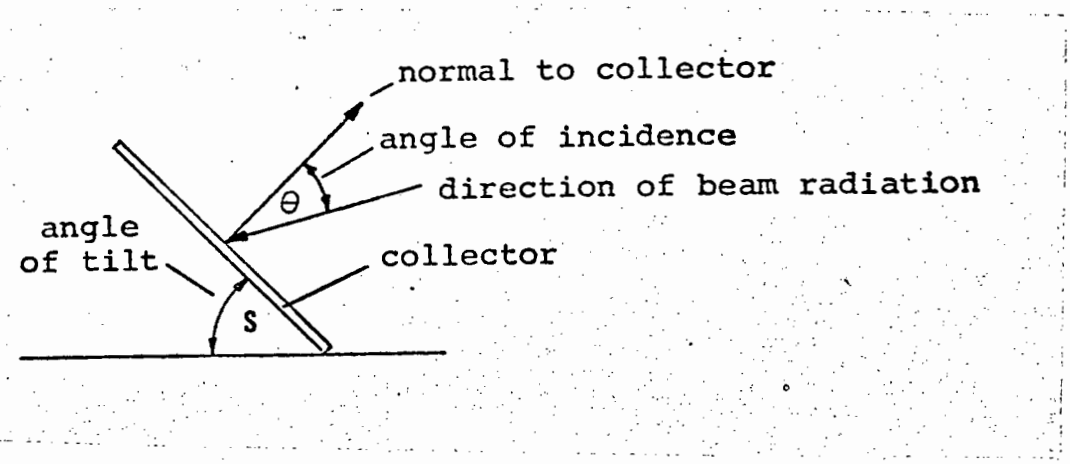

Fig. 3.2.1. Angle of Incidence

$$\cos\theta = \cos(L - s)\cos\delta\cos\omega + \sin(L - s)\sin\delta \quad (3.2.1.)$$

from (9)

where L = the latitude of the place (south is negative)

δ = declination of the sun

s = the angle between the horizontal and the plane of the collector (angle of tilt; negative for north facing)

ω = hour angle (solar noon being zero and each hour equalling 15^{o} of longitude; mornings positive and afternoons negative)

To account for difference between the longitude of the location in question L_{loc} and the longitude of the standard meridian for the local time zone L_{st} an equation is introduced to determine the solar time T.

$$T = T_{st} + E + 4\,(L_{st} - L_{loc}) \quad (3.2.2.)$$

where T_{st} = the standard time (or local clock time)

and E = the equation of time (in minutes)

The equation of time E is a correction factor introduced to account for the various perturbations in the earth's orbit and the rate of rotation which affects the time the sun appears to cross the observer's meridian. The value of E is obtained from published charts and Fig. 3.2.3. shows the variation of E throughout the year.

Fig. 3.2.3./.....

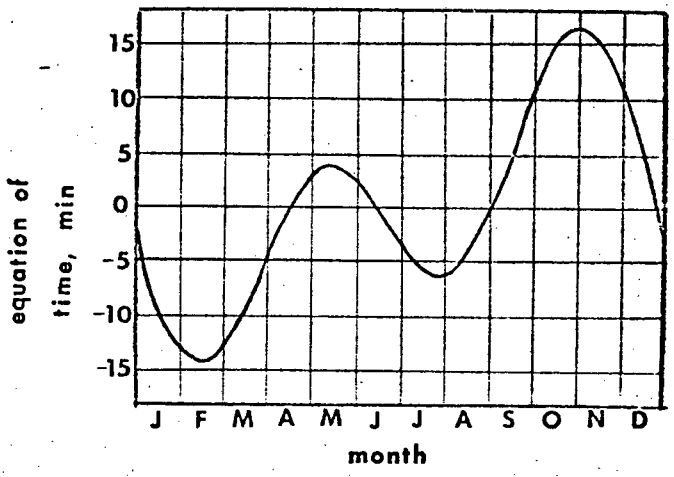

Fig. 3.2.3. The Equation of Time for the Year

The hour angle $\omega = (12 - T) \times 15$ (3.2.3.)
since the earth rotates 15^0 longitude each hour.

The declination δ is obtained from the following equation (from(9))

$$\delta = 23{,}45 \sin \left(360 \frac{284 + n}{365} \right) \quad (3.2.4.)$$

where n is the day of the year.

The radiation falling on the collector occurs as beam and diffuse radiation (see section 2.4.).

The direction of the diffuse radiation is extremely difficult to assess accurately, since it comes from parts of the sky dome other than the sun. However, Lui and Jordan (11) have derived equations to assess the amount of diffuse radiation falling on a tilted surface. Since, experimentally, no equipment was available to constantly determine the diffuse and beam radiation separately, this equation is not considered. The error in assuming all the radiation measured on the tilted surface to have the direction of the beam component is very small (see appendix 8.7.).

To predict the collector performance it will be necessary to determine the exchange of radiation between the collector surface and the sky. The sky can be considered as a blackbody at an equivalent sky temperature T_{sky}. This temperature accounts for the fact that the atmosphere

is not/...

is not at a uniform temperature and radiates at certain wavelengths only. Several techniques have been presented to relate this temperature to the ambient air temperature. However influences of clouds and ground reflectance were not considered in these interpretations. The various techniques prove to have negligible difference in effect on the final performance of the collector. Whillier (11) assumes the sky temperature T_{sky} to be $6^{o}C$ less than the ambient temperature. This value is used in this model

$$T_{sky} = T_{amb} - 6 \qquad (3.2.5.)$$

The radiation between a plane surface at temperature T, with emittance E, and area A and the sky is then

$$Q = EA\ \sigma(T_{sky}^{4} - T^{4}) \qquad (3.2.6.)$$

where σ = Stefan Boltzmann constant = $5,6697 \times 10^{8}\ W/m^{2}\ {}^{o}K^{4}$

3.3. FLAT PLATE COLLECTOR

For a flat place collector without optical concentration the flux of incident radiation is 1100 W/m^{2} maximum and the wave length range is from 0,3 to 3,0 μ m.

3.3.1. Energy Balance

To begin this analysis, an energy balance is considered on the collector. The radiant heat absorbed into the collector is distributed into useful heat and various losses.

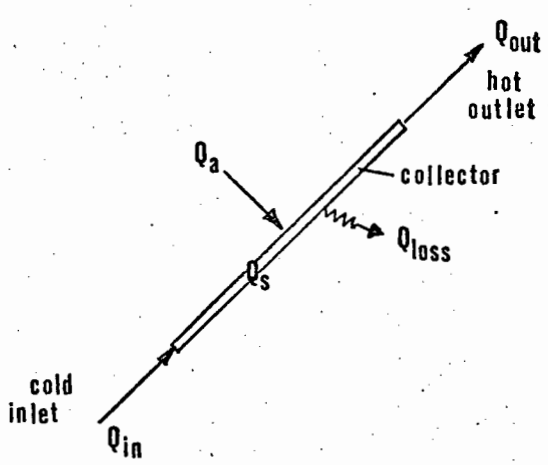

Fig. 3.3.1. The Flow of Energy through the Collector

An energy/....

An energy balance from Fig. 3.3.1. gives

$$Q_{in} + Q_a = Q_s + Q_{loss} + Q_{out} \qquad (3.3.1.)$$

This becomes

$$\text{Rad } (\tau\alpha)_e \, A_c = Q_s + Q_{loss} + Q_u \qquad (3.3.2.)$$

Where Q_a = radiant energy absorbed = Rad $(\tau\alpha)_e$ A_c

Rad = the radiation falling on the collector

$(\tau\alpha)_e$ = the effective transmittance-absorptance product of the collector cover

A_c = the collector area

Q_s = the energy stored in the collector

Q_u = the useful heat transferred by the working fluid = $Q_{out} - Q_{in}$

Q_{loss} = the energy losses from the collector to the surroundings.

The collector performance can be determined using the collector efficiency η_c, defined as the ratio of the useful heat gained over a period of time to the incident radiation over the same time period

$$\eta_c = \frac{\int Qu \, d\tau}{\int \text{Rad} \times A_c \, d\tau} \qquad (3.3.3.)$$

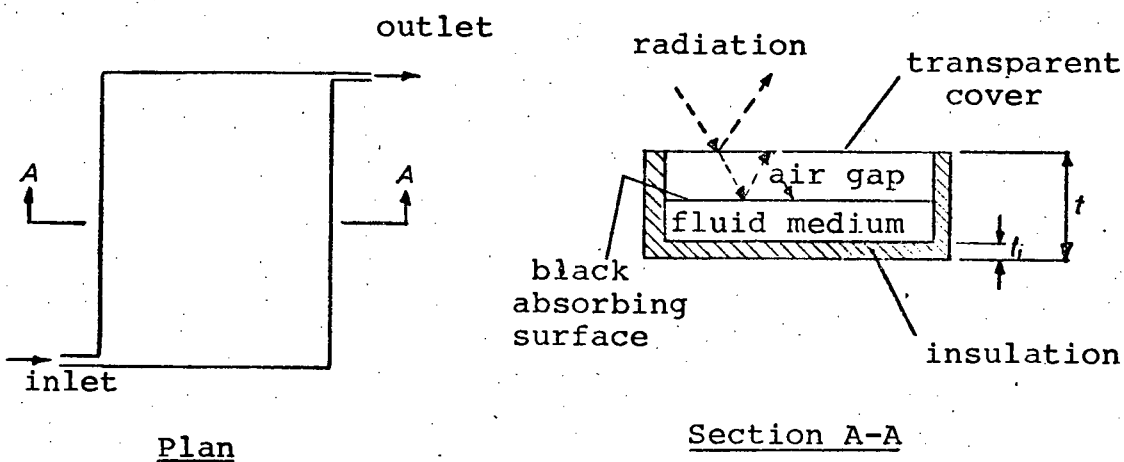

Fig. 3.3.2. Collector Model

Fig. 3.3.2. shows a simplified diagram of the model. The analysis which follows is based on derivations presented by Whiller (11) and Duffie and Beckman (9).

3.3.2./...

3.3.2. The Transparent Cover

For a surface transparent to incident radiation, the sum of the absorptance, reflectance and transmittance is unity. These properties are a function of wavelength and angle of incidence θ of the incoming radiation, the refractive index n and the extinction coefficient K of the material. K and n for solar energy applications are assumed to be independent of the wave length. (14)

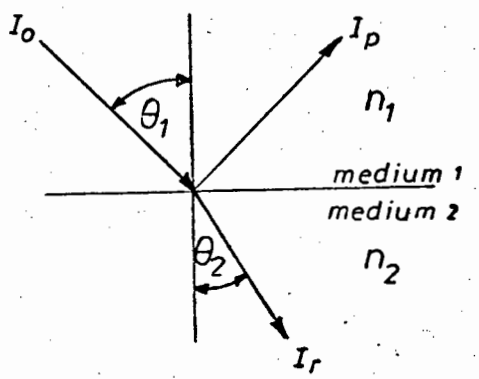

Fig. 3.3.3. Angle of Incidence θ_1, and Refraction θ_2.

For mediums with refractive indices n_1 and n_2 respectively, Fresnal derived a relationship for the reflection of non-polarised radiation (14).

$$\frac{I_r}{I_o} = \rho(\theta_1) = \frac{1}{2}\left[\frac{\sin^2(\theta_2 - \theta_1)}{\sin^2(\theta_2 + \theta_1)} + \frac{\tan^2(\theta_2 - \theta_1)}{\tan^2(\theta_2 + \theta_1)}\right] \quad (3.3.3.)$$

and by Snell's law (14)

$$\frac{n_1}{n_2} = \frac{\sin\theta_2}{\sin\theta_1} \quad (3.3.4.)$$

then for radiation at normal incidence (i.e. $\theta_1 = 0^o$)

$$\rho(\theta^o) = \left(\frac{n_1 - n_2}{n_1 + n_2}\right)^2 \quad (3.3.5.)$$

Reflection losses occur at two interfaces of the cover

Fig. 3.3.4./...

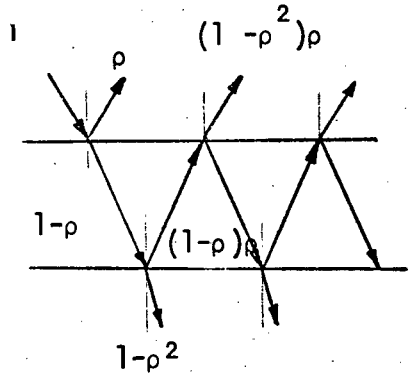

Fig. 3.3.4. Transmission through the Cover.

Neglecting absorption, and assuming air to be on either side of the cover, the beam depletes by the same amount at each surface. $(1-\rho)$ of the initial beam strikes the second surface. $(1-\rho)^2$ passes through and $(1-\rho)\rho$ is reflected. So the beam continues to deplete at each surface.

A sum of all these terms gives the transmittance of the cover, neglecting absorption.

$$\tau_r = (1-\rho)^2 \sum_{n=0}^{\infty} \rho^{2n} = \frac{1-\rho}{1+\rho}$$

i.e. having accounted for reflection only, the transmittance, at an angle of incidence θ, is

$$\tau_r(\theta) = \frac{1-\rho(\theta)}{1+\rho(\theta)} \qquad (3.3.6.)$$

To determine the transmittance due to absorption, Bouger's law is applied (14). This assumes that the absorbed radiation is proportional to the local intensity in the medium and the distance the radiation travels through the medium, x.

$$dI = IKdx$$

K is the extinction coefficient assumed to be constant. Integrating across the cover thickness, the transmittance due to absorption only is found to be

$$\tau_a(\theta) = \frac{I_c}{I_o} = e^{-Kt_c/\cos\theta_2} \qquad (3.3.7.)$$

and the total transmittance $\tau(\theta) = \tau_r(\theta)\,\tau_a(\theta)$ (3.3.8.)

Fig. 3.3.5. /....

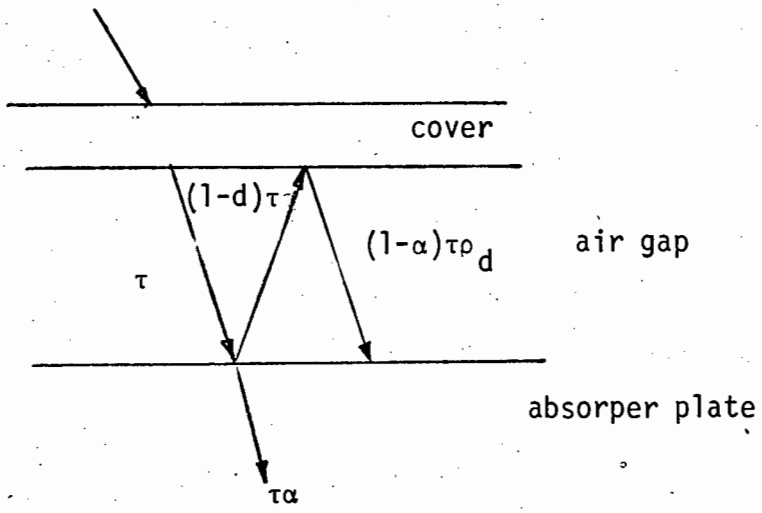

Fig. 3.3.5. Absorption of Solar Radiation by the Absorber Plate

Some of the radiation that passes through the cover and impinges on the absorber is reflected back to the cover and in turn reflected back to the absorber. The situation is similar to that described in Fig. 3.3.4. and is illustrated in Fig. 3.3.5. Of the incident energy $\tau\alpha$ is absorbed by the plate, $(1 - \alpha)\tau$ is reflected back to the cover. This is diffuse radiation and $(1 - \alpha)\tau\rho$ is again relected. ρ_d is the relection due to diffuse radiation.

This multiple reflection is summed as the transmittance absorptance product

$$(\tau\alpha) = \tau\alpha \sum_{n=0}^{\infty} \left[(1 - \alpha)\rho_d\right]^n = \frac{\tau\alpha}{1 - (1 - \alpha)\rho_d} \qquad (3.3.9.)$$

where $\rho_d = 1 - \tau_r$ (3.3.10.)

3.3.3. Heat Loss Coefficients

To assess the heat loss, Q_{loss} an overall loss coefficient, U_o, is introduced to simplify the analysis, and the following assumptions are made.

(i) Flow is steady.

(ii) Heat flow through the cover and insulation is one dimensional.

(iii) /....

(iii) The temperature drop through the cover is negligible.

(iv) Ambient temperatures are the same all around the collector.

(v) Dust and dirt on the cover have negligible effect.

(vi) The entire collector is at the mean plate temperature, T_p.

Consider the thermal network in Fig. 3.3.6.

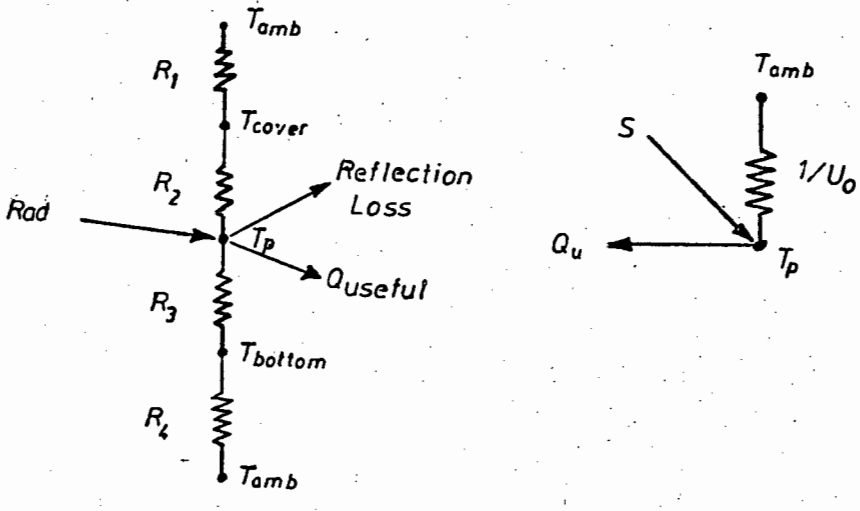

Fig. 3.3.6. (a) Thermal Network for the Collector. (b) Equivalent Thermal Network.

Solar energy, Rad, is absorbed into the plate. This is converted into useful work Q_u and losses occur through the top, bottom and edges of the collector.

Bottom and edge losses are represented by R_3 and R_4. R_3 represents the resistance to heat flow through the insulation, while R_4 represents the convection and radiation resistance to the ambient air. Since $R_3 >> R_4$, R_4 is assumed to be negligible and equal to zero.

The bottom loss coefficient $U_b = k/t_i$ (3.3.11.)

where k is the thermal conductivity and t_i is the thickness of the insulation.

The edges loss coefficient $U_e = \frac{k}{t_i} \frac{t \times \text{perimeter}}{A_c}$ (3.3.12.)

where t is the thickness of the collector, and one dimensional sideways heat flow around the perimeter of the collector is assumed.

The losses/...

The losses through the top of the collector, by radiation and convection are represented by R_1 and R_2.

R_2 represents the resistance to loss between the plate and cover. These are considered as two parallel plates in assessing the heat transfer between them.

$$R_2 = \frac{1}{h_{p-c} + h_{r,p-c}} \qquad (3.3.13.)$$

where h_{p-c} and $h_{r,p-c}$ are the plate to cover convection and radiation coefficients, respectively.

R_1 is the cover to sky resistance to radiation and convection. The convection term is represented by a wind coefficient h_w and $h_{r,c-s}$ is the cover to sky radiation coefficient.

$$R_1 = \frac{1}{h_w + h_{r,c-s}} \qquad (3.3.14.)$$

Thus, the top loss coefficent

$$U_t = \frac{1}{R_1 + R_2} = \left[\frac{1}{h_{p-c} + h_{r,p-c}} + \frac{1}{h_w + h_{r,c-s}} \right]^{-1} \qquad (3.3.15.)$$

The plate to cover convection coefficient h_{p-c}, can be found by considering the heat transfer, with natural convection, between two parallel flat plates, inclined at an angle to the horizontal. For solar collector calculations the data presented by Duffie and Beckmann (9) shows a relationship between Nusselt and Grashof numbers, for 45^{o}planes, with heat flow upwards and $10^4 < Gr < 10^7$

$$Nu = 0{,}093\ (Gr)^{0{,}310} \qquad (3.3.16.)$$

where Nusselt No. $Nu = \frac{h\ell}{k}$ (3.3.17)

and $Gr = g \frac{\beta\ \Delta T\ \ell^3}{\nu^2}$ (3.3.18.)

h = heat transfer coefficent.

ℓ = plate to cover spacing

k = thermal conductivity

g = gravitational constant

β = volumentric coefficient of expansion of air

Δ T /....

ΔT = temperature difference between the plates (^{o}C)

ν = kinematic viscosity

Equation (3.3.16.) can be expressed in dimensional form for a temperature of $10^{o}C$ (9)

$$h_{10} = 1,14 \frac{\Delta T^{0,310}}{\ell^{0,070}} \qquad (3.3.19.)$$

For other temperatures

$$\frac{h_T}{h_{10}} = 1 - 0,0018 (\bar{T} - 10) \qquad (3.3.20.)$$

Where $\bar{T}$ is the average temperature between the two plates (in ^{o}C)

i.e. $$h_{p-c} = \frac{1,14 \Delta T^{0,310}}{\ell^{0,070}} \left[1 - 0,0018 (\bar{T}-10)\right] \qquad (3.3.21.)$$

(where ℓ is the plate to cover spacing in cms.)

The radiation coefficient from the plate to the cover is

$$h_{r,p-c} = \sigma \frac{(T_p^{\,2} + T_c^{\,2})(T_p + T_c)}{1/\varepsilon_p + 1/\varepsilon_c - 1} \qquad (3.3.22.)$$

and the radiation coefficient from the cover to the sky is

$$h_{r,c-s} = \sigma \varepsilon_c (T_c^{\,2} + T_s^{\,2})(T_c + T_s) \qquad (3.3.23.)$$

The heat loss coefficient for flat plates exposed to winds (9) is given as

$$h_w = 5,7 + 3,8 V_w \qquad (3.3.24.)$$

where V_w is the wind velocity.

σ is Stefan Boltzmann constant.

T_p and T_c are the plate and cover temperatures, respectively.

ε_p and ε_c are the plate and cover emissivities, respectively.

The cover temperature can be found by an iterative technique, assuming the initial cover temperature and using the following equation

$$T_c = T_p - \frac{U_t (T_p - T_a)}{h_{p-c} + h_{r,p-c}} \qquad (3.3.25).$$

Using the /.....

Using the assumed value of T_c; h_{p-c}, $h_{r,p-c}$, $h_{r,c-s}$ and U_t are calculated. T_c is then assessed using equation (3.4.25.) This new value of T_c becomes the assumed value of T_c and the iteration continues until the assumed and calculated values are equal.

The overall loss coefficient U_o is then evaluated.

$$U_o = U_t = U_b + U_e \qquad (3.3.26.)$$

These loss coefficients were calculated assuming no absorption occured in the collector cover.

To account for this absorption of energy an effective transmittance-absorptance product $(\tau\alpha)_e$ is introduced.

Returning to Fig. 3.4.6.(a), the solar energy absorbed by the cover is Rad $(1 - \tau_a)$. The loss without absorption is $\frac{1}{R_2}(T_p - T_c)$ and with absorption is $\frac{1}{R_2}(T_p - T_c')$.

Where $T_c' > T_c$ since a small amount of energy is absorbed in the cover. If $U_2 = \frac{1}{R_2}$, $U_1 = \frac{1}{R_1}$ and $U_t = \frac{1}{R_1 + R_2}$ then the difference

between the two loss terms is

$D = U_2 \left[(T_p - T_c) - (T_p - T_c')\right]$ which is shown (9) to be

$$\text{Rad}\,(1 - \tau_a)\,\frac{U_o}{U_1}$$

This gain in energy is thus considered in the following equation

$$(\tau\,\alpha)_e = (\tau\,\alpha) + (1 - \tau_a)\,\frac{U_o}{U_1} \qquad (3.2.27.)$$

and $U_1 = h_w + h_{r,c-s}$

A finite /...

A finite difference technique is introduced to determine the mean plate temperature after a time interval $\Delta\tau$.

Returning to the energy balance equation (3.3.1.) and using the following values :

Energy stored in the collector in time interval $\Delta\tau$

$$Q_s = W_c \frac{dT_p}{d\tau} \qquad (3.3.28.)$$

where W_c is the thermal capacity of the collector

dT_p is the difference in plate temperature over the time interval $d\tau$.

$$\text{Energy loss } Q_{loss} = U_o A_c (T_p - T_{amb}) \qquad (3.3.29.)$$

$$\text{Useful heat transferred } Q_u = \dot{m}_c c_p (T_{co} - T_{ci}) \qquad (3.3.30.)$$

where T_{co} and T_{ci} are the collector outlet and inlet temperatures, respectively.

then (3.3.2.) becomes

$$W_c \frac{dT_p}{d\tau} = \text{Rad } (\tau\alpha)_e A_c - \dot{m}_c C_p (T_{co} - T_{ci}) - U_o A_c (T_p - T_{amb}) \qquad (3.3.31.)$$

The new mean plate temperature is then

$$T_{pnew} = T_{pold} + \frac{\Delta\tau}{W_c} \left[\text{Rad } (\tau\alpha)_e A_c - \dot{m}_c C_p (T_{co} - T_{ci}) - U_o A_c (T_{p_{old}} - T_{amb}) \right] \qquad (3.3.32.)$$

From equation (3.4.2.) the instantaneous collector efficiency is then

$$\eta_c = \frac{\dot{m}_c C_p (T_{co} - T_{ci})}{\text{Rad} \times A_c} \qquad (3.3.33.)$$

while the efficiency for the whole day

$$\eta_{solar} = \frac{Q_{solar}}{\text{Tot.Rad.(for the day)} \times A_c} \qquad (3.3.34.)$$

where Q_{solar} /...

where $Q_{solar} = \Sigma \dot{m}_L C_p \Delta T_{solar} \Delta t$ (3.3.35.)

ΔT_{solar} = the temperature difference between the water leaving and entering the solar tank during draw off.

Δt = the time period for which water is drawn off.

3.4. THE SOLAR STORAGE TANK

The storage tank can be modelled in two ways.

(a) Non-stratified simulation

This type of solution assumes that the tank is at a uniform temperature (throughout its vertical height).

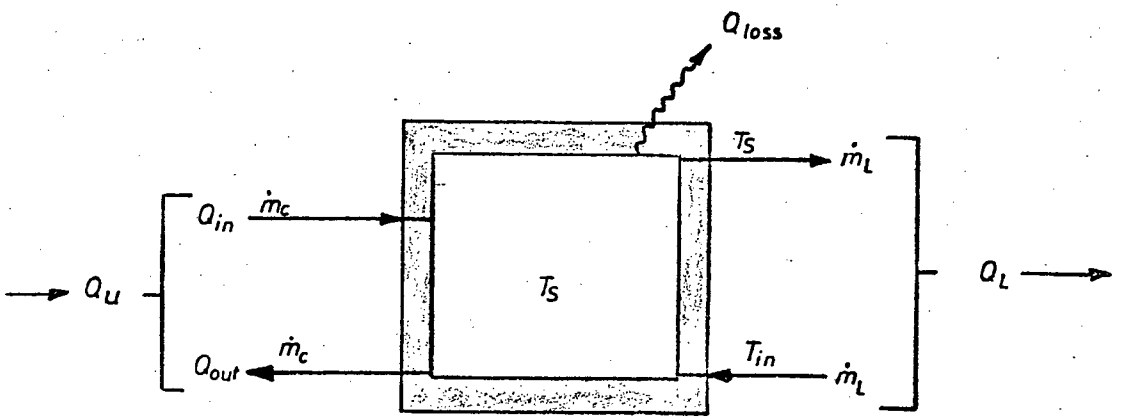

Fig. 3.4.1. Non-stratified Tank model

The energy storage capacity of a liquid storage unit operating over a finite temperature difference ΔT_s in time $\Delta\tau$ is

$$Q_s = (MC_p)_s \frac{(\Delta T_s)}{\Delta\tau} \quad (3.4.1.)$$

where M is the mass of liquid with specific heat capacity Cp.
The rate of energy gain from the collector

$$Q_u = Q_{in} - Q_{out} = \dot{m}_c C_p (T_{co} - T_s) \quad (3.4.2.)$$

where $\dot{m}_c$ is the thermosyphon mass flow rate through the collector and T_{co} is the temperature of water from the collector.

The rate /....

The rate of energy removal to the load is

$$Q_L = \dot{m}_L C_p (T_s - T_{in}) \qquad (3.4.3.)$$

where $\dot{m}_c$ is the draw off flow rate and T_{in} is the inflowing water temperature.

The thermal losses $Q_{loss} = (UA)_s (T_s - T_a)$ (3.4.4)

where $(UA)_s$ is the loss coefficient area product.

Applying an energy balance to this system

$$W_s \frac{\Delta T_s}{\Delta \tau} = Q_u - Q_L - Q_{loss} \qquad (3.4.5.)$$

where the thermal capacity is $W_s = MC_p$ and

ΔT_s is the temperature difference over the time period $\Delta\tau$

$$\Delta T_s = T_{s,new} - T_{s,old} \qquad (3.4.6.)$$

$T_{s,old}$ and $T_{s,new}$ are the temperatures of the tank at the beginning and end of the time period $d\tau$, respectively.

For a finite time increment this new tank temperature is then

$$T_{s,new} = T_{s,old} + \frac{\Delta\tau}{W_s} \left[Q_u - Q_L - (UA)_s (T_{s,old} - T_a)\right] \qquad (3.4.7.)$$

(b) Stratified tank simulation

This type of model does not assume a uniform temperature over the entire vertical dimension of the tank.

The tank is sectioned as shown in Fig. 3.4.2.

The equation (3.4.2.) then holds for each section of the tank (which is assumed to have constant temperature over its vertical height). This simulates the real situation in which the incoming water seeks its own density level (provided that it enters at a low velocity).

Fig. 3.4.2. /...

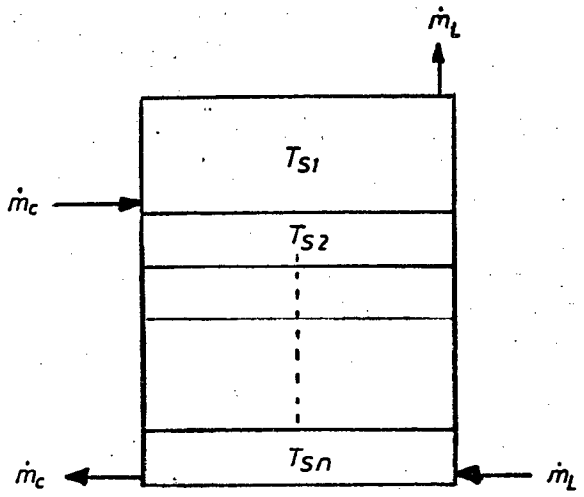

Fig. 3.4.2. Stratified Tank

The criteria for tank sectioning is based on experimental data (8) in which the water temperature of the upper tank section was found to be quite uniform down to the upriser pipe level. Below this the temperature profile was nearly linear down to the tank bottom.

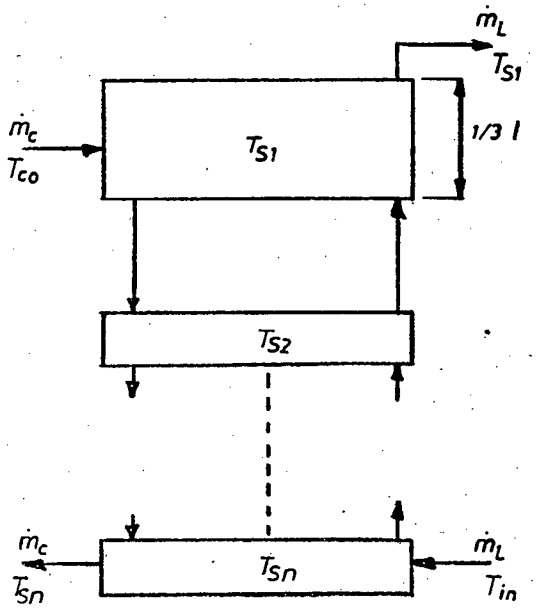

Fig. 3.4.3. Tank Sections

The water from the collector enters into the upper section 1, of the tank/...

the tank. The sections 2 to n are of the same size.
The thermosyphon and load mass flow rates are assumed equal for all sections.
The new temperatures for each section are obtained by applying equation (3.4.7.).
For the jth section

$$T_{sj,new} = T_{sj,old} + \frac{\Delta\tau}{W_{sj}} \left[\dot{m}_c C_p \left(T_{s(j-i)old} - T_{sj,old}\right) + \dot{m}_L C_p \right.$$

$$\left. \left(T_{s(j+i)old} - T_{sj,old}\right) - (UA)_j \left(T_{sj,old} - T_{amb}\right) \right] \qquad (3.4.8.)$$

3.5. THE PIPES

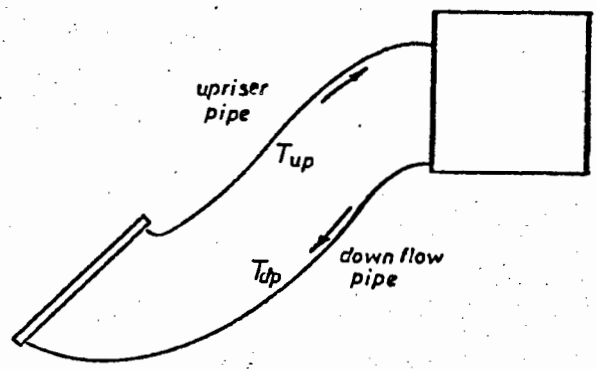

Fig. 3.5.1. Thermosyphon Flow Circuit Pipes

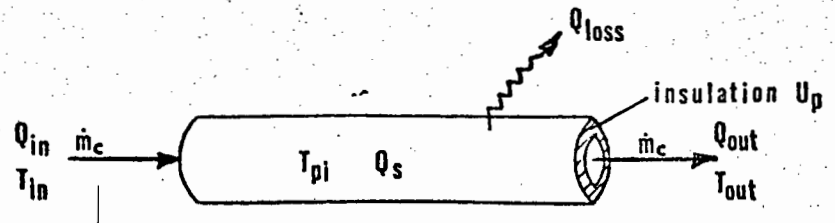

Fig. 3.5.2. Pipe Simulation

An energy /....

An energy balance from Fig. 3.5.2. gives $Q_{in} = Q_s + Q_{loss} + Qout$.

Since $Q_u = Q_{out} - Q_{in}$, and $Q_s = W_{pi} \frac{\Delta T_{pi}}{\Delta \tau}$, where $\Delta T_{pi} = T_{pi,new} - T_{pi,old}$ is the temperature difference over a time period $\Delta\tau$, then

$$W_{pi} \frac{\Delta T_{pi}}{\Delta \tau} = Q_u - Q_{loss} \qquad (3.5.1.)$$

and $$T_{pi,new} = T_{pi,old} + \frac{\Delta \tau}{W_{pi}} \left[\dot{m}_c C_p (T_{in} - T_{pi,old}) - (UA)_{pi} (T_{pi,old} - T_{amb})\right] \qquad (3.5.2.)$$

Equations (3.3.32.), (3.4.8.) and (3.5.2.) are used to determine the mean plate temperature, tank temperatures and pipe temperatures throughout the day, given the initial temperatures at start of the day.

CHAPTER 4

THE COMPUTER SIMULATION MODEL

The Wang 2200 computer was programmed for the solution of temperatures, flow rates and efficiencies. The program was based on the theory presented in Chapter 3.

A systems diagram of the model is shown in Fig. 4.1.1.

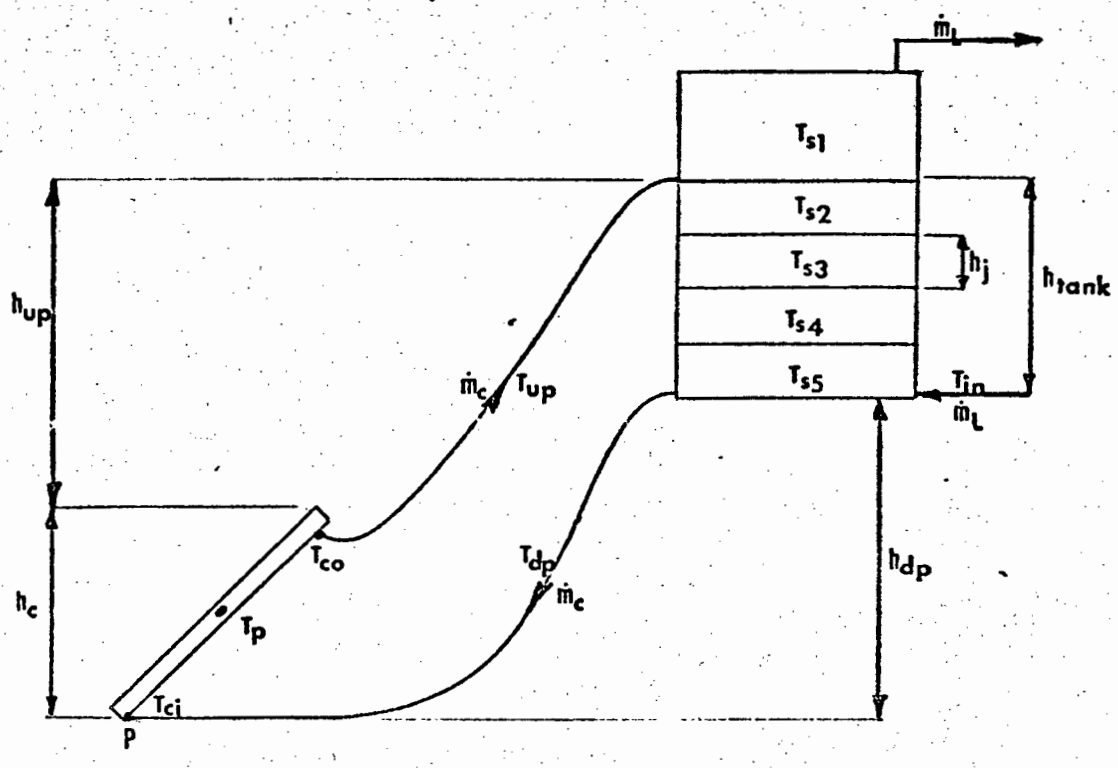

Fig. 4.1.1. Systems Diagram of the Computer Model.

4.1. ASSUMPTIONS

The following assumptions were made in developing this model.

(i) The entire collector is at the mean plate temperature T_p

$$T_p = (T_{ci} + T_{co}) / 2 \qquad (4.1.1.)$$

(ii) No absorption of radiation or heat loss due to wind occurs in the/....

in the pipes.

(iii) The storage tank is multi-sectioned, each section representing a portion of the tank wall, insulation and water. The top section, s_1, is from the top of the tank down to the upriser pipe inlet. The other sections are divided equally, while the bottom section, s_5, includes the bottom of the tank insulation and the down flow pipe exit.

(iv) The ambient temperature, T_{amb}, is assumed to be the same for the tank and collector.

(v) At the initial starting time of the program, for each day, $T_{up} = T_{co}$, $T_{dp} = T_{ci}$

(vi) After each time interval $\alpha\tau$, $T_4 = T_{dp}$, $T_{co} = 2T_p - T_{ci}$

4.2. LOSS COEFFICIENTS

The loss coefficients for the pipes and tank were determined experimentally. A known quantity of water was trapped in the pipes (and tank) and the temperatures were observed with respect to time.

Using equations (3.5.2.) for the pipes and (3.4.5.) for the tank with zero flows, the factors U_{up}, U_{dp} and U_s were calculated.

4.3. THE THERMAL CAPACITIES

Thermal capacity = $W = MC_p$

$$= V \times p \times Cp \qquad (4.3.1.)$$

The volumes V, were calculated from the physical parameters of the system components, while the values of density ρ, and specific heat capacity Cp were determined at the temperature of the water in the particular section.

4.4. THERMOSYPHON MASS FLOW RATE

A U-tube principle was used to assess the thermosyphon head causing flow.

The pressure difference at point P (see Fig. 4.1.1.) was calculated using the weight of water on either side of P.

The tank/....

The tank temperature $T_{tank} = \sum_{2}^{5} (T_j h_j)/h_{tank}$ (4.4.1.)

where h_j is the height of each section of the tank.

The pressure difference causing flow is

$$\Delta p = \left[(\sum_{2}^{5} h_j \rho_j)(h_{tank} + h_{dp} \rho_{dp} - h_{coll}\rho_{coll} - h_{up}\rho_{up}) \right] \quad (4.4.2.)$$

The relationship between pressure head and mass flow rate was determined experimentally. Flows were mostly inside the laminar flow region and had the relationship of a geometrical regression

$$\dot{m}_c = a\Delta p^b \quad (4.4.3.)$$

where a and b were constants.

(See appendix 8.4. for further details)

4.5. THE PROGRAM

A flow chart of the program is shown in Fig. 4.5.1.

Various size stratification models were tested in the early stages of building the tank model. A 4-stratified tank appeared to be the most accurate. However, a 5-stratified tank system proved to be more accurate.

A time interval of $\Delta\tau$ of 5 minutes was found to be adequate except during high flow rate draw off periods where 1 minute intervals were used.

Initial system temperatures, hot water draw off times and flow rates, were recorded and stored in data files. Radiation, wind velocity and ambient temperatures, experimentally measured, were averaged out over hourly periods and stored in the same data files.

Computation was started at 0730 hours when thermosyphon flow was about to begin and collector and tank temperatures began to rise.

The calculated temperatures, flow rates and efficiencies were printed out as the time was incremented throughout the day.

4.5.1. /...

Fig. 4.5.1. Flow Diagram of the Computer Program

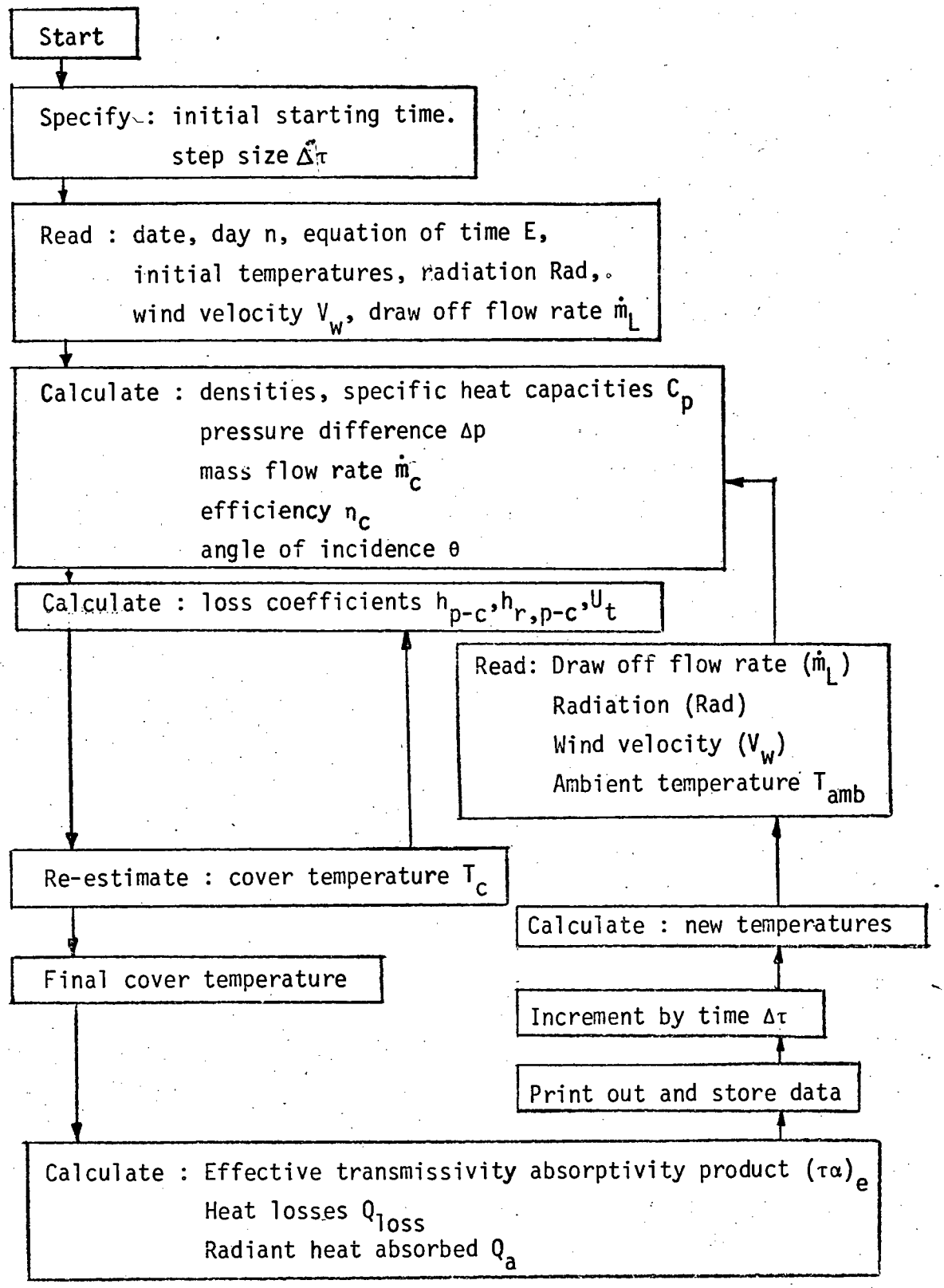

4.5.1. A step by step detailed description of the operation of the program.

This description of the program is an expansion of the flow chart of Fig.4.5.1., giving the step by step proceedure and equations utilized.

(i) It is required to specify the initial starting time, so that the data at that time can be obtained from the data file. The step size $\Delta\tau$ must be specified.

(ii) The data file is then inserted and the following information is read : date; day of the year (n); equation of time (E); initial temperatures T_{co}, T_{ci}, T_A, T_B, T_C, T_D, at the initial starting time; radiation (Rad); wind velocity(V_w); ambient temperature(T_{amb}); and the draw off flow rate ($\dot{m}_L$).

(iii) The values of T_A, T_B, T_C, and T_D, the tank temperatures are converted to T_{s1}, T_{s2}, T_{s3}, T_{s4}, and T_{s5} using equations (8.6.1.) described in the appendix 8.6.

The initial upriser pipe temperature T_{up} is assumed equal to the collector outlet temperature T_{co}.

The initial downflow pipe temperature T_{dp} is assumed equal to the collector inlet temperature T_{ci}.

The mean plate temperature $T_p = (T_{ci} + T_{co})/2$

(iv) Using the temperatures in the various sections, the densities ρ and the specific heat capacities Cp are calculated with equations (8.6.2.) and (8.6.3.) (see appendix 8.6.).

The pressure difference Δp at point P (see Fig. 4.1.1.) is then calculated with equation (4.4.2.) and hence the thermosyphon mass flow rate $\dot{m}_c$ is obtained utilizing equation (4.4.3.).

The instantaneous efficient $\eta_c = \dfrac{\dot{m}_c C_p (T_{co} - T_{ci})}{Rad \times A_c}$ is thencalculated from equation (3.3.33.)

(v) The time /..

(v) The time is converted to solar time T, using equation (3.2.2.). The hour angle w = (12 - T) x 15 from equation (3.2.3.), and the declination δ is obtained from equation (3.2.4.).

The angle of incidence is calculated using equation (3.2.1.).

(vi) A value for the cover temperature T_c is assumed and the loss coefficients h_{p-c}, $h_{r,p-c}$, $h_{r,c-s}$, and h_w are calculated using equations (3.3.21. to 24.) The top loss coefficient U_t is then obtained with equation (3.3.15.). The cover temperature is now calculated using equation (3.3.25.), and if it is not the same as the assumed temperature the iteration continues until the value of T_c is the same before evaluating the loss coefficients.

(vii) The angle of refraction θ_2 of the radiation through the transparent collector cover is enumerated from equation (3.3.4.) and utilized to determine the reflectance $\rho(\theta)$ from equation (3.3.3.).

The transmittance due to reflection only $\tau_r(\theta)$, absorption only $\tau_a(\theta)$ and the total transmittance $\tau(\theta)$ are obtained from equations (3.3.6. to 8.). The transmittance-absorptance product $(\tau\alpha)$ is then calculated from equation (3.3.9.).

(viii) The bottom loss coefficient U_b and edges loss coefficient U_e are assessed from equations (3.3.11. and 12.). The overall loss coefficient U_o is then determined with equation (3.3.26.) and the effective transmittance absorptance product $(\tau\alpha)_e$ with equation (3.3.27.).

(ix) The heat losses Q_{loss}, useful heat Q_u and heat absorbed Q_a in the collector are determined using equations (3.3.29.), (3.3.30.) and (3.3.2.).

(x) The required data is printed and stored.
The time is incremented by $\Delta\tau$

(xi) The new mean plate tank and pipe temperatures are then calculated /...

calculated using equation (3.3.32.), (3.4.8.) and (3.5.2.) respectively.

The new collector inlet temperature $T_{ci} = T_{dp}$ and outlet temperature $T_{co} = 2T_p - T_{ci}$.

(xii) At this new time, the draw off flow rate ($\dot{m}_L$), radiation (Rad), wind velocity (V_w) and ambient temperature (T_{amb}) is read from the data file.

(xiii) The program then returns to step (iv) and continues until all the readings in the data file are processed.

CHAPTER 5

THE EXPERIMENT

A solar water heating system was designed and built to simulate a domestic system, and to compare the results with those obtained using the computer model.

5.1. APPARATUS

Fig. 5.1.1. is a systems diagram showing the basic layout of the apparatus.

Water is supplied to the system from the mains.

The time clock was used to operate the solenoid valve, to supply water at preselected times, chosen to simulate domestic conditions. This water then flowed through the water meter, measuring the quantity of water supplied, and before entering the bottom of the storage tank the temperature of this cold water was measured with a thermocouple connected to a chart recorder.

The tank temperatures were measured at four different heights with thermocouples connected to the chart recorder. The cold water at the bottom of the tank flowed out into the downflow pipe to the collector. About halfway along this pipe the thermistor and a thermometer were inserted. The thermistor was connected to a specially designed circuit, from which the thermosyphon flow could be assessed.

Closer to the collector, along this downflow pipe, two valves were located, one to drain the system, the other to seal off the pipe so as to create a no flow situation (this was required for the calibration of the thermistor).

At the pipe entrance to the collector, the collector inlet temperature was measured. The water then passed into the collector where

it was /....

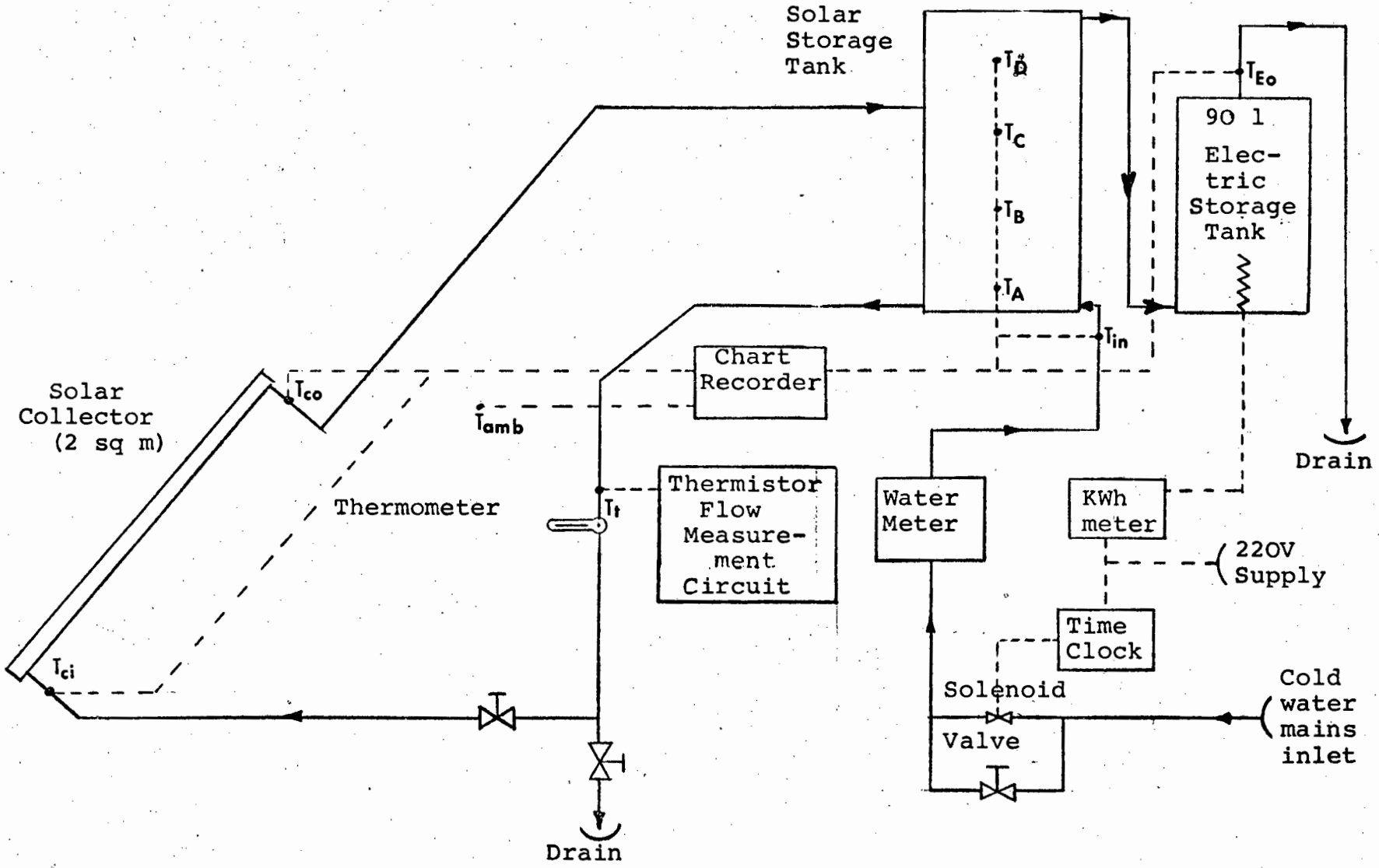

Fig. 5.I.I Systems diagram for the solar water heater

it was heated by solar radiation. The heated water seeking its own density level rose to the top of the collector. In passing into the upriser pipe, a thermocouple connected to the chart recorder measured the collector outlet temperature. This pipe carried the water back into the solar storage tank.

This completed the thermosyphon flow circuit.

Hot water was drawn off from this solar storage tank by a push through system, whereby cold water was fed into the system pushing the hot water out at the top of the tank.

This hot water was fed into the bottom of an electric geyser. The amount of electrical energy consumed to maintain the water at a constant preselected temperature, was measured on a kilowatt-hour meter. The exit temperature of the water at the top of this geyser was recorded with the aid of a thermocouple.

5.1.1. The Collector

The collector (see Fig.5.1.2.) was a 2 square meter Hamworthy/Van Leer solar heat exchanger. (see specifications in appendix 8.8.).

This particular collector was available for use at the start of the project and provided the basic collector requirements.

According to Chinnery (10), the use of a solar water heater with electric auxilliary heating for four people, requires a minimum absorber area of 1,8m^2 and a minimum total tank capacity of 180 litres. This collector was therefore suitable for simulating these conditions.

The absorber plate was a stainless steel envelope coated with matt black paint. It was insulated with 25 mm thick polyurethane foam. 3 mm perspex was used as a transparent cover. The absorber frame was made from aluminuim with a base sheet of galvanised steel.

The collector /....

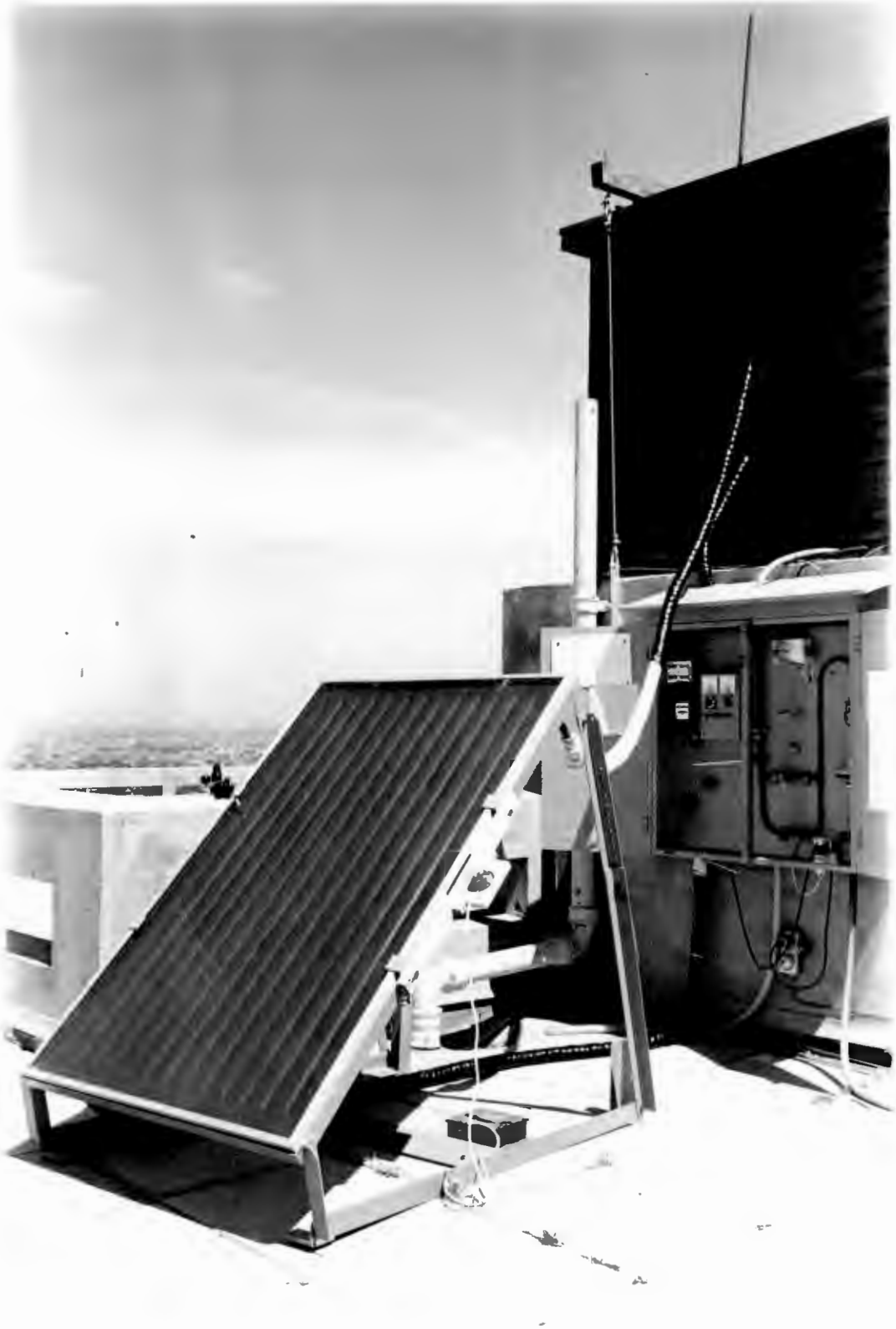

Figure 5.1.2 The Solar Collector

The collector support was designed and built such that the angle of tilt could be adjusted. The mechanism was placed so that the collector was facing due north, and an angle of tilt of 44^{o} from the horizontal was set for the tests.

5.1.2. Storage Tanks

To simulate domestic conditions it was necessary to select the appropriate type and size of storage tank. Most existing middle class 'white' houses in South Africa have an electrical hot water heating system. Also for families to be assured of a constant hot water supply, solar energy is not totally reliable (especially during winter in the Cape). The type of system selected was therefore a solar tank feeding an electrical geyser.

A 2 m^2 absorber requires approximately a 100 litre tank, while Chinnery (10) recommends, with electrical auxilliary heating, a total minimum tank capacity of 180 litres for 4 people.

A 135 litre solar tank and a 90 litre electrical tank were chosen for the experimental circuit (see Fig. 5.1.3. and Fig. 8.3.2.).

The solar tank was a "Kwikot" Solar Water Heater, code 21355 and the electrical tank was a "Kwikot" Vertical Multiple electric water heater, code 2020.

The solar storage tank was placed more than 600 mm above the top of the collector (at a 44^{o} angle of tilt).

The heat loss coefficient was determined experimentally (see appendix 8.3. ii).

5.1.3. Pipes

The thermosyphon flow circuit was connected using 1" diameter reinforced nylon hose. Asbestos rope was wound around the pipes providing insulation.

The loss-coefficients were determined experimentally (see appendix 8.3. iii).

5.1.4. /...

Figure 5.1.3 The Storage Tanks

5.1.4. Instruments

Temperatures were recorded on a Phillips PM 9833 multipoint recorder using copper-constantan thermocouples.

Zeal thermometers with an accuracy of $0,2^{o}C$ were used as well (as a double check and during non test periods).

Four thermocouples were inserted into the solar tank at various heights (see Fig 3.3.3.), giving temperatures T_A, T_B, T_C and T_D.

The thermosyphon mass flow rates were measured using a thermistor (type FS 23D) inserted into the downflow pipe. The thermistor was connected to an electronic circuit designed so that the change in voltage across the thermistor due to a certain flow rate was registered on a meter and the actual flow was then read off on a calibration chart. (A detailed explanation appears in section 5.2.3.)

Radiation was measured using a solarimeter mounted on the collector support mechanism, at the same angle of tilt as the collector, and recorded on the Phillips PM 9833 multipoint recorder.

Wind velocity was measured on a Casella anamometer, also mounted on the collector support mechanism. This technique actually measured only instantaneous wind velocities.

Hot water was drawn off at preselected times using an Electroboy Universal Time Switch (Type U 596) connected to a solenoid valve. A (Kent S.A.) watermeter measured the quantity of water drawn off.

The amount of electricity consumed by the electrical geyser was recorded on a Landis and Gyr (Type CL 272) kilowatt-hour meter.

5.2. EXPERIMENTAL PROCEDURE

Before the actual tests could be performed on the solar water heating system, it was necessary to experimentally determine the loss coefficients of the solar storage tank and pipes. To measure

the thermosyphon /..

Figure 5.1.4 The Instrument Box
(a) the thermistor circuit
(b) the kWh meter
(c) the timer clock
(d) the water meter

the thermosyphon flow rate various techniques were tested in the circuit and certain calibrations were necessary.

5.2.1. The Tank Loss Coefficients

To assess the heat losses from the solar storage tank during operation, it was necessary to know the value of the loss coefficient for the tank insulation.

The experimental procedure adopted was as follows.

The tank was filled with hot water. The temperaturesat various positions inside the tank were recorded over a two day period.

No flow occured to or from the tank and the drop in temperatures over periods of constant ambient temperatures were evaluated.

The loss coefficient was then calculated using a mathematical analysis (described in appendix 8.3.ii).

5.2.2. The Loss Coefficients of the Pipes

The technique for determining the loss coefficients for the upriser and downflow pipes was similar to that for the tank.

The pipes were sealed off at their ends so that no flow occured.

The temperatures at both ends of the pipes, and also midway along the downflow pipe, were measured with respect to time.

The loss coefficients were then evaluated mathematically (appendix 8.3.iii).

5.2.3. Thermosyphon Mass Flow Rate

To theoretically calculate the thermosyphon mass flow rate knowing the temperatures throughout the system, it is essential to know the relationship between the pressure and the mass flow rate. This relationship was determined experimentally.

A pump and rotameter were inserted into the thermosyphon flow

circuit at/...

circuit at the collector inlet.

The flow was altered at various temperatures, and the pressure head was read on an inclined water monometer.

The theoretical evaluation of these results (appendix 8.4. i.) enabled the prediction of the thermosyphon mass flow rate.

It was necessary to measure experimentally the rate of thermosyphon flow rate while the solar water heater was in operation.

However, any obstruction in the flow line would prevent flow, as the system operates at extremely low pressures (of the order of 100 N/m^2).

A rotameter was tested. It was inserted in the cold water downflow pipe. The flow was obstructed, and there was insufficient pressure in the system to create continuous flow, (due to the weight of the rotameter float, and the extra bends required in the flow circuit).

An injection system was tried. Using a hypodermic syringe, water-proof coloured ink was injected into the flow line. However, the colour dispersed, in the 25 mm diameter pipe, and by the time it had travelled 0,5 meters it was impossible to evaluate the flow rate.

Another scheme considered was to have a light beam focused on a reflecting disc, mounted in a clear plastic or glass tube, in the flow line. The disc would spin at different speeds for varying flow rates. This could be enumerated by an electronic eye and counter system. The disadvantage lay in the difficulty to produce a disc and bearing system suitable for a 25 mm diameter tube, and the involved circuitry necessary.

Another technique of measuring flow was to use a type of hot wire anamometer. A current is passed through the wire and the water flow causes the wire to be cooled. The amount of cooling is dependent on the flow rate and can be assessed by determining the voltage drop across the wire.

A thermistor was chosen to determine the flow rate, using the

above /....

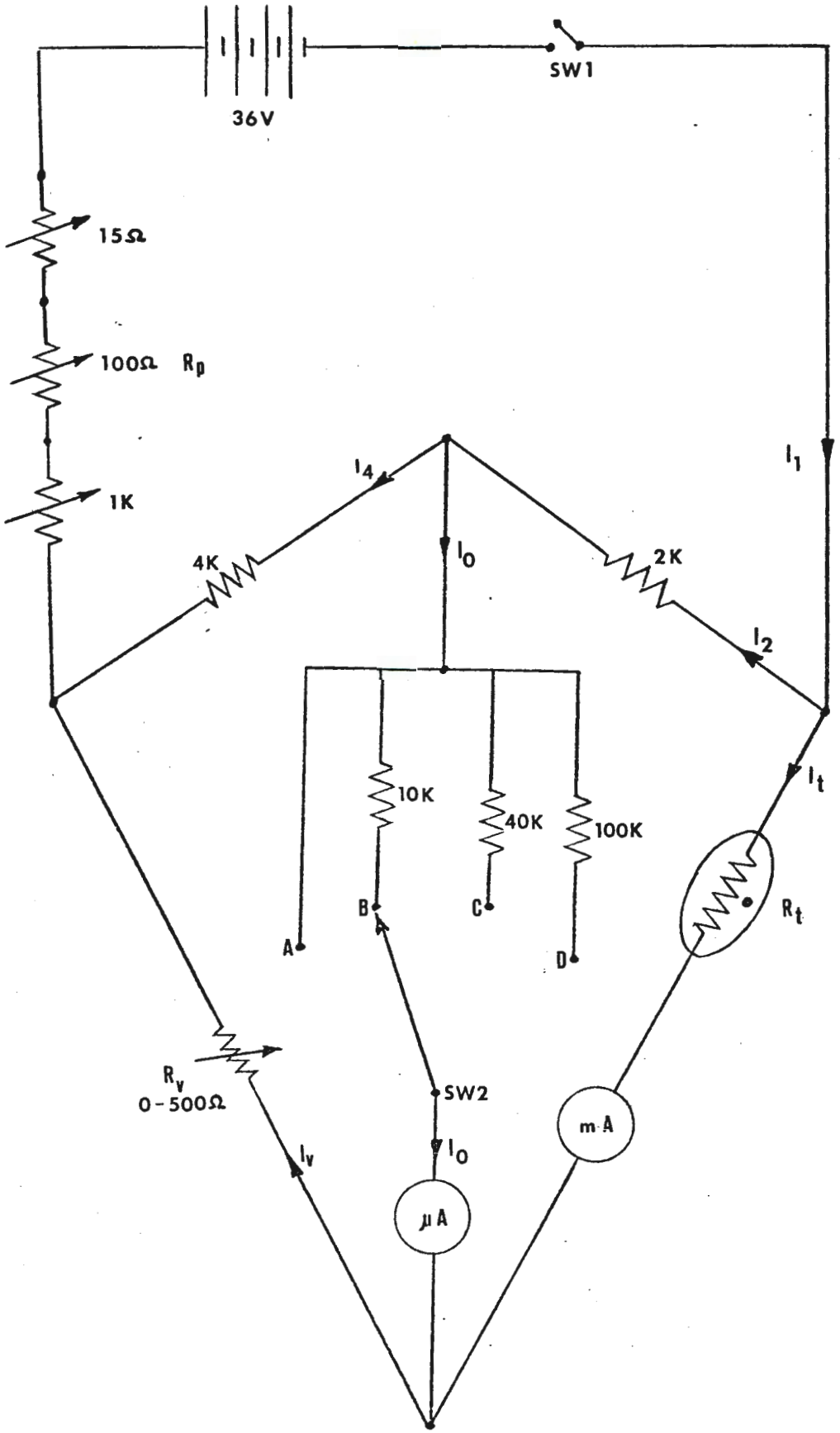

Fig. 5.2.1 Circuit diagram of the thermosyphon mass flow rate apparatus

above principle. It was small enough to be positioned in the flow line without affecting the flow rate.

The thermistor was inserted into the downflow pipe about midway between the tank and the collector (see Fig. 5.1.1.). It was connected to a specially designed electronic circuit (shown in Fig. 5.2.1.). This circuit was designed so that the rate of flow at any temperature could be determined. (Since the temperature of the water in the system continually changes, the water temperature in the downflow pipe changes.) The voltage drop across the thermistor varies differently at different temperatures and hence it was important to know the temperature of the water flowing past the thermistor. A thermometer was inserted into the downflow pipe, next to the thermistor, enabling the temperatures to be read when the flow rates were required.

This system was calibrated in two stages.
(i) At zero flow rates, it was necessary to have the zero reading across the bridge circuit (Fig. 5.2.1.) for varying temperatures. This was achieved by calibrating Rv at varying temperatures T_t, at zero flow with I_o = 0 and I_t = 40mA. (I_t was chosen to be 40mA.)

Over the systems temperature range this current was found to be optimum to heat the thermistor to a high enough temperature, so that cooling of the wire by the water flow could create a sufficiently large voltage drop which could be read off on the bridge circuit . (See graph 8.4.1.).

(ii) At increasing flows I_o was calibrated at varying temperatures I_t, with I_t maintained constantly at 40mA. As the water flows past the thermistor, it is cooled and the resistance (R_t) of the thermistor changes. The current through the thermistor I_t is maintained at 40mA by altering the resistances R_p, hence the voltage across the bridge varies and is registered in the form of a change in the current I_o (see graph 8.4.2.).

The procedure for reading the flow was as follows:-

(a) Read the temperature T_t

(b) /...

(b) Set the value of Rv accordingly (from graph 8.4.1. in appendix 8.4.)

(c) Switch on the circuit and adjust resistance R_p until I_t = 40mA

(d) When the gauges are steady read off the value of I_o (μA).

(e) Find the flow rate $\dot{m}_c$, at the temperature I_t and meter reading I_o, on the calibration chart. (graph 8.4.2. in the appendix 8.4.)

5.2.4. The Solar Water Heater in Operation

Two sets of tests were conducted on the solar water heating system. For both of these sets of tests the angle of tilt of the collector was kept constant, at 44^o from the horizontal, (10^o larger than the latitude angle of Cape Town) simulating a stationary domestic set up for year round performance. The collector was set facing due north.

Test set I was conducted during December 1976 and January 1977. The aim of this set of tests was to simulate various domestic draw off times and quantities.

Draw off quantities varied from 100 to 200 litres and the times of draw off were set to simulate mainly bathing, showering and washing in the mornings and evenings. A few tests also included draw offs set for mid-day, to simulate washing of utensils for lunch time meals and mid-morning to account for hot water required to wash clothes.

The hot water draw off flow rates were low (below 0,035 Kg/s). This avoided the mixing of the cold incoming water with the warm tank water. The minimum time setting period on the time clock was 15 minutes, which meant that a flow rate had to be set according to the quantity of draw off required. (For a 15 minute draw off flow rates were low, which suited the type of simulation required.

The solar water heater was in continual operation and readings were taken from 07h00, when the collector water temperature was just beginning to rise, until 19h00 at which time the sun had disappeared behind the mountain to the west of the test site.

Temperatures /...

Temperatures and radiation were recorded continually during the day while wind velocities were read at half hourly intervals and thermosyphon mass flow rates were read at the beginning and end of draw off periods and at half hourly intervals during non draw off times.

Test set II : This set of tests were conducted during autumn, in April and May 1977; to observe the effect of high draw off flow rates on the experimental and theoretical systems; to compare these results; to examine how the times when water was drawn off would influence the thermal performance of the system; and to see how these test results differed from test set I results.

The draw off quantities varied from 90 to 220 litres. Draw off flows were high (up to 0,27 litres per second). This meant that draw off periods were required to be short: in fact too short to use the time clock. A gate valve was therefore operated manually (as would be the case in a domestic household). The draw off times and the quantities of water drawn off were read. Draw off times were not chosen to particularly simulate domestic draw offs but more to evaluate how different times would alter the performance of the system.

The system was operating continuously. Measurements began at 07h30 at sunrise till sunset at about 18h00. (The sun actually was hidden behind the mountain from 16h30.)

Temperatures and radiations were recorded continually. The wind velocity was read off every half hour, while the thermosyphon flow rate was read during and just after draw offs and at half hourly intervals at non draw off periods.

Ten days of results for tests I and II are presented in the following chapter, with detailed graphs of the thermal performance, predicted and measured, for a day from test set I and a day from test set II.

CHAPTER 6

RESULTS

6.1. AMBIENT CONDITIONS

All the days for test set I were clear, cloudless days. The ambient conditions were similar for all these days. Graph 6.I. shows a typical set of curves of radiation, ambient temperature and wind velocity (for the 24 December 1977).

The radiation falling on the collector increased steadily from sunrise until 12h30 when it reached a peak of about 900 W/m^2. It then decreased uniformly as the sun descended.

The total radiation for the day varied slightly for each of the five days, probably due to the varying pollution and atmospheric constituents on each day. The average total radiation for one day was 13,32 kWh.

The ambient temperature curves all had the same shape, increasing slowly and consistenly until about 15h00, and then decreasing until sunset when the temperature returned to approximately that at sunrise.

The wind velocities and directions were haphazard and no definite pattern was observed.

The ambient conditions for test set II varied. Some days were cloudy or partially cloudy, some days clear. Large fluctuations in radiation occured during cloudy periods, but the overall shapes of the radiation and ambient temperature curves were similar to those presented for 24/12/76. Radiation obviously only began rising slightly later and returned to zero earlier due to seasonal fluctuation in the times of sunrise and sunset. Ambient temperatures were also generally lower than for test set I, while wind velocities were once again haphazard. (Details of radiation, ambient temperature and wind velocity for 10/5/77 appear in appendix 8.9. graph 8.9.7.)

6.2./....

Graph 6.1 Solar insolation,ambient temperature and wind velocity for 24.12.76

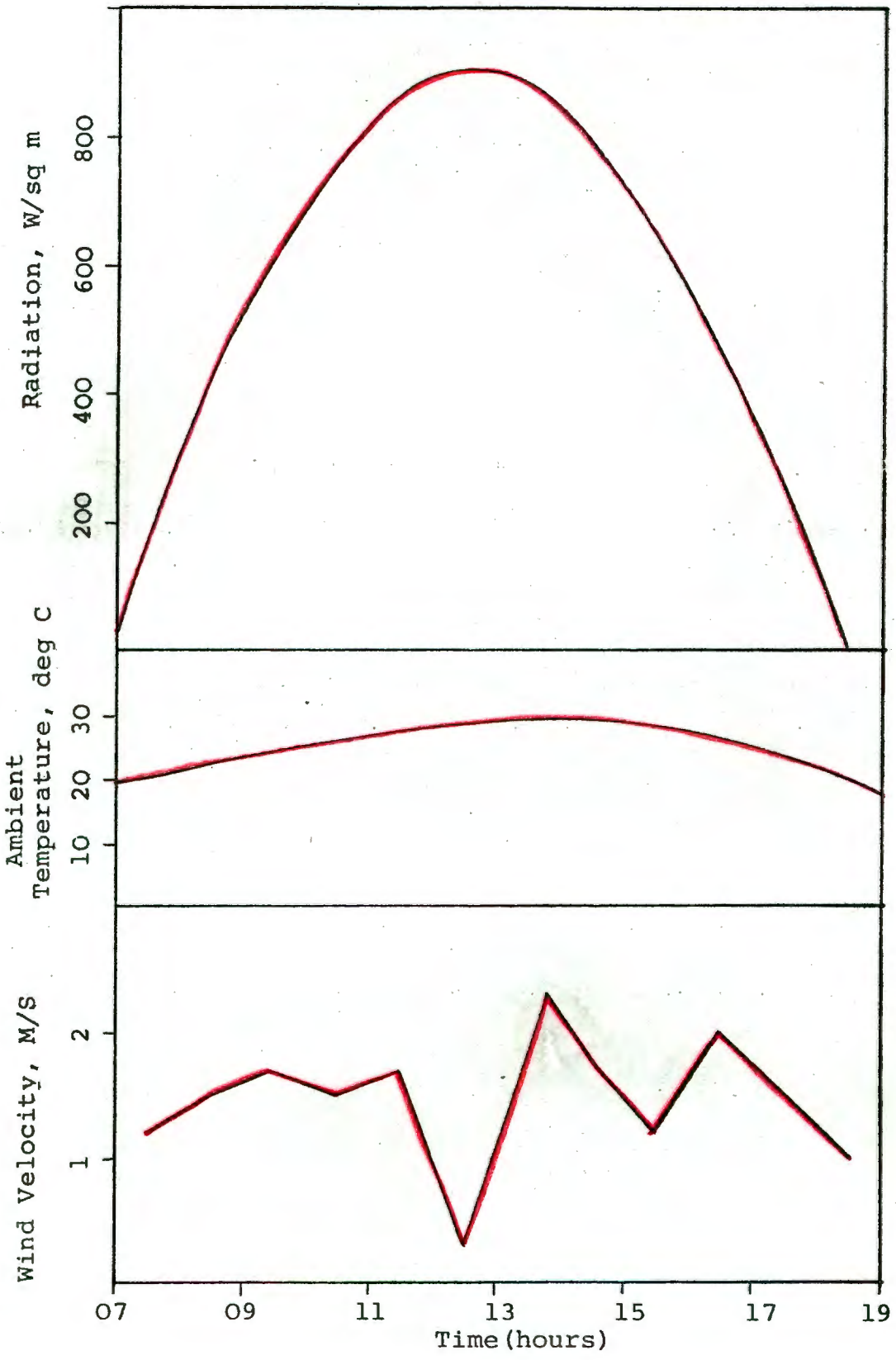

6.2. DRAW OFF

The draw off quantities and times varied from day to day and for the two sets of tests as described in section 5.2.2.

Details of exact draw off times and quantities are given in the appendix 8.9.1.

6.3. THERMAL PERFORMANCE

6.3.1. Experimental Performance

The collector temperatures (collector inlet, outlet and mean plate temperatures), solar storage tank temperatures, and thermosyphon mass flow rates were measured experimentally and graphs were drawn.

A typical set of curves (for 24/12/76) is shown in graph 6.2., together with the draw off flow rates for that day.

The collector temperatures increased from just after sunrise, when the radiation was sufficiently high, till about 15h30. The ambient temperature then began to decrease while the radiation was steadily dropping. The collector therefore began losing heat to its surroundings and its temperature declined fairly rapidly.

A sharp decrease in collector temperatures occured at 13h00, at which time hot water was drawn off while cold water was introduced into the system. The collecter temperatures began to increase rapidly again as soon as the draw off was stopped (at 13h15).

The tank temperatures (which were initially still quite high from the previous day) dropped sharply as water was drawn off for early morning washing. As the water began to circulate from the collecter the tank temperatures increased until about 15h30 after which they remained constant.

During the lunch hour draw off, the bottom tank section temperature decreased sharply while cold water was introduced into this section of the tank. The upper tank section temperatures remained constant during this draw off period since only 21 litres were drawn off (enough to fill only the bottom tank section.

The thermosyphon /...

Graph 6.2 Experimental results for 24.12.76

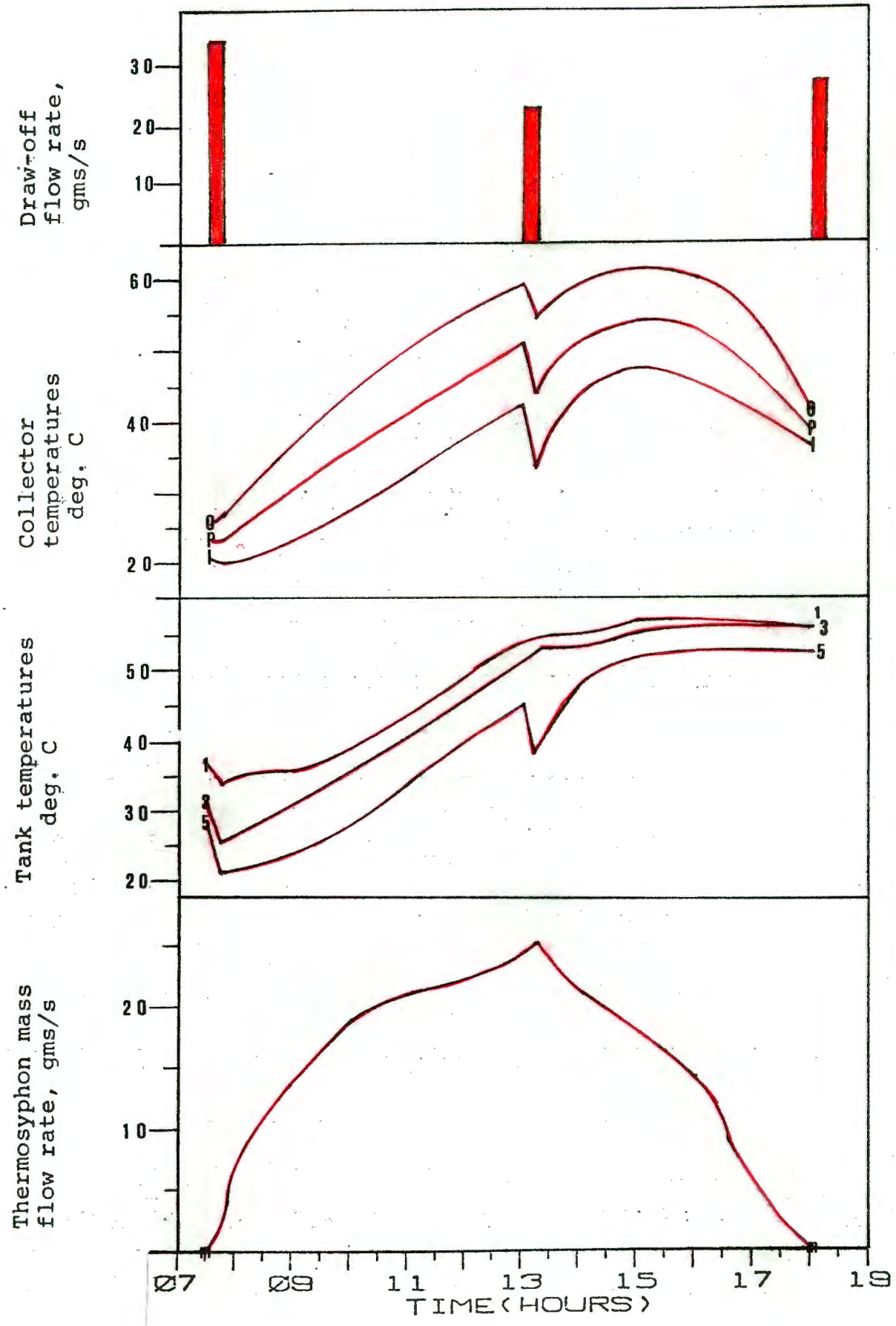

The thermosyphon mass flow rate increased from just after sunrise until 13h00, and then decreased to zero at about an hour and a half before sunset (at 18h00).

At 07h30, 31 litres of hot water was drawn off at a flow rate of 0,0344 kg/s, for 15 minutes.

The water in the tank, which was still warm from the previous day, began to drop in temperature as cold water was introduced. This temperature difference caused a mass flow rate. The collector inlet temperature therefore decreased slightly and then began to rise, while the outlet temperature increased immediately.

The radiation and ambient temperature increased causing the collector temperature to continually increase. Hence the thermo-syphon flow increased and the warm water circulating from the collector entered the tank and raised its temperature.

The process continued until 13h00 when hot water was again drawn off.

Cold water entering the bottom of the storage tank, at about $24^{o}C$ immediately reduced the temperature of the water in the lower part of the tank. Consequently there was an increase in mass flow rate (due to the sudden large difference in densities of water in the system), and as this water moved down the pipe to the collector, the collector temperatures suddenly decreased.

Only 21 litres of water was draw off between 13h00 and 13h15 and therefore the upper section temperatures of the tank remained constant.

At 13h15 the draw off stopped. Since the radiation and ambient temperature were still high, the collector immediately heated up. The cold water at the bottom of the tank moved down into the collector and was replaced by warmer water from the upper parts of the tank. The hot water from the collector outlet circulated into the top of the tank and the system temperatures began to even out. The difference in temperature throughout the system grew smaller and hence the circulation flow rate decreased.

The system/...

The system temperatures reached a maximum at about 15h30 when the ambient temperature was at its highest. Thereafter the collector temperatures began to drop and the flow decreased rapidly to zero.

The tank temperatures remained approximately constant, at their maximum, after 15h30 losing a small quantity of heat through the tank insulation.

6.3.2. Mathematical Predictions

Various theoretical simulation models were tested (see appendix 8.9.2.). The results for the 24/12/76 (shown in graph 6.3.) are considered to be representative of the thermal performance predictions for a single day. (This prediction model was a 5-section tank model, Solasim 5B, the details of which appear in appendix 8.9.2.)

The initial experimental collector and tank temperatures were used in the computer program, and draw off times and flow rates were exactly the same as for the experiment.

The collector temperatures increased until 13h00 when a dip occured during the lunchtime draw off of hot water. They began increasing rapidly again until about 15h30 when they reached their maximum, and then decreased.

The tank temperatures initially decreased as water was drawn off (from 07h30 to 07h45) and then increased until 13h00. Another draw off occured during which time the tank bottom section temperature sharply decreased while the tank mid-sections remained at approximately constant temperature and the top tank section temperature continued to increase (since the inflowing water from the collector was still at a higher temperature). At 13h15 draw off stopped. The tank bottom and mid-section temperatures began to increase. However, the collector outlet temperature had dropped to below the tank top section temperature and therefore the tank top section temperature began to decrease slowly. By 13h45 the collector outlet was once again at a higher temperature than the tank and the tank top section temperatures began to rise.

At 16h00 /....

Graph 6.3 Theoretically predicted results for 24.12.76

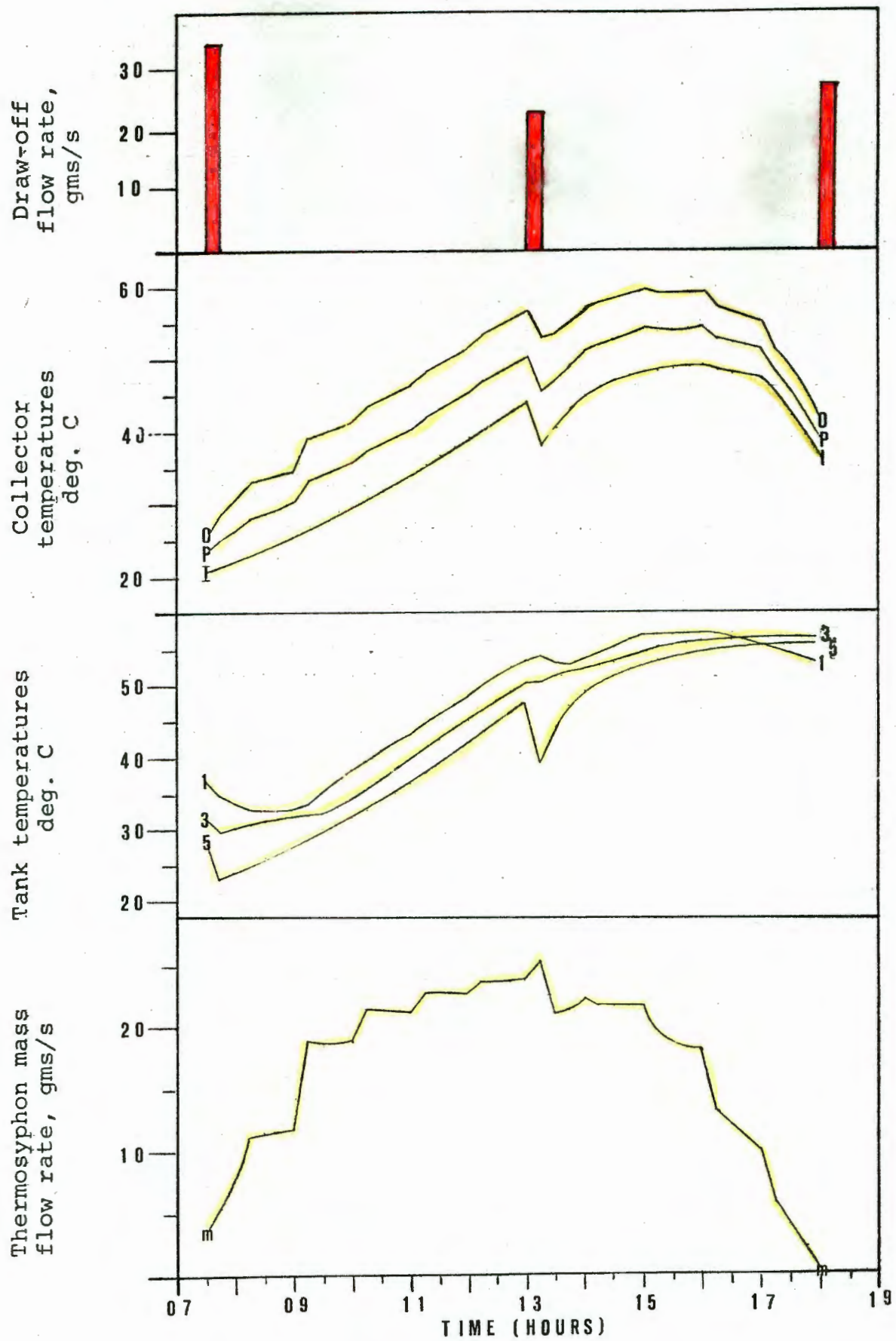

At 16h00 the collector temperature, decreasing rapidly, fell below the tank temperatures. The top tank section temperature began to decrease. Since convection in the tank was not considered in the mathematical model, the decreasing temperature in the tank top section did not affect the temperatures in the sections below. The tank top section temperature therefore dropped below the temperatures in the sections below. (To be referred to from now on as a "cross over" effect.)

The thermosyphon flow rate had already begun at the start of the program (07h30) and increased until 13h15 and then decreased to zero at 18h00. Stepwise variations in mass flow rate occured, which coincided with the stepwise input of radiation and ambient temperature into the program.

A sudden decrease in flow rate occured at 13h15 when the tank top section temperature began dropping, decreasing the system temperature difference and hence the flow rate. This was followed by an increase in flow from 13h30 to 14h00 when the system temperature difference increased.

The daily efficiencies of the solar water heating system , η solar are shown in table 6.1.

Test Set	Date	η solar (%)	
		experimental	theoretical
I	20/12/76	32,2	31,5
	21/12/76	34,9	35,2
	22/12/76	20,4	19,4
	23/12/76	36,0	36,4
	24/12/76	29,0	26,6
II	29/4/77	40,3	41,3
	30/4/77	26,7	26,4
	5/5/77	25,4	22,4
	7/5/77	44,5	42,8
	10/5/77	37,0	36,8

Table 6.1. Daily efficiencies for 10 tests

There were /...

These were calculated by determining the ratio of heat used (in the total water drawn off for the day), to the total radiation falling on the collector for the day.

The large variation in daily efficiencies was mainly due to variations in water draw off times and quantities, and ambient conditions.

The daily efficiences were well predicted by the mathematical model with a maximum deviation of 3% from the experimental values.

CHAPTER 7

DISCUSSION AND CONCLUSIONS

Having measured the actual results obtained during the experiment and having made predictions of the thermal performance of the solar water heating system using the computer simulation model, these experimental and predicted results were then compared.

7.1. AMBIENT CONDITIONS

The measured conditions for each day were fed into the computer program as follows :

The radiation, ambient temperature and wind velocity measurements read during the experiment were averaged out over hourly and during draw off periods. These average values were then fed into the computer program, so that they changed in a stepwise manner.

7.2. TEST SET I

A comparison of theoretically predicted and experimental results for a typical day (24 December) is presented in graph 7.2.1. and discussed here.

The collector mean plate temperature was well predicted, with slight discrepancies occuring before 10h00 and after 15h30. The collector outlet temperature was predicted to be lower than measured values during the main insolation period while the collector inlet temperature was predicted to be higher than the experimental values.

The tank top and mid-section temperatures were well predicted for most of the day while the bottom section temperature was predicted slightly higher than measured values.

The thermosyphon mass flow rate was fairly well predicted but tended to be slightly above experimental flow rates.

At 07h30 thermosyphon flow had theoretically already begun while

the measured /...

Graph 7.2.1 Experimental and theoretical results for 24.12.76

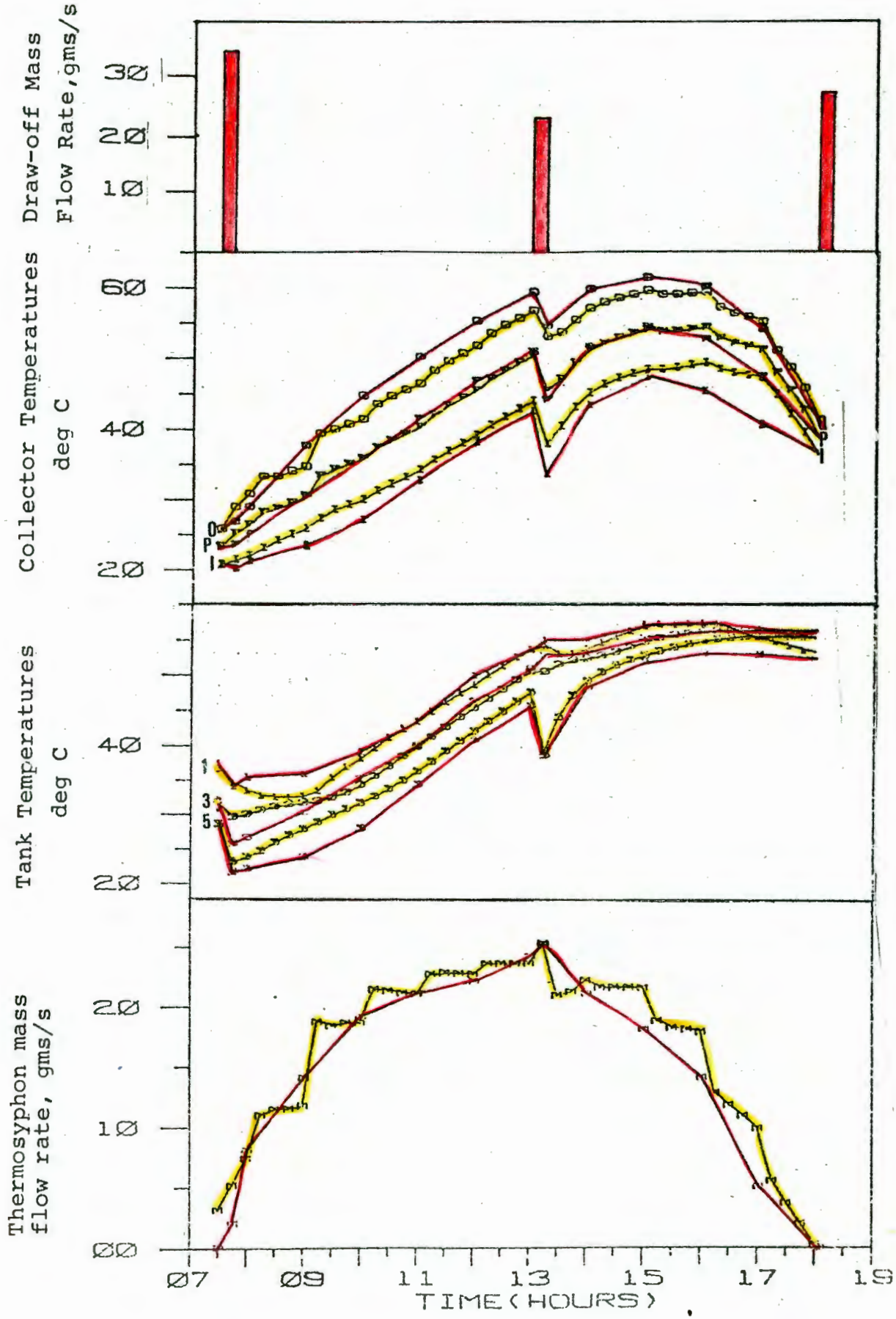

the measured values indicated zero flow. This discrepancy occured since theoretically the temperature differences in the system indicated that flow should have taken place, but to have begun the actual circulation of water a slightly larger temperature difference was required to develop sufficient pressure to overcome the initial static inertia.

The temperature of the water in the tank bottom section was higher than that in the collector at 07h30. Since flow was theoretically taking place at this time the warmer tank water entering the collector increased the predicted collector temperatures (above the experimental values). The cold water entering the tank during the 07h30 to 07h45 draw off reduced tank temperatures. The predicted temperatures did not drop as low as the experimental mid and bottom tank section temperatures since the experimental flow was lower than the predicted flow which at this time was circulating warmer water from the upper sections to the lower tank sections.

As soon as the draw off stopped at 07h45 the bottom and mid tank section temperatures increased due to the circulation of warmer water from the upper tank sections. However, the predicted top section temperature dropped, since colder collector outlet water was flowing in, while the experimental top section temperature rose. This increase was due to the fact that experimentally the temperature of this section was determined by using equation 8.6.1. (see appendix 8.6.).

$$\text{i.e. } T_{s1} = T_C + (T_D - T_C)\ 116/200$$

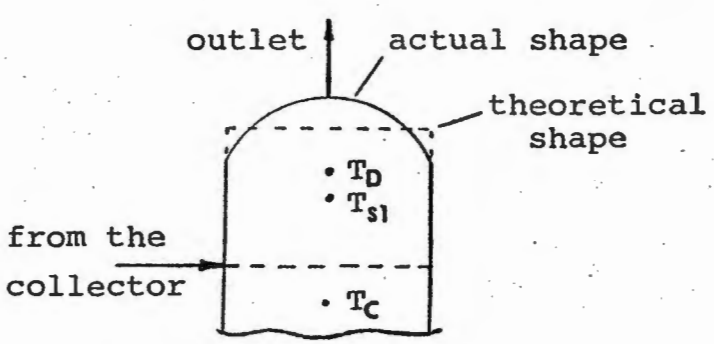

Fig. 7.2.1. Upper Tank Section

From /....

From Fig. 7.2.1. the experimental temperature of the top section T_{s1} was the temperature at the mid point of this section. However the portion of water above point T_{s1} was at a higher temperature than T_{s1} and would therefore tend to increase the temperature T_{s1}.

Throughout the day the bottom tank section temperature was predicted to be higher than experimentally measured. In the theoretical model convection in the tank was not considered. Hence, experimentally the coldest tank water was continually being convected to the bottom of the tank and remained there since the outlet pipe to the collector was slightly above the lowest part of the tank (see Fig. 7.2.2.).

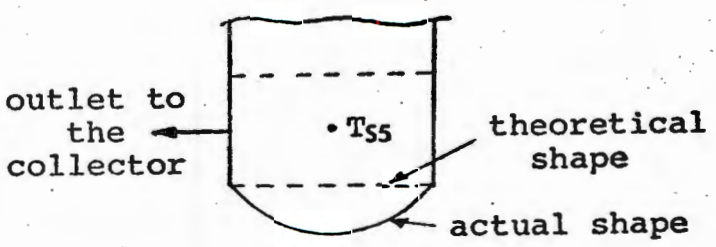

Fig. 7.2.2. Lower Tank Section

The colder water below T_{s5} experimentally reduced the temperature of T_{s5} while theoretically its temperature was only affected by the warmer water from the upper tank sections, and heat losses to the ambient air.

Since the tank bottom section temperature was predicted slightly high, this had a similar affect on the predicted collector inlet temperature, which was also predicted to be slightly above the actual values throughout the day.

After 16h00 the discrepancy between predicted and experimental tank bottom section temperature increased causing a larger discrepancy in collector inlet temperature to occur and thus causing the prediction of the mean plate temperature to be high. This "cross over" effect in predicted tank temperatures is explained in section 6.3.2.

in the /...

(in the previous chapter).

The collector outlet temperature was predicted to be lower than in the experiment, during the main insolation period.

Mean plate temperatures were experimentally assumed to be mid way between collectorinlet and outlet temperatures, and determined using equation 4.1.1. i.e. $T_p = (T_{ci} + T_{co})/2$. The mean plate temperatures were well predicted until 16h00. The theoretical model used the mean plate temperature T_p and the collector inlet temperature T_{ci} to determine the collector outlet temperature T_{co}, i.e. $T_{co} = 2T_p - T_{ci}$ Since the collector inlet temperatures were predicted slightly high and the mean plate temperatures were correctly predicted, the collector outlet temperatures were predicted slightly low.

The thermosyphon flow rates were theoretically determined from the temperatures in the system (see section 4.4 and 8.4. for detailed explanation). The discrepancies between the predicted and experimental flows were a direct result of any discrepancies occuring in the predicted tank and collector temperatures.

Discrepancies could in addition be imputed to the fact that experimental flows were measured only at an 81% level of confidence.

7.3. *TEST SET II*

The previous test set simulated domestic conditions with draw off times and quantities. However, to achieve automatic simulation with the equipment available it was necessary to have 15 minute draw off periods using slow draw off flow rates. This also avoided the occurrence of "mixing" in the solar storage tank during draw offs, allowing the system to be mathematically modelled and the thermal performance to be predicted.

To simulate domestic conditions more accurately it was necessary to draw off hot water quickly and over short periods. This set of tests was therefore conducted to observe the effect of high draw off flow rates. The times and quantities of hot water drawn off were varied

from day /...

from day to day. Theoretical predictions were made of the system performance on these days and the results of one day (10 May 1977) super-imposed on the experimental results are presented in graph 7.3.1. and discussed here. (Detailed curves of the collector and tank temperatures appear in graphs 7.3.2. and 7.3.3. respectively.)

The comparison of predicted and experimental collector temperatures shows the predicted temperatures to become further displaced from the measured values, after each draw off period.

A similar effect occured in the tank.

Experimentally "mixing" occured in the tank during draw offs whereas this was not considered in the mathematical model.

At 07h55 when water was drawn off at a mass flow rate of 0,163 Kg/s, cold water at 17,1^{o}C was introduced into the tank. This mixed with the warm tank water, decreasing the temperature of the bottom half of the tank's water (the lower three sections of the tank) to below 25^{o}C. However, in the predicted model the bottom section temperature dropped considerably while the upper section's temperatures decreased, but not as quickly.

The prediction temperatures appeared to be quite accurate until the 12h00 draw off of 50 litres at 0,168 Kg/s.

Once again mixing occured in the experiment. Predicted tank temperatures were higher than experimental values, and hence in the collector as well. Until the next draw off at 14h40 temperatures continued to be predicted too high and this was accentuated during this next draw off period.

A "cross over" of tank temperatures then occured in the predicted model (similar to what happened in the late afternoon for test set I) The predicted flow at about 15h30 was much larger than the measured flow, while the collector outlet temperature had fallen below that at the top of the tank. Since no convection was considered in the tank model the colder water flowing in from the collector did not move to the bottom of the tank but reduced the temperature of this

top section /...

GRAPH 7.3.2

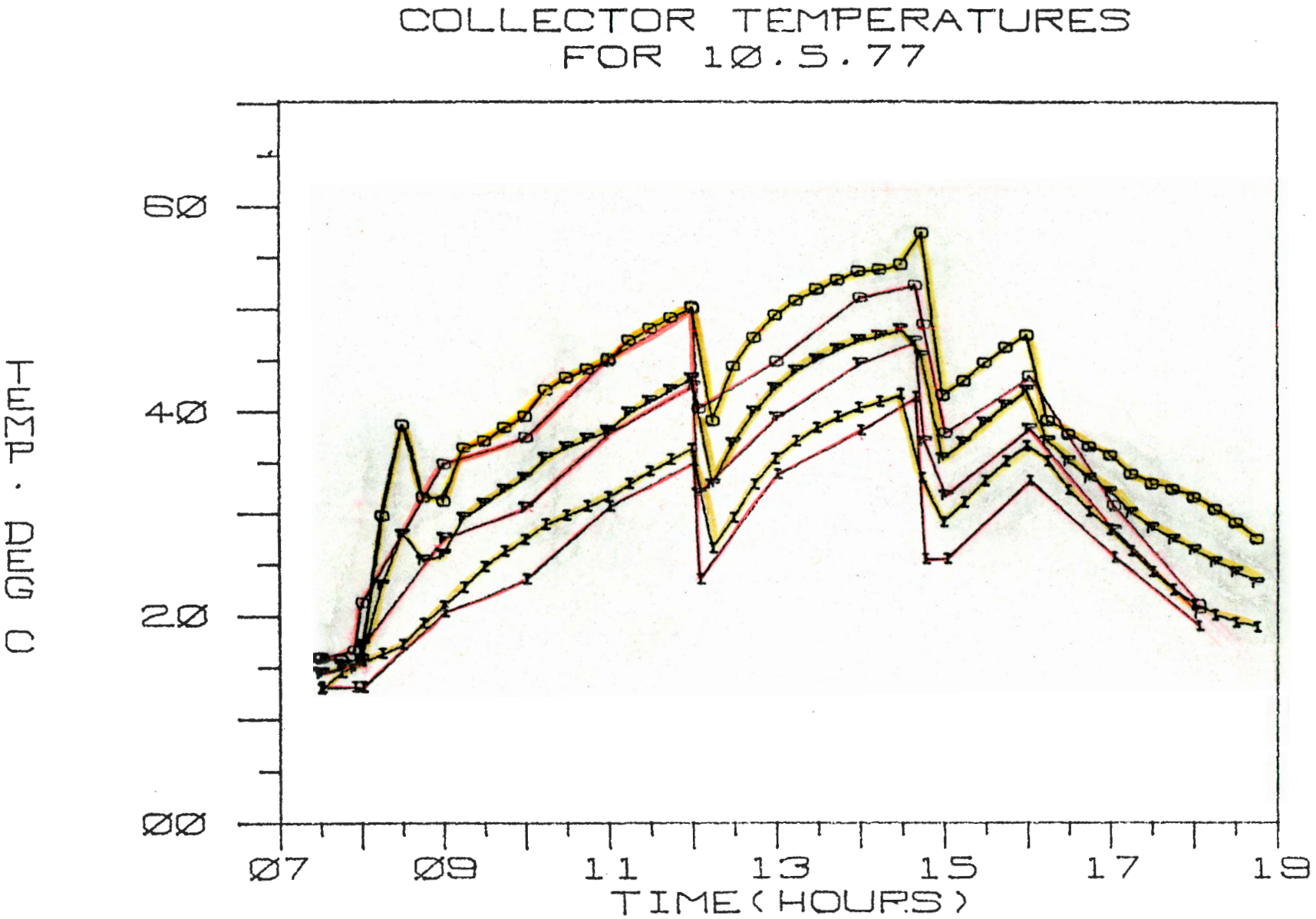
COLLECTOR TEMPERATURES
FOR 10.5.77
TEMP. DEG C
00
20
40
60
07
09
11
13
15
17
19
TIME(HOURS)

GRAPH 7.3.3

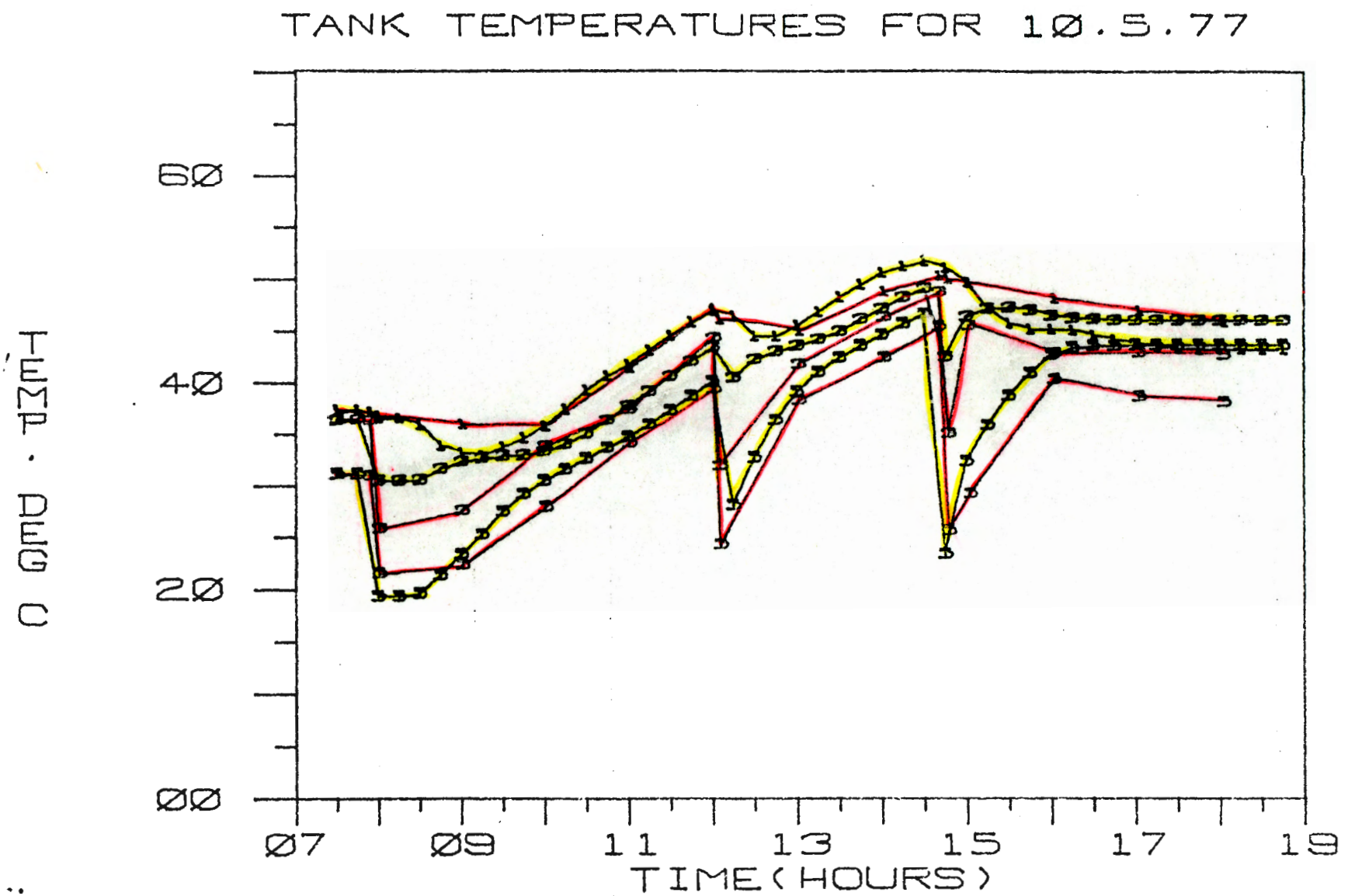
TANK TEMPERATURES FOR 10.5.77
60
40
20
00
TEMP. DEG C
07
09
11
13
15
17
19
TIME(HOURS)

top section to below that of the tank lower sections.

Two points on the predicted collector temperature graph appear to be out of place, at 08h30 and 14h45. These will be explained in relation to the thermosyphon mass flow rate.

The experimental flow increased from 07h30 until about 11h00 with increase in radiation, temperatures and difference in system temperatures. It remained more or less constant until the 14h40 draw off when it suddenly increased due to the introduction of higher density cold water into the tank. The flow then decreased rapidly to zero at 17h30. This decrease was due to the fall off in collector temperatures after 14h45. The collector began to regain heat between 15h00 and 16h00 but the radiation was too low at that time to raise the outlet temperature above the top tank section temperature. In fact, the mean plate temperature was lower than the mean tank temperature hence flow was almost non existent.

The predicted flows were similar to experimental flows until 14h40, after which they superceded the latter. Predicted thermosyphon flow only began after 08h15. Due to the no flow condition prior to this time, the predicted collector outlet water heated up to well above the measured temperatures. This created sufficient temperature difference through the system to generate flow. The circulating cold water from the collector inlet then had the effect of reducing the predicted collector outlet temperature to approximately the same value as measured in the experiment. Once the predicted collector outlet temperature had dropped reducing the system temperature difference again (at 08h45), the predicted mass flow rate dropped slightly (08h45 to 09h00).

At 09h00 the average hourly radiation was increased and so the predicted collector temperatures and flow rates began rising. The flow increased sharply with the higher radiation, and then remained almost constant for the next hour, following the step-wise input of average hourly radiation.

At the 12h00 draw off the collector temperatures dropped sharply,

the outlet /...

the outlet temperature falling below that at the top of the tank. Accordingly a slight dip occured in the predicted flow rate curve, followed by a slight increase as the collector once again gained heat.

At 14h40 51 litres of hot water was drawn off for five minutes. The following results occured in the computer simulation . The cold water reduced the temperature of the lower half of the tank, the bottom section temperature decreasing by 22°C. By 14h40 (when draw off was stopped) the collector inlet temperature had decreased by 8°C while the mean plate temperature had only dropped by 3°C. Since the collector outlet temperature T_{co} was calculated from the inlet inlet and mean plate temperatures, T_{ci} and T_p respectively ($T_{co} = 2T_p - T_c$), the outlet temperature increased. This created a sudden surge in flow rate which circulated the cold water from the bottom of the tank through the entire collector and into the top section of the tank. The collector temperatures decreased swiftly until 15h00 to below the mean tank temperature, promptly decelerating the flow.

From 15h00 to 16h00 the predicted flow remained constant while the collector was struggling to regain its heat. However, by 16h00 the collector began to lose heat to the cooling environment and the flows plummeted to zero by 17h30.

7.4. EFFICIENCY

Instantaneous collector efficiencies were calculated from equation (3.3.33.) which gives the ratio of useful heat in the collector at that time instant to the radiation falling on the collector at that instant. However, these calculations were invalid since the basic assumption of steady state conditions, upon which the efficiency equation was formulated, was incorrect. Unsteady conditions were created during draw offs and for about an hour afterwards. There was also a time lapse between the radiation falling on the collector and the corresponding effect it had on collector temperatures and thermosyphon flows. Therefore, instantaneous collector efficiencies could not be assessed for this solar water heating system. However, daily efficiencies were calculated. The experi-

mental /...

mental and theoretically predicted daily efficiencies for 5 days of test I and 5 days of test II are presented in table 6.1.

These efficiencies were well predicted by the theoretical model. The large fluctuations in efficiency indicate that there were many variables influencing the performance of the collector. The main factors being the radiation, ambient temperature and water draw off quantity and times.

Due to the simultaneous influence of all these factors it was difficult to assess their exact individual effects on the efficiency. However, a general indication was evident and the following evaluations were made :

(i) The efficiency increased with increasing quantity of water drawn off, up to 200 litres. The optimum draw off was between 150 and 200 litres.

(ii) Draw offs during high radiation periods only affected the system temperatures for a while and the temperatures were regained rapidly. The efficiencies increased for larger and more draw offs during the main insolation periods.

(iii) The rate of draw off did not have any effect on the efficiencies.

The amount of electrical energy required, Q_{elec}, to maintain the geyser water at a preset temperature ($60^{o}C$) fluctuated according to the water draw off quantity and times, the radiation and the ambient temperature.

Without the solar heating system, Q_{elec} was a function of only water draw off, quantity and mains cold water inlet temperature, T_{in} (which on an average was about $21^{o}C$ in summer and $17^{o}C$ in autumn).

Q_{elec} was found to be about 13KWh/day for a draw off of 152 litres per day (draw off set C.) without solar water heating, and varied between 3 and 5 KWh/day with solar water heating, on clear days. This presented an 8 to 10 KWh/day savings on sunny days.

7.5. /...

7.5. ACCURACY

The accuracy of the experimental measurements was as follows:

(i) The temperature measurement in the system, taking into account thermocouple calibration (accurate to $0,2^{o}C$) and a chart recorder error of 0,5%, was accurate to 1%.

(ii) The radiation, using the solarimeter (accurate to 1%) and chart recorder, was measured with a 1,5% accuracy.

(iii) The ambient temperature was measured using a thermocouple in the instrument box, a few feet away from the collector and below the wooden hut where the storage tanks were mounted. This meant that the actual ambient temperature immediately around the collector, that around the storage tanks and that measured in the instrument box, may have differed by a few degrees. A thermocouple was mounted in the hut next to the tanks and found to have a maximum of $5^{o}C$ difference, and an average of $0,5^{o}C$ difference, to that measuring ambient temperature in the instrument box. This possible error in ambient temperature contributed slightly to the errors in the thermal predictions.

(iv) The measurement of thermosyphon mass flow rate had large errors (up to 19%). The errors were accumulative, and appeared in : the calibration of R_v with temperature (see section 5.2.3., 3% error); the reading of thermistor temperature, I_t (2% error); the setting of resistance R_v (2% error); the accuracy with which I_t could be maintained at 40mA (2% error); the fluctuation of the gauge reading of I_o, due to temperature fluctuations (5% error); and the calibration of I_o with mass flow rate $\dot{m}_c$ at various temperatures (5% error). It was found, however, that with experience of working with the system the assessment of $\dot{m}_c$ became more accurate.

(v) The water draw off quantity was measured using a water meter capable of reading to 0,5 litres. The draw off times were set on a time clock for test I with an accuracy of 1%. The draw off flow rates were then calculated, having a maximum possible error of 2%.

(vi) The electrical energy consumed by the electrical geyser was measured on a Kilowatt hour meter with a 0,2% accuracy.

7.6. /...

7.6. CONCLUSIONS

The theoretical solar water heater simulation model presented, predicted the thermal performance accurately for low draw off flow rates, and fairly accurately at high draw off flow rates.

System temperatures, mass flow rates and daily efficiencies could be closely predicted for similarly designed solarwater heating systems, in any place, using this computer simulation model with the necessary modifications.

Instantaneous efficiencies were not predictable using the mass flow rates and temperatures across the collector.

The solar heating system daily efficiency varied with draw off times and quantities, ambient temperatures and radiation (from 20% to 45%).

Although mass flow rates correlated well in the graphs presented, it is not recommended that a thermistor and circuit for thermosyphon flow measurement be used due to the inaccuracy, the experience required and the problems encountered in designing, fitting, calibrating and operating this system.

Possible improvements could be made on the theoretical model by :

(i) Including the effect of convection currents in the tank.

(ii) Feeding in data in half or quarter hourly intervals instead of hourly intervals.

(iii) Increasing the number of sections in the tank.

(iv) Interpolating the data fed in, over hourly intervals instead of using single average values for each hour.

APPENDIX

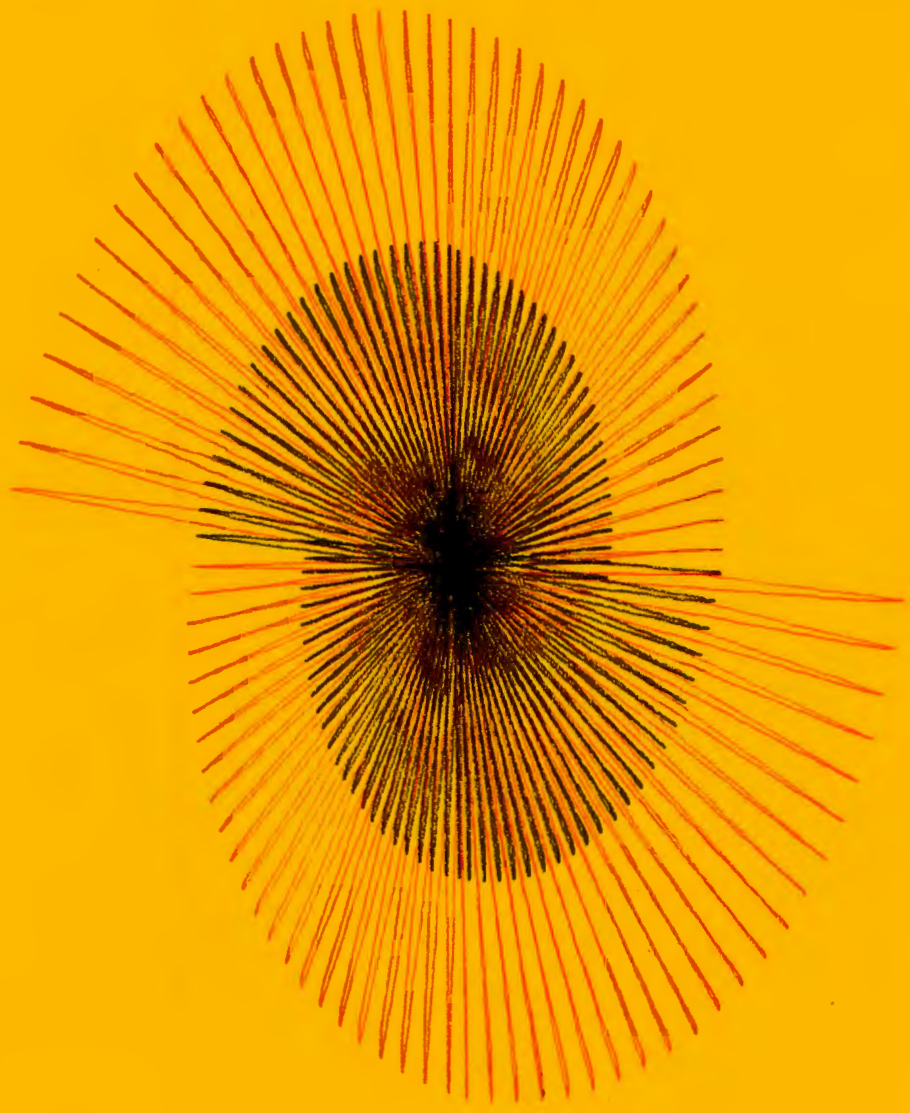

APPENDIX

A few specimen calculations and theoretical elaborations are given for further clarification and verification of the theory presented.

8.1. ANGLE OF INCIDENCE

The latitude of Cape Town L = 34^{o}S (i.e. - 34)

The angle of tilt of the collector s = 44^{o} (i.e. - 44)

The standard and local meridians $L_{st} = 30^{o}E$, $L_{loc} = 19,5^{o}E$

For the 24 December, the day of the year n = 358

From (3.3.2.) declination $\delta = 23,45 \sin \left[360 \ \frac{284 + 358}{365}\right]$

$= -13,25^{o}$

The equation of time E = 0,3 mins from Fig. 3.2.3.

e.g. at 08h00 $T_{st} = 8$

equation (3.2.2.) $T = 8 + (0,3 + 46)/60$

$= 0846$ hours

$= 8,77$ hours

equation (3.2.3.) $w = (12 - 8,77) \times 15$

$= 48,50^{o}$

equation (3.2.1.) $\cos \theta_T = \cos \ 10^{o} \cos (-13,25) \cos (48,5) + \sin (10) \sin (-13,25)$

i.e. $\theta_T = 53,52^{o}$

8.2. TRANSMITTANCE - ABSORPTANCE PRODUCT

The refractive index for air $n_1 = 1$

for the perspex cover $n_2 = 1,25$

According to the specifications p = 0,04

To check this at normal incidence $\theta = 0^{o}$

(3.4.5.) $$p\ (0^{o}) = \left[\frac{n_1 - n_2}{n_1 + n_2}\right]^2$$

At $\theta_1 = 53{,}52^0$

equa. (3.3.4.) gives $\sin \theta_2 = \frac{n_1}{n_2} \sin \theta_1$

i.e. $\theta_2 = 40{,}66^0$

then (3.3.3.) $\rho(\theta_1) = \frac{1}{2} \left[\frac{\sin^2(\theta_2 - \theta_2)}{\sin^2(\theta_2 + \theta_1)} + \frac{\tan^2(\theta_2 - \theta_1)}{\tan^2(\theta_2 + \theta_1)} \right]$

$\rho(\theta_1) = 0{,}02$

from (3.3.6.) $\tau_r(\theta_1) = \left(\frac{1 - \rho}{1 + \rho} \right)^3$

$\tau_r(\theta_1) = 0{,}78$

The cover thickness $t_c = 3$ mm
and the extinction coefficient for perspex $K = 0{,}2/\text{in}$
$= 0{,}00787/\text{mm}$

then $Kt_c = 0{,}02361$

from (3.3.7.) $\tau_a(\theta_1) = e^{-Kt_c/\cos\theta_2}$

$= \underline{0{,}97}$

and $\tau(\theta) = \tau_r(\theta)\, \tau_a(\theta)$

$= \underline{0{,}76}$

$\rho_d = 1 - \tau_r$

$= \underline{0{,}22}$

For the plate $\alpha = 0{,}92$
then (3.3.9.) gives $(\tau\alpha) = \frac{\tau . \alpha}{1-(1 - \alpha)\, \rho_d}$

$= \underline{0{,}71}$

8.3. /...

8.3. LOSS COEFFICIENTS

(i) Collector

The polyurethane insulation of the collector has a heat rate of

$$U_b = 1 \text{ W/m}^2\,^{o}\text{C} \quad \text{(from the collector specifications)}$$

and thickness $t_i = 25$ mm

(3.4.11.) gives $U_b = k/t_i$

$\therefore$ the thermal conductivity $k = 0{,}025$ W/m ^{o}C

and

$$Ue = \frac{k}{t_i} \times \frac{t \times \text{perimeter}}{A_c}$$

$$= \underline{0{,}0919} \text{ W/m2 } ^{o}\text{C}$$

For natural convection between two plates inlined at 45^{o} to the horizontal $Nu = 0{,}093\ (Gr)^{0,310}$ from (3.3.16).

From the physical parameters of the collector and at 08h00 on 24/12/76

mean plate temperature $T_p = 25^{o}$C

$g = 9{,}81$ m/s^2

$\ell = 0{,}015$ m

$\nu = 9{,}022 \times 10^{-7}$ m^2/s, $\rho = 997$ kg/m^3

$\mu = 890 \times 10^{6}$ kg/ms

$\beta = 255 \times 10^{-6}\ ^{o}K^{-1}$

then

$$Gr = \frac{g\beta\Delta T\ell^3}{\nu^2}$$

$$= 1{,}037 \times 10^{4}\ \Delta T$$

$\Delta T \simeq 4^{o}$C

$\therefore$ $Gr = 4{,}4148 \times 10^{4}$

since $10^4 < Gr < 10^7$ equation (3.4.16) can be applied and the plate to cover convection coefficient

$$h_{p-c} = \frac{1{,}14\ \Delta T^{0,310}}{\ell^{0,070}} \left[1 - 0{,}0018\ (\bar{T}-10)\right]$$

$$= \underline{1{,}663}$$

From (3.3.22.) with $\sigma = 5{,}669 \times 10^{-8}$ W/m^2 ^{o}K

ε_p /.....

$$\varepsilon_p = 0,92$$
$$\varepsilon_c = 0,63$$
$$T_p = 25^oC$$
$$T_c = 21^oC$$

$$h_{r,p-c} = \frac{5,669 \times 10^{-8} (298^2 + 294^2)(298 + 294)}{1/0,92 + 1/0,63 - 1}$$

$$= \underline{3,513}$$

$$h_{r,c-s} = 5,669 \times 10^{-8} \times 0,63(294^2 + 288^2)(294 + 288)$$

$$= \underline{3,521}$$

$$h_w = 5,7 + 3,8 \times 1,5$$

$$= \underline{11,4}$$

$$U_t = \left[\frac{1}{1,663 + 3,513} + \frac{1}{11,4 + 3,521}\right]^{-1}$$

$$= \underline{3,84}$$

$$U_o = 3,84 + 1 + 0,0919$$

$$= \underline{4,93}$$

$$(\tau\alpha)_e = 0,71 + (1 - 0,97)\frac{4,93}{14,92}$$

$$= \underline{0,72}$$

(ii) Tank

The loss coefficient area product was determined experimentally for the whole tank,(as explained in section 5.2.1.). The loss coefficient was then assessed using the following mathematical analysis.

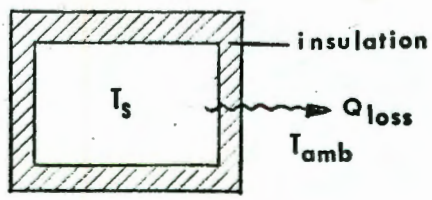

Fig. 8.3.1. Tank losses

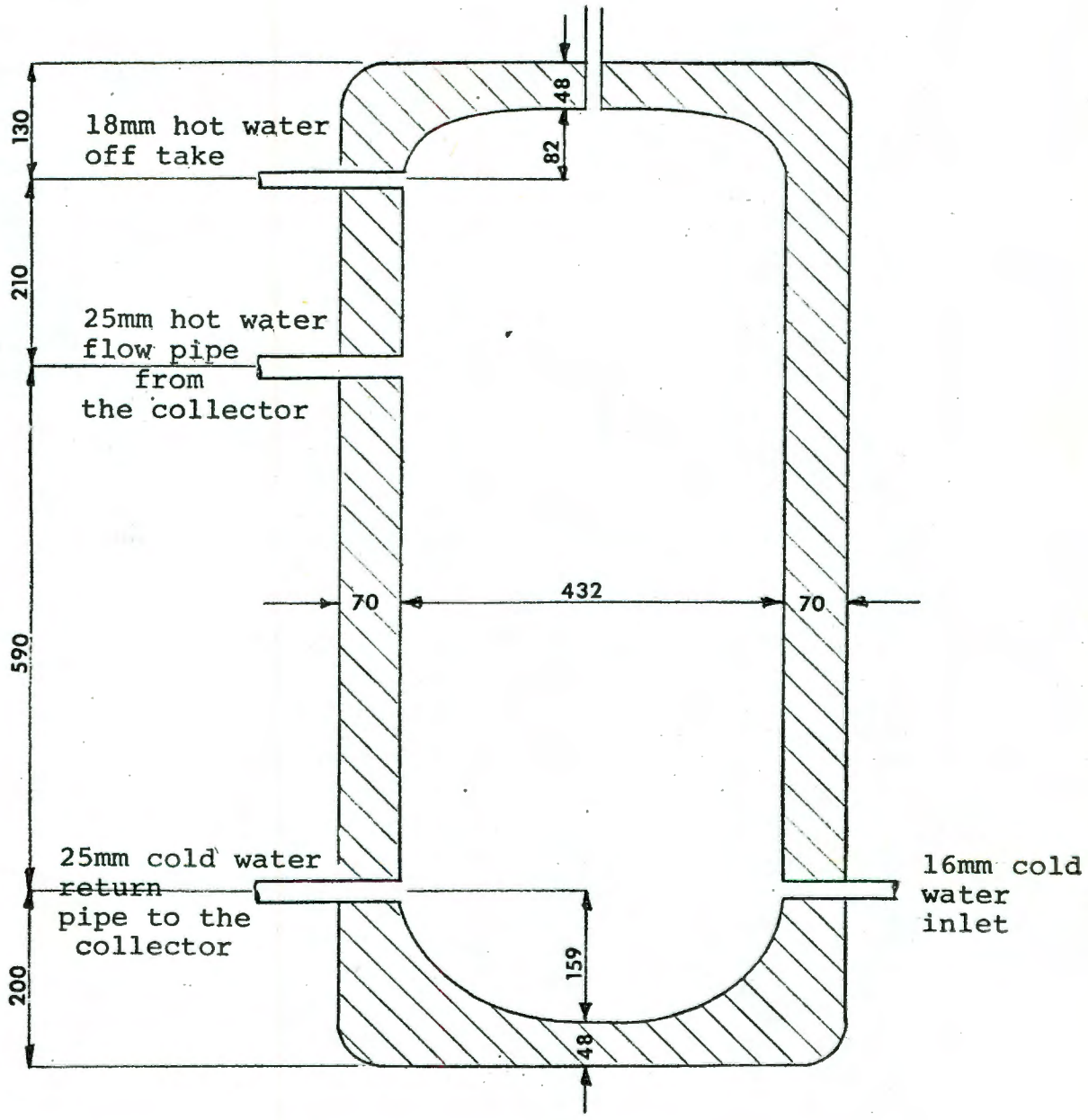

Fig. 8.3.2 A cross-section through the solar storage tank

The thermal loss $Q_{loss} = (UA)_s(T_s - T_a)$ (8.3.1.)

The energy stored over a time period $\Delta\tau$ =

$$Q_s = MC_p \frac{\Delta T_s}{\Delta\tau} \quad (8.3.2.)$$

An energy balance of $Q_s = Q_{loss}$ gives

$$(UA)_s = \frac{MC_p}{\Delta\tau} \frac{\Delta T_s}{(T_s - T_a)} \quad (8.3.3.)$$

The mean value of $(UA)_s = 7{,}92$ KJ/$_{hr^oC}$

The area A is the surface area of the tank.

From Fig. 8.3.3. a height of 908 mm and a diameter of 432 mm was used.

The area A_s = 1,52 m^2

Whence U_s = 5,19 KJ/$_{hr^oCm^2}$

This is an average for the whole tank.

The technique of obtaining loss coefficient area products for the 5 - stratified model is to determine the surface areas of the sections.

From Fig. 8.3.3. the surface areas of the sections are

$As_1 = \frac{\pi d^2}{4} + \pi dhs_1 = 0{,}508\ m^2$

$As_2 = As_3 = As_4 = \pi dhs_2 = 0{,}218\ m^2$

$As_5 = \pi dhs_5 + \frac{\pi d^2}{4} = 0{,}364\ m^2$

Since the average loss coefficient U = 1,442 x 10^{-3} KW/$^oCm^2$

Then $(UA)_{s_1} = 7{,}325 \times 10^{-4}$ KW/^oC

$(UA)_{s_2,s_3,s_4} = 3{,}144 \times 10^{-4}$ KW/^oC

$(UA)_{s_5} = 5{,}255 \times 10^{-4}$ KW/^oC

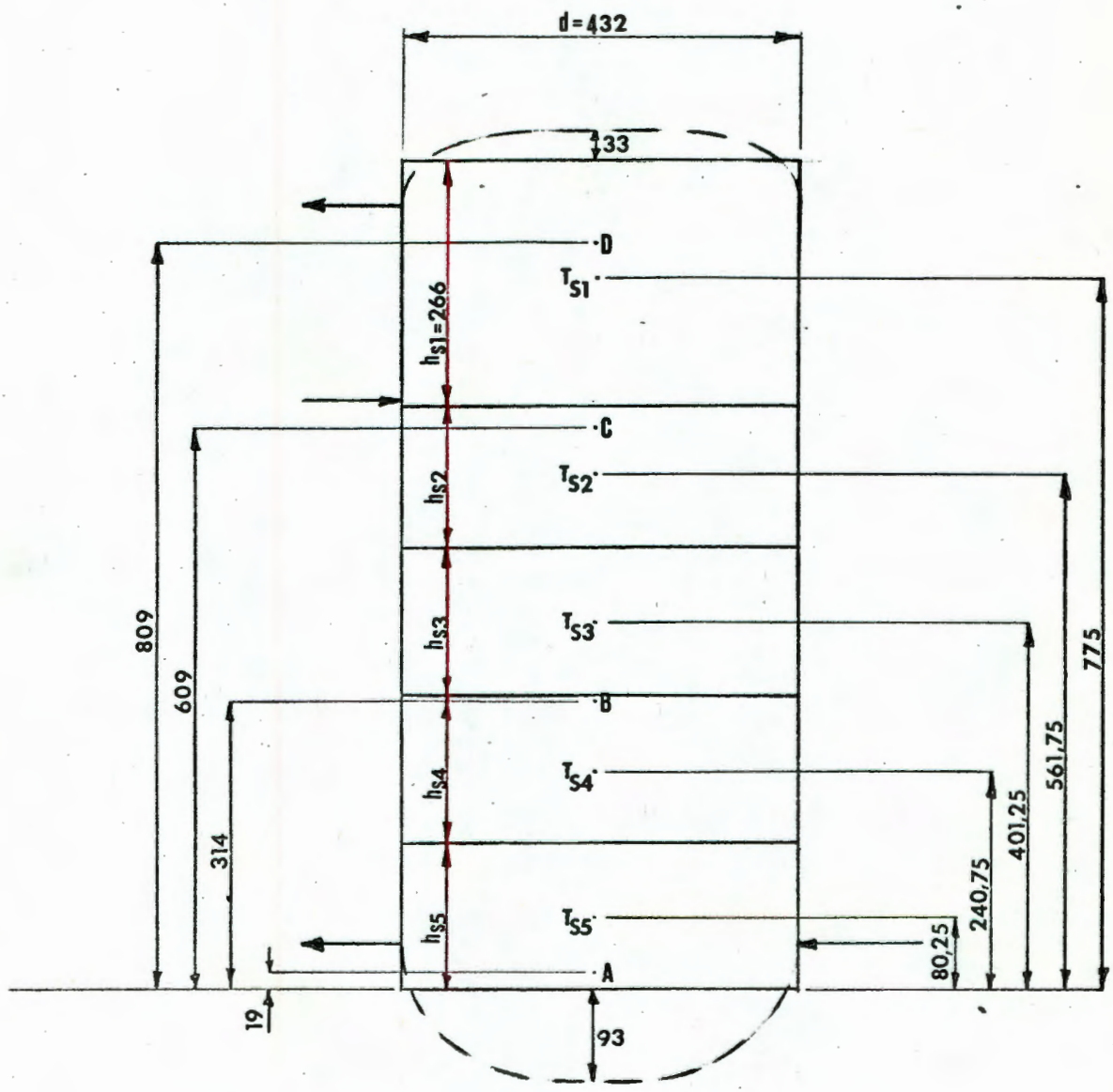

Section heights: $h_{S2} = h_{S5} = h_{S3} = h_{S4} = 160,5$mm

Thermocouple positions: A,B,C,D

Section temperature reference points: T_{S1} , T_{S2} , T_{S3} T_{S4} , T_{S5}

Fig.8.3.3 5-Section Tank Simulation Model

(iii) Pipes

The determination of the loss coefficients for the upriser and downflow pipes was the same as for the tank.

The temperature drop with respect to time was experimentally determined (see section 5.2.2.) and equation (8.3.3.) was used for the pipes.

$$(UA)_{pi} = \frac{MC_p}{\Delta\tau} \frac{\Delta T_{pi}}{(T_{pi} - T_a)}$$

where ΔT_{pi} is the temperature difference in the pipe over a time $\alpha\tau$.

For the upriser pipe $(UA)_{up} = 4,7\ W/^oC$

and for the downflow pipe $(UA)_{dp} = 20,0\ W/^oC$

The discrepancy in these values is due to the difference in length (and thus surface areas) of the pipes and the fact that there is a gate valve mid-way along the downflow pipe.

8.4. THERMOSYPHON MASS FLOW RATE

8.4.1. Theoretical Determination

To determine the mass flow rate theoretically, it is necessary to obtain a relationship between the pressure head in the system and the mass flow rate.

Theoretically it would be extremely difficult to calculate this relationship using pipe friction, head losses, entrance losses, losses in the bends and head losses through the collector and tank. Experimentally it becomes quite simple.

Using a pump, rotameter and monometers as described in section 4.4., the flow was altered and the pressure was recorded at various temperatures.

Since the change in viscocity of water is quite considerable over the operating temperatures (μ = 1002 x 10^{-6} $Kg/_{ms}$ at 20^oC and 463 x 10^{-6} $Kg/_{ms}$ at 60^oC), it would be expected that the pressure mass flow rate relationship would be different at various temperatures.

The results/...

The results of the experiment showed a large scatter in readings. This was probably because temperatures throughout the system were not the same as that in the downflow pipe. It was also extremely difficult to maintain a constant temperature throughout the test. The temperature fluctuated up to $3^{o}C$ and an average had to be taken.

Since, during operation of the solar water heater, the temperatures throughout the system are different, it would be impossible to determine an exact pressure-flow relationship at any one temperature. A mean curve was therefore drawn and observed to describe a relationship of

$$\dot{m} = a \Delta p^{b}$$

Using the Wang 2200 Geometric Regression program, the equation was found to have values

$$\left.\begin{aligned} \dot{m} &= 3{,}55316 \times 10^{-4}\ \Delta p^{0{,}910928} \quad \text{for } \Delta p < 100\ N/m^2 \\ \text{and } \dot{m} &= 1{,}18995 \times 10^{-3}\ \Delta p^{0{,}6448} \quad \text{for } \Delta p > 100\ N/m^2 \end{aligned}\right\} \quad (8.4.1.)$$

To calculate the pressure difference at the collector inlet (point P) in the computer model, it was necessary to know the weight of water in the pipes, tank and collector on either side of point P.

The water in the tank influencing flow lies between the collector inlet and outlet pipes. The tank was sectioned as shown in Fig. 8.4.1. The weight of water in the tank between inlet and outlet to the collector $= g \sum_{3}^{5} h_{sj}\rho_j / 0{,}59$

$$= g\,(42\rho_5 + 282\rho_4 + 36\rho_3 + 230\rho_2)/590$$

Fig. 8.4.1.

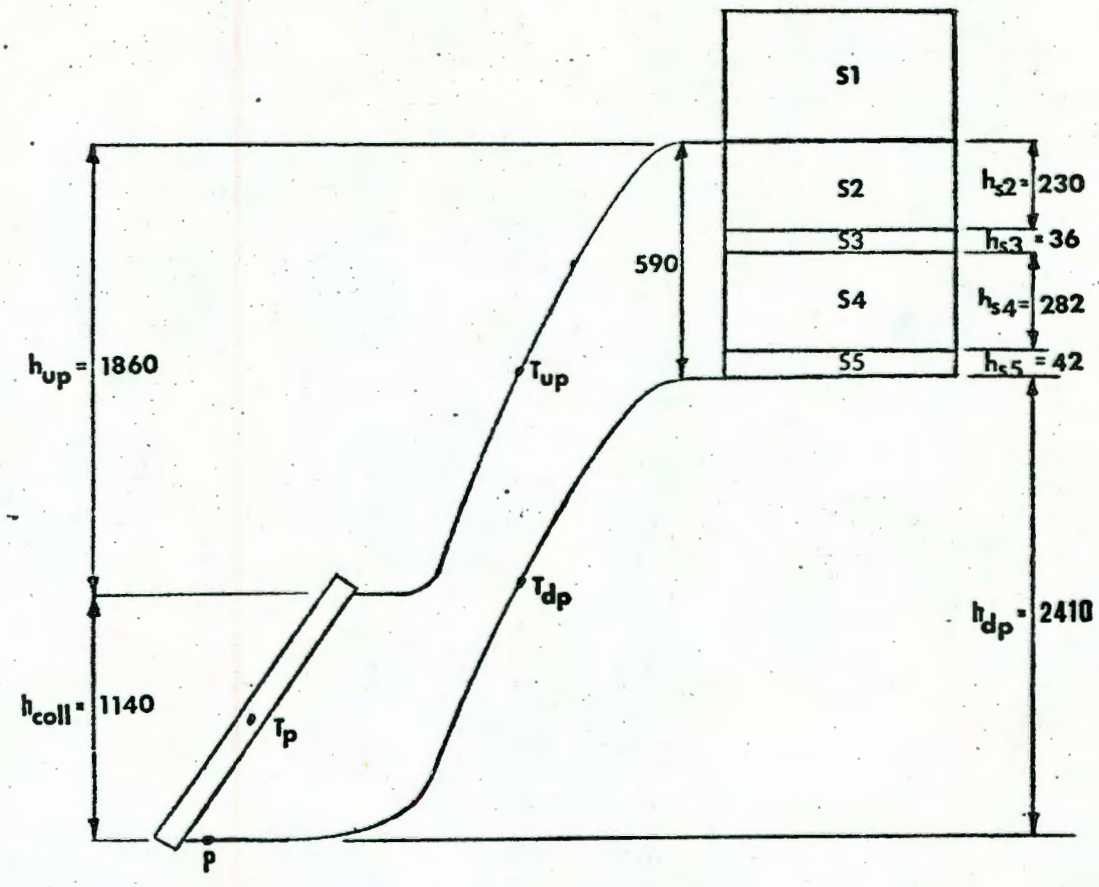

Fig. 8.4.1. Systems Diagram Showing Pressure Heads Used to Calculate the Theoretical Thermosyphon Flow .

The pressure difference (from 4.4.2)

$$\Delta p = g \left(42\rho_5 + 282\rho_4 + 36\rho_3 + 230\rho_2\right)/590 + 2{,}41 \times \rho_{dp}$$

$$- 1{,}14\rho_{coll} - 1{,}86\rho_{up} \qquad (8.4.2.)$$

With known temperatures throughout the system, densities can be calculated, hence the pressure difference Δp and the mass flow rate $\dot{m}_c$.

8.4.2. Experimental Determination

Thermosyphon mass flows were determined as described in section 5.2.3.

Graph 8.4.1 Calibration of the variable potential, R_v in the thermistor circuit

(I_t=40mA; I_o=0mA; zero flow)

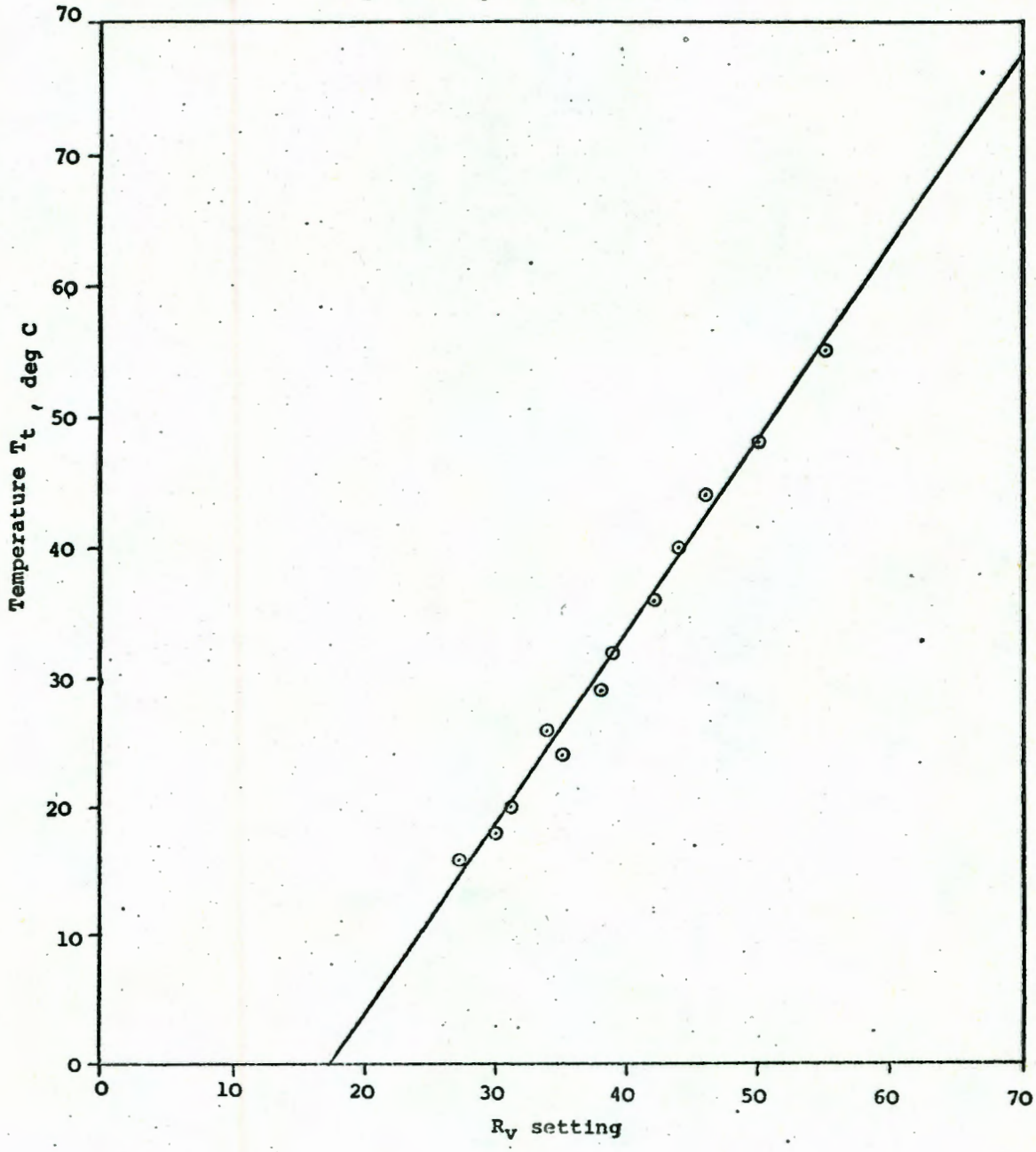

Graph 8.4.2 Thermistor calibration chart

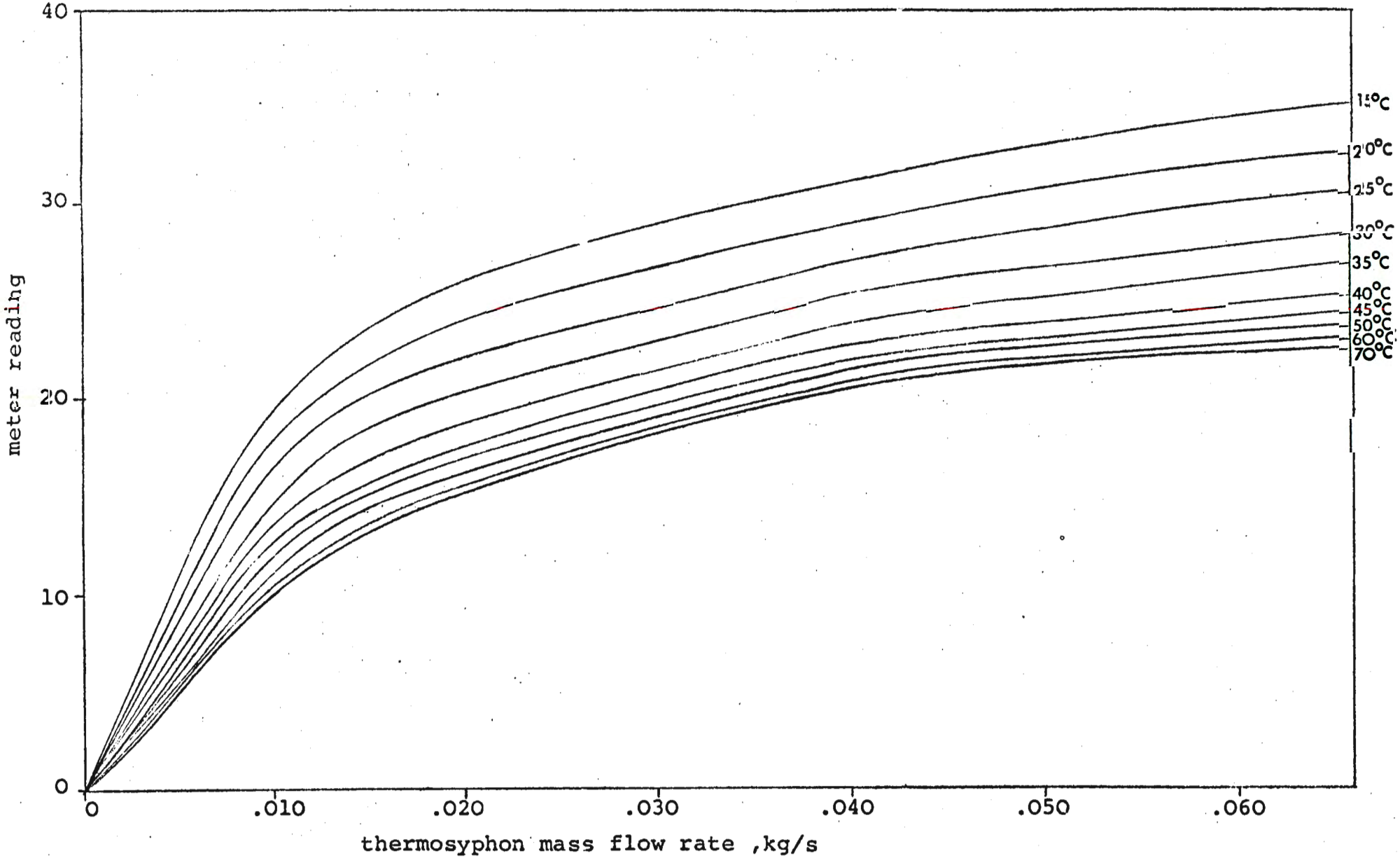

8.5. EFFICIENCIES

The overall efficiency was determined using

$$\eta_{overall} = \frac{Q\ overall}{Tot.Rad. \times Ac + Qelec} \qquad (8.5.1.)$$

The total Radiation (Tot.Rad.) was calculated by finding the area under the radiation curve for the whole day.

$$Q\ overall = \Sigma\ \dot{m}_L C_p\ (T_{Eo} - T_{in})\ \Delta t \qquad (8.5.2.)$$

This is the total thermal heat drawn off from the entire system during one day's operation.

Qelec is the amount of electrical energy used to maintain the water in the electrical geyser at a preset constant temperature, during one day's operation.

$\eta_{overall}$ therefore shows the ratio of the net heat drawn off from the entire system, to the sum of the radiant and electrical energy received by the system, during one day.

8.6. COMPUTER DETAILS

(i) The initial tank temperatures used, at the start of the program, were assessed from Fig. 8.3.3. assuming linear temperature distribution vertically between the thermocouples.
The tank section temperatures were then

$$\left.\begin{aligned} Ts_1 &= T_C + (T_D - T_C)\ \frac{166}{200} \\ Ts_2 &= T_B + (T_C - T_B)\ \frac{240}{295} \\ Ts_3 &= T_B + (T_C - T_B)\ \frac{87}{295} \\ Ts_4 &= T_A + (T_B - T_A)\ \frac{222}{295} \\ Ts_5 &= T_A + (T_B - T_A)\ \frac{61}{295} \end{aligned}\right\} \qquad (8.6.1.)$$

(ii) The calculation of density of water from the temperature was performed using an equation assessed using the Wang Geometric Regression program.

The relationship/...

The relationship between temperature T and density ρ was

$$\rho = 1000,93 - 0,199T + 1,53 \times 10^{-2}T^2 - 9,72 \times 10^{-4}T^3 + 2,28 \times 10^{-5}T^5 - 2,51 \times 10^{-7}T^5 + 1,06 \times 10^{-9}T^6 \qquad (8.6.2.)$$

where ρ is in kg/m^3 and T is in ^oC

(iii) The specific heat capacity of water C_p at a temperature T was also obtained from equations assessed using the Wang Geometric Regression program.

For $T < 35^oC$

$$C_p = 4,24 - 8,57 \times 10^{-3}T + 4,97 \times 10^{-4}T^2 - 1,33 \times 10^{-5} + 1,33 \times 10^{-7}T^4$$

For $T > 35^oC$ (8.6.3.)

$$C_p = 4,125 + 3,76 \times 10^{-3}T - 9,99 \times 10^{-5}T^2 + 1,19 \times 10^{-6}T^3 - 4,81 \times 10^{-9}T^4$$

(iv) Thermal capacities used were for the water only. The metal and insulation of the collector or tank, were not considered since the heat capacities of these parts were relatively very small, as proven below.

For the collector, the mass of the steel envelope through which the water flowed, was

$M = \rho V = 14,12$ Kg (from specifications given in section 4.3.) at 20^o.

$C_p = 0,11$ KJ/$^{Kg^oC}$

$\therefore W = MC_p = 1,553$ KJ/^oC

For the insulation $\rho = 24$ Kg/m^3, $C_p = 0,7$ KJ/Kg^oC at 20^oC

$M = \rho V = 1,2$ Kg

$W = 0,084$ KJ/^oC

while for the water at 20^oC, $W = 33,49$ KJ/^oC

However/....

However, using the value for water $W = \rho VCp = 0{,}008\ \rho Cp\ KJ/^{o}C$

for the collector produced alternate large fluctuations above and below the actual collector outlet and mean plate temperatures, every 15 minutes. A damping factor therefore had to be introduced. A trial and error technique proved that it had to be incorporated into the collector thermal capacity, and was found to be equal to 2,5. The thermal capacity was therefore expressed as $W = 0{,}08\ f_d\ \rho\ Cp$, where f_d was the damping factor. $\therefore\ W = 0{,}020\ \rho\ Cp$.

(v) The Wang 2200 computer did not provide enough space to store the experimental data, retrieve this data, process the data, print out and store the calculated data and draw graphs, in one program. A series of programs was set up.

SOLAFILE was created to store average hourly experimental data.

SOLASIM was the main program which predicted the thermal performance of the solar water heater, using the data provided in SOLAFILE. It printed out the predicted results and stored them in a data file called THEOFILE.

Another two programs were required to obtain plots of the theoretical results (THEOPLOT) and experimental results (EXP-PLOT).

8.7. RADIATION ERRORS

(i) Errors in assuming the radiation to be only beam radiation.

The total radiation Rad, on the tilted surface consists of two components Rad_b, beam radiation, and Rad_d, diffuse radiation.

$$Rad = Rad_b + Rad_d$$

According to Duffie and Beckman (9), a surface tilted at slope s from the horizontal sees a portion of the sky dome given by $(1 + \cos s)/2$ if the diffuse radiation is uniformly distributed over the sky dome. This is also the conversion factor for diffuse radiation

$$Rad = Rad_b + Rad_d\ (1 + \cos s)/2$$

For $s = 44^{o}$, $Rad = Rad_b + Rad_d\ (0{,}89)$

From experimentation /...

From experimentation it was found that Rad_d varied between 9% and 100% of the total radiation, on a clear day at 12h30 and sunset respectively.

The direction of the diffuse radiation is from all parts of the sky dome and therefore enters the collector from all possible angles. To theoretically determine the losses due to the angle at which the radiation strikes the collector cover would mean assuming an angle of incidence for the diffuse radiation.

The total diffuse radiation for one clear day was found to be about 14% of the total radiation. Using the conversion factor, $Rad_d(0,89)$ the diffuse radiation is about 12% of the total. The direction varies from 0^o to 90^o.

If it is assumed that a 50% error is made in considering the direction of diffuse radiation to be the same as that for beam radiation, the total error would then be in the region of 6%, which is not significant.

8.8. COLLECTOR SPECIFICATIONS

The solar collector used in the experiment had the following specifications :-

a) Dimensions
- Length : 1780 mm
- Width : 1135 mm
- Height : 65 mm
- Area : 202 m^2
- Weight : 40 kg

b) Pressures — Static

Low pressure : Test 70 kPa

Working 40 kPa

Dynamic low pressure subjected to 400 000 cycles at 27kPa.

c) Temperatures — Unit can withstand temperature range from 15^oC to 140^oC

d) Absorbtivity — 0,92 or greater to 50 microns

e) /....

e) Emissivity 0,92

f) Corrosion Resistance Unaffected by water containing 200 ppm chloride and temporary hardness of 140 ppm.

g) Construction

(i) Stainless steel envelope : 0,45 mm, low carbon stainless steel resistance welded

(ii) Absorber frame : 6063 Ts Aluminium corrosion resistant alloy.

(iii) Base sheet : 0,6 mm Galvanised steel, 138 grms/m^2 Zinc coating per face.

(iv) Insulation : 25 mm polyurethane foam in slab form. Heat rate 1,0 W/$m^2{}^oC$

(v) Cover : 3 mm perspex
reflectivity 0,04
transmissivity 0,92
max temperature 160^o

(vi) Cover to plate distance : 15 mm

(vii) Paint : Maximum selectivity matt black paint.

8.9. DETAILS OF RESULTS

8.9.1. Tables

Table 8.9.1. shows the maximum ambient and tank temperatures, total radiation, the type of draw off of hot water and the daily efficiencies for each of the 10 days from test sets I and II.

The draw off times and flow rates are elaborated in tables 8.9.2 and 8.9.3.

Table 8.9.1. /...

Table 8.9.1. Results of 10 Tests

Test. Set	Date	Max T_{amb} (^{o}C)	Max T_{tank} (^{o}C)	Tot. Rad (Kwh)	Draw off		η_{solar}	$\eta_{overall}$
					(ℓ)	(set)		
I	20/12/76	27,1	53,4	13,21	162	a	32,2	46,2
	21/12/76	23,6	52,0	13,34	185	b	34,9	55,7
	22/12/76	24,8	52,5	13,47	150	b	20,4	33,6
	23/12/76	34,3	60,7	13,23	156	b	36,0	47,0
	24/12/76	29,0	57,4	13,33	125	c	29,0	36,7
II	29/4/77	32,2	49,8	10,83	218	m	40,3	48,1
	30/4/77	27	43,8	8,30	100	m	26,7	31,6
	5/5/77	19,2	44,3	10,36	93	m	25,4	32,8
	7/5/77	20,8	47,8	11,80	152	m	44,5	58,5
	10/5/77	21,0	49,7	12,7	150	m	37,0	45,8

Table 8.9.2. Water Draw Off Settings

Set	Flow times	Simulation
a	07h30 to 07h45 08h00 to 08h15	breakfast washing, baths and showers
	18h00 to 18h30 18h45 to 19h15	dinner, washing, bathing,
b	07h30 to 07h45 08h00 to 08h15	breakfast, washing, bathing, showering
	13h30 to 13h45	lunchtime washing.
	18h00 to 18h30 18h45 to 19h15	washing, bathing.
c	07h30 to 07h45	washing, showering.
	13h00 to 13h15	washing
	18h00 to 18h15	washing
	18h45 to 19h00	bathing
	19h30 to 19h45	
m	manual draw off, varying for each day (see table 6.3.)	

Table 8.9.3. Manual draw off times and flow rates

Day	Draw off times	Flow rate (kg/s)
29/4/77	07h30 to 07h45	0,1419
	13h00 to 13h02	0,2667
	16h40 to 16h45	0,1600
	17h00 to 17h05	0,1833
30/4/77	12h25 to 12h29	0,1500
	17h00 to 17h15	0,0719
5/5/77	10h55 to 11h00	0,1533
	14h10 to 14h15	0,1567
7/5/77	08h45 to 08h50	0,1433
	10h00 to 10h05	0,1500
	16h00 to 16h07	0,2133
10/5/77	07h55 to 08h00	0,1633
	12h00 to 12h05	0,1667
	14h40 to 14h45	0,1700

8.9.2. Simulation Models and Graphs

The various techniques of obtaining theoretical solutions are described here, together with the graphs of results using these methods for the 24/12/76.

The experimental results are superimposed on these graphs to show the prediction accuracy of these models.

SOLASIM 4 :

Initially a 4 - stratified tank model was used, (the tank was divided into 4 sections, as shown in Fig. 8.9.1.) in the theoretical simulation of the solar water heater.

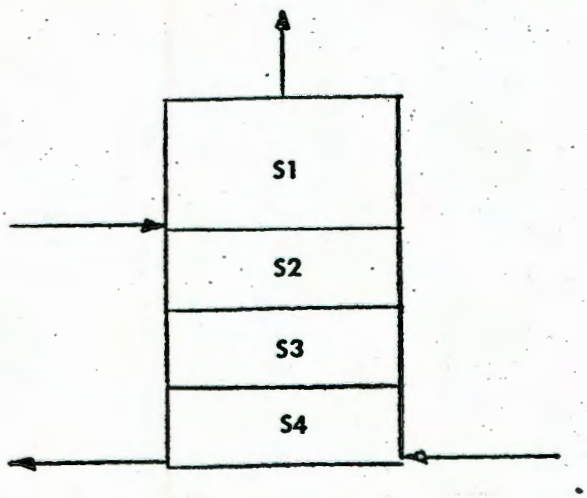

Fig. 8.9.1. 4 - Stratified Tank Model

SOLASIM 4A

The first solution technique employed was to determine both the collector outlet and mean plate temperature, after a time interval $\Delta\tau$, by evaluating the heat lost or gained over this period of time (using equation 3.3.32.).

The results of this model are presented in graphs 8.9.1., 8.9.2. and 8.9.3. with the appropriate experimental results superimposed, for the 24 December 1976.

This technique resulted in the mean plate temperature being close to the collector outlet temperature and well above the collector inlet

temperature /...

temperature, and not mid-way between the two, as expected.

The experimental mean plate temperature was assumed to be mid-way between collector inlet and outlet temperatures.

The shape of the experimental and predicted curves were similar, but not satisfactory, and another prediction technique was employed.

SOLASIM 4B

Again using the 4 - stratified tank model, and a heat balance to obtain the mean plate temperature at each finite step interval, the collector outlet temperature was this time determined assuming the mean plate temperature to be mid-way between the collector inlet and outlet temperature (from equation 4.1.1.)

$$T_{co} = 2T_p - T_{ci}$$

The results are presented in graphs 8.9.4, 8.9.5. and 8.9.6, for 24/12/76.

The shape of the curves were similar to those predicted using the SOLASIM 4A model, but were closer to the experimental results. This model was therefore more accurate than the previous model but was not entirely satisfactory and there was room for improvement.

SOLASIM 5B

It was decided to increase the number of sections in the theoretical tank simulation model to five.

Using the same technique as in SOLASIM 4B to determine the collector outlet temperature, thermal performance of the solar water heater was then predicted. (These results are shown in graphs in chapter 6, and discussed in chapter 7. See graphs 6.3. and 7.2.1.)

Once again the general shapes of the curves were similar to the predicted curves of SOLASIM 4A and 4B but more accurate than both previous models.

This theoretical model was also used to predict the thermal performance of the system for high draw off flow rates.

Plots of /...

Plots of these results for the 10/5/77 appear in graphs 7.3.1.,7.3.2. and 7.3.3., while the ambient conditions recorded on that day appear in graph 8.9.7.

GRAPH 8.9.1 SOLASIM 4A

COLLECTOR TEMPERATURES FOR 24/12/76

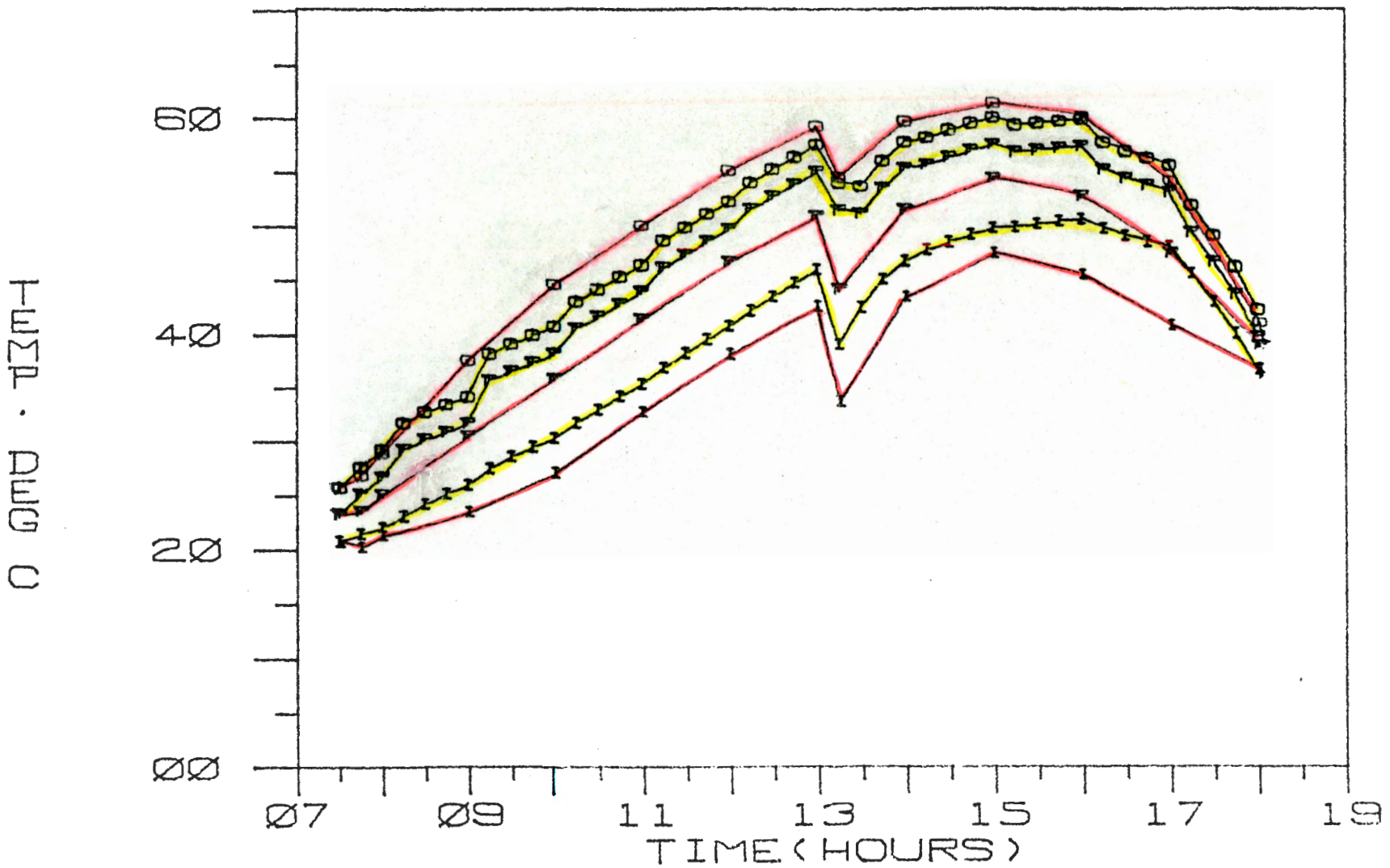

GRAPH 8.9.2 SOLASIM 4A

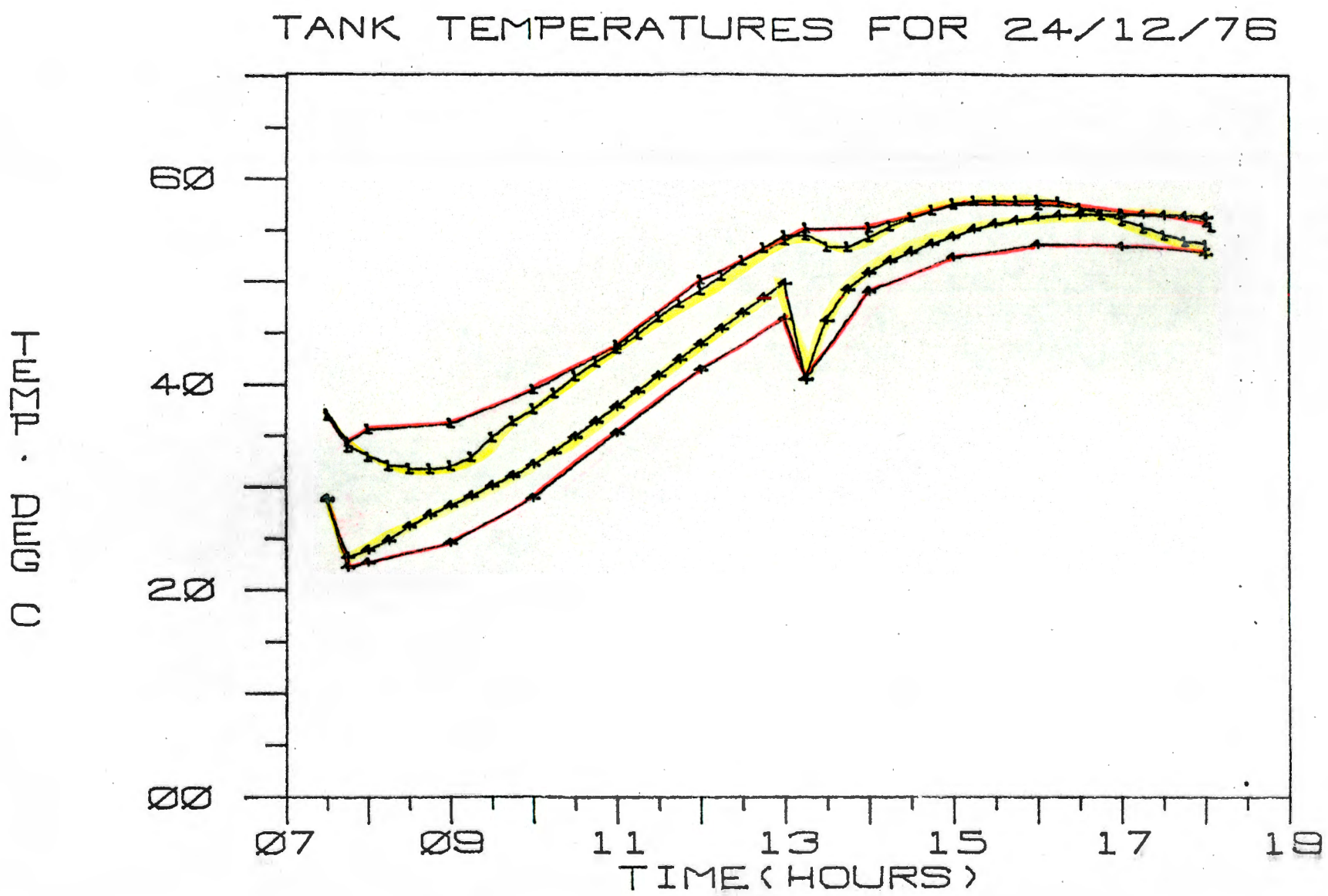

GRAPH 8.9.3 SOLASIM 4A

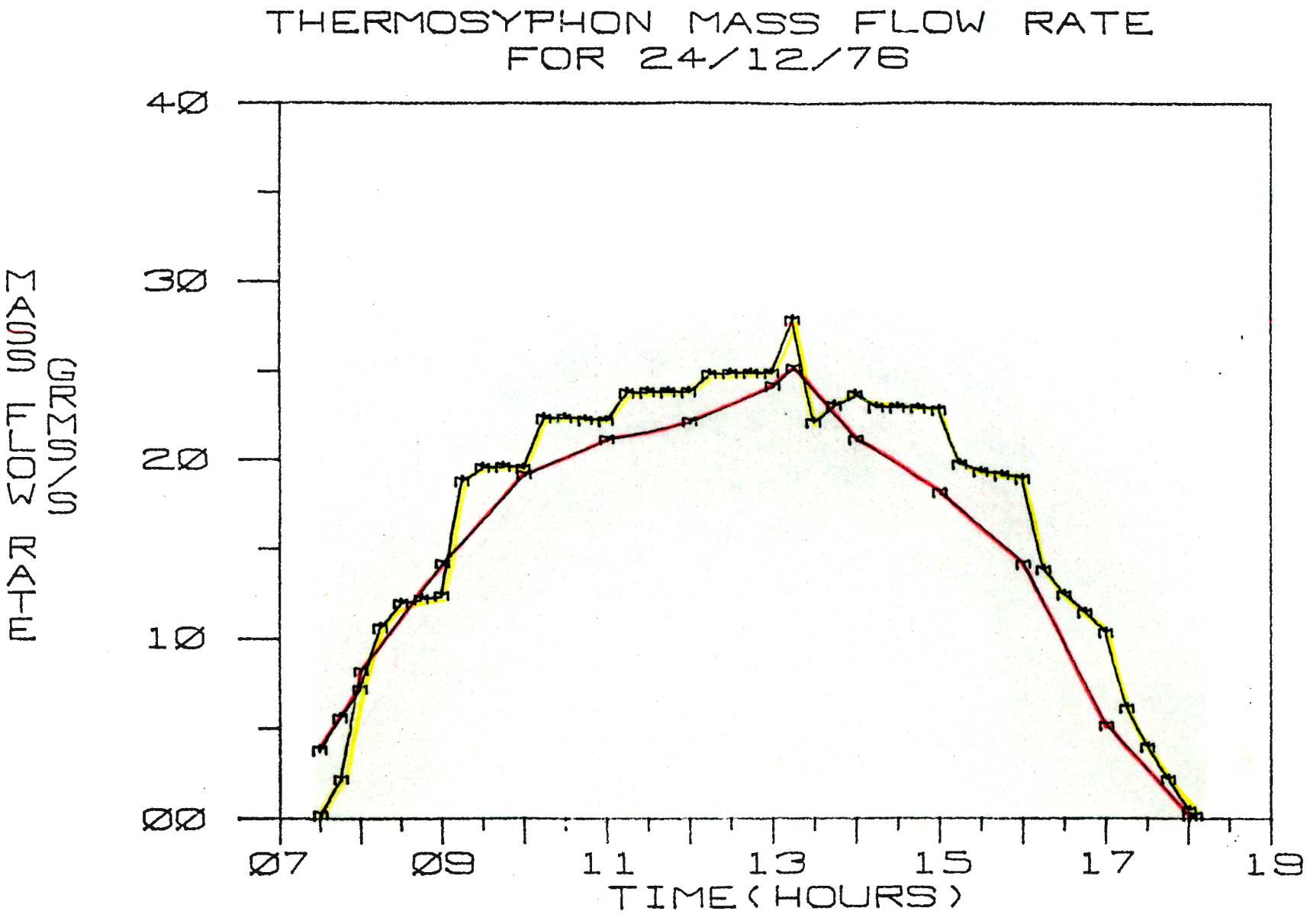

GRAPH 8.9.4 SOLASIM4B

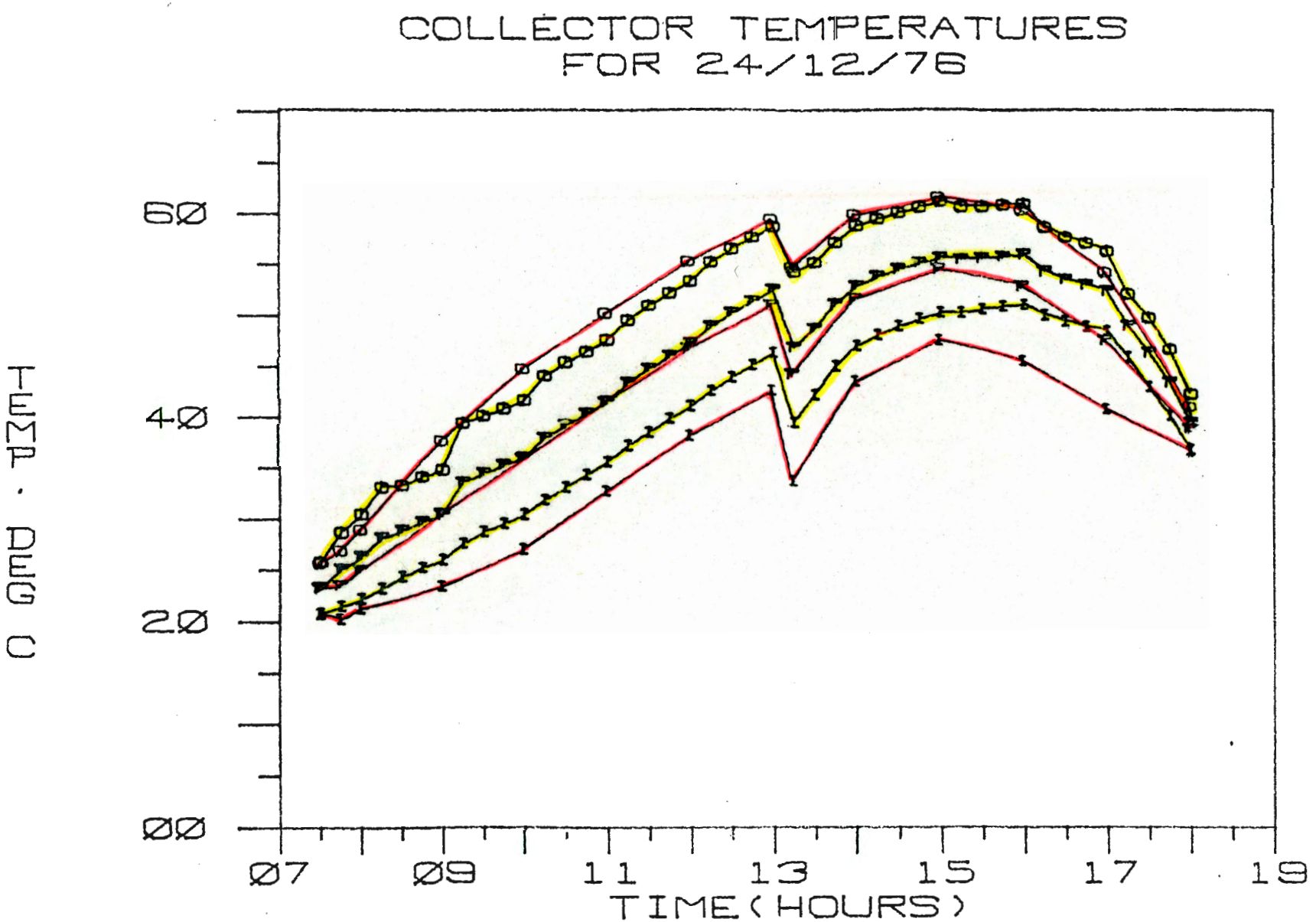

GRAPH 8.9.5 SOLASIM 4B

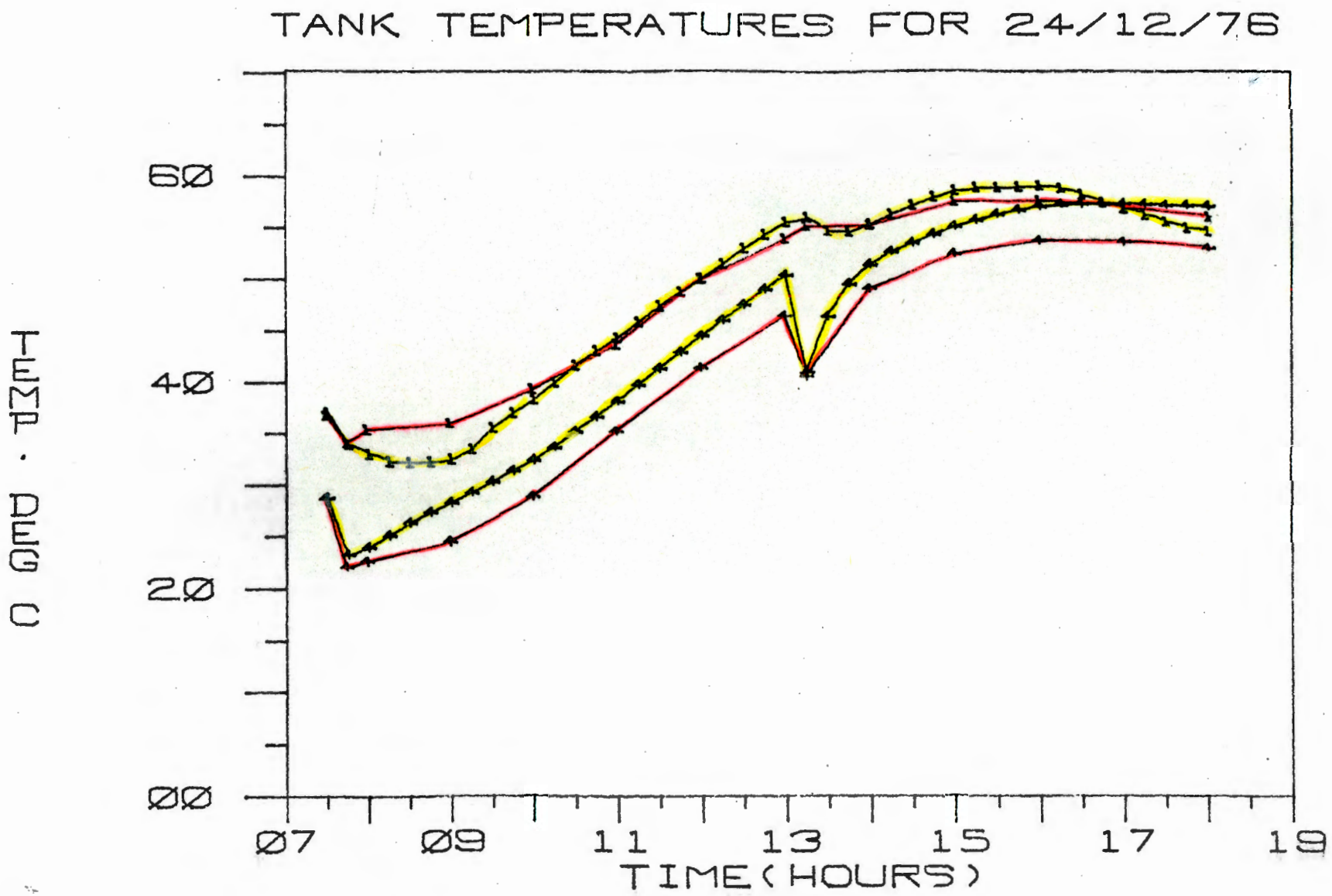

GRAPH 8.9.6 SOLASIM4B

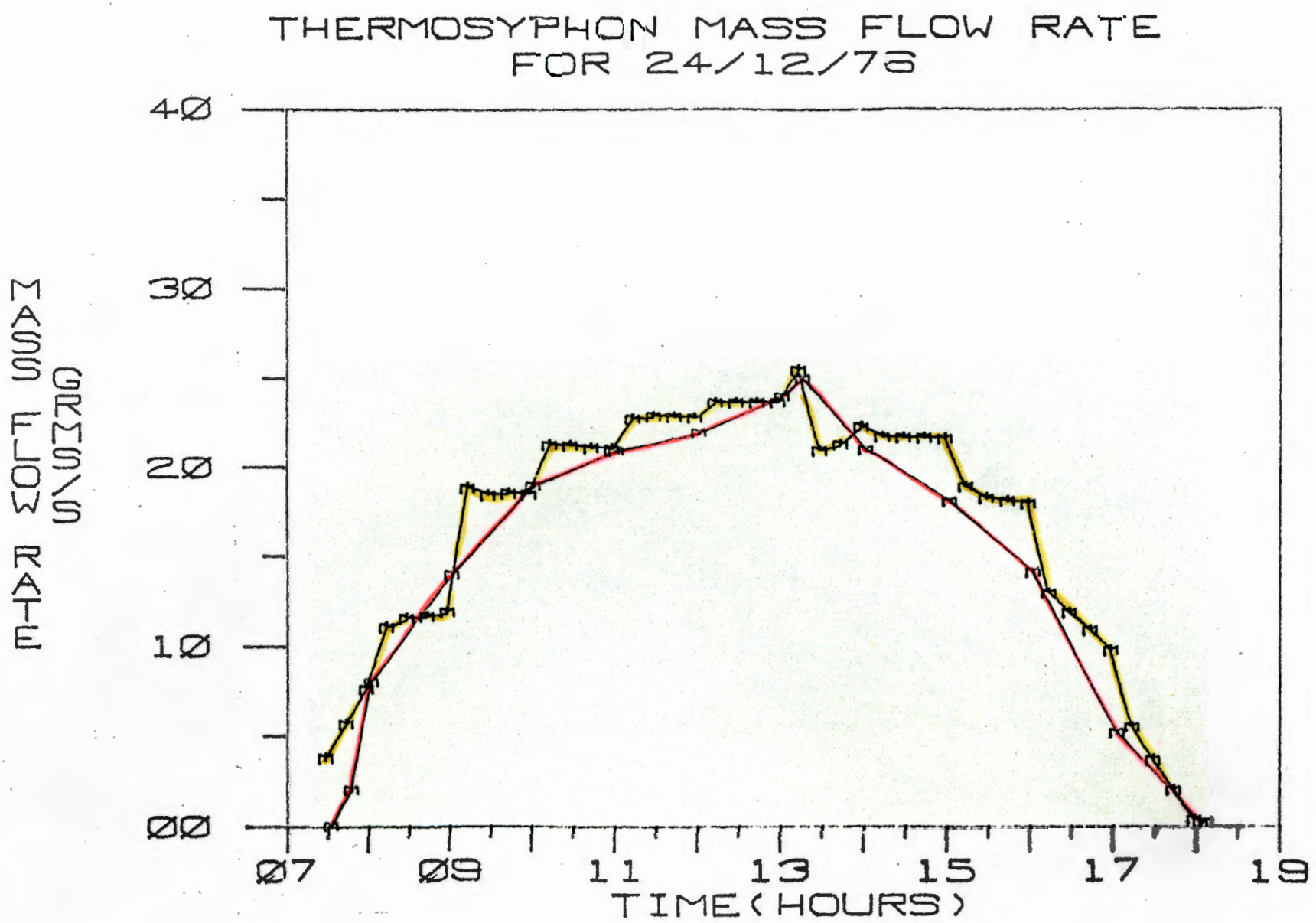

Graph 8.9.7 Solar insolation,ambient temperature and wind velocity for 10.5.77

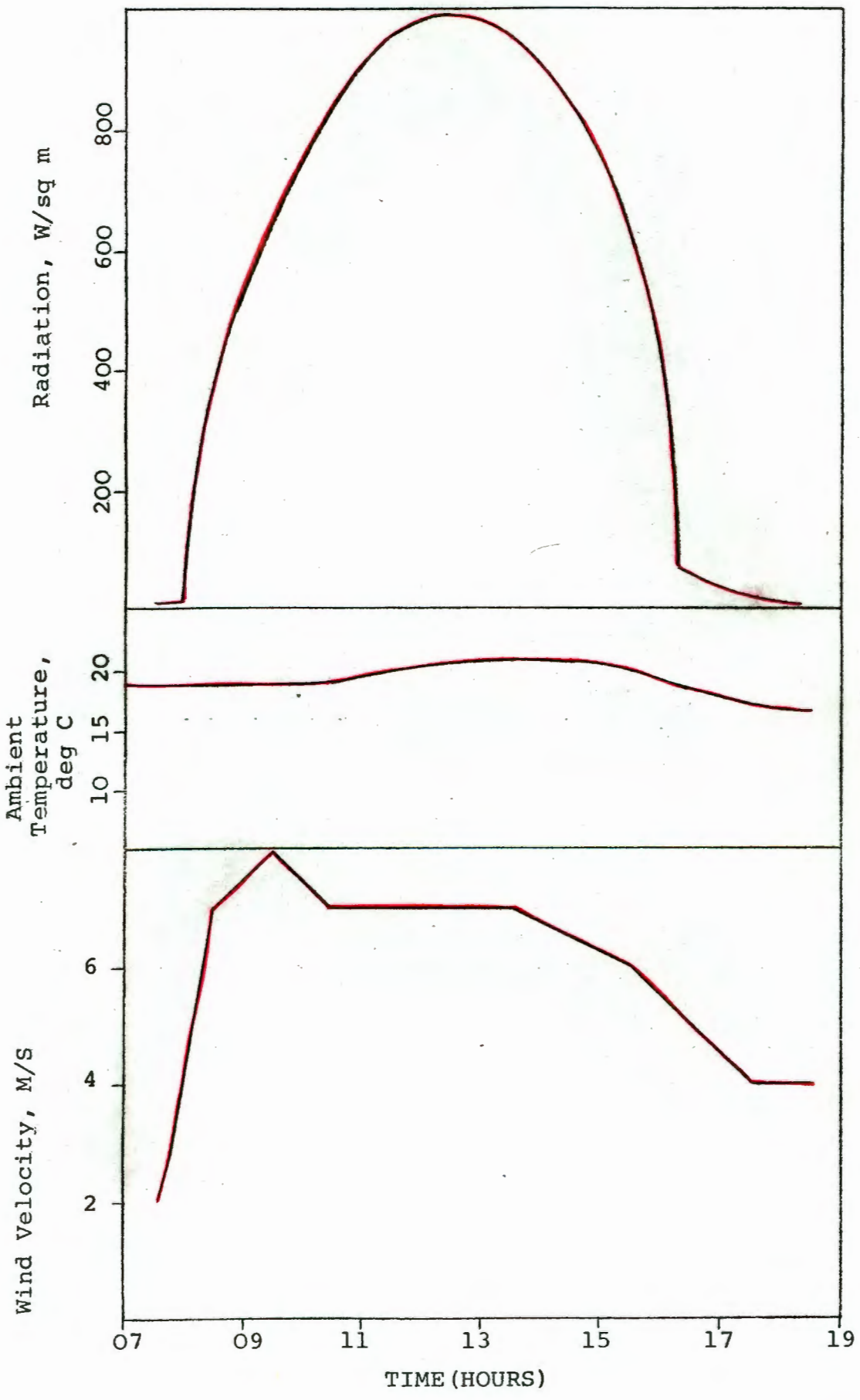

REFERENCES

1. Hottel H.C. and Woertz B.B. "The performance of flat plate solar heat collectors", Trans. A.S.M.E. 64, 91, 1942.

2. Whillier A. "Prospects for the engineering utilization of solar energy in South Africa", S.A.Mech. Eng. Oct. 1956.

3. Bliss R.W. "The derivations of several plate efficiency factors useful in design of flat plate solar heat collectors", Solar Energy, 8, 83, 1959.

4. Close D.J. "The performance of solar water heaters with natural circulation", Solar Energy, 6, 33, 1962.

5. Desa V.G. "Solar Energy utilisation at Dacca", Solar Energy 8,83, 1964.

6. Gupta C.L. and Garg H.P. "System design in solar water heaters with natural circulation", Solar Energy, 12,163 1968.

7. Ong K.S. "A finite-difference method to evaluate the thermal performance of a solar water heater", Solar Energy 16, 137, 1974.

8. Ong K.S. "An improved computer program for the thermal performance of a solar water heater", Solar Energy 18, 183, 1976.

9. Duffie J.A. and Beckman W.A. "Solar Energy Thermal Processes", John Wiley & Sons, New York, 1974.

10. Chinnery D.N.W. "Solar Water Heating in South Africa", C.S.I.R. Research Report 248, 1-79, C.S.I.R. 1971.

11.(a) Lui H. and Jordan R.C. "Availability of solar energy for flat plate solar heat collectors".

(b) Whillier A. "Design factors influencing solar collector performance"/...

performance", Low Temperature Engineering Applications of Solar Energy, ASHRAE, New York, 1967.

12. Dutkiewicz R.K. and Gryzagoridis J. "Solar Energy Course", University of Cape Town, 1976.

13. "Introductory Guide to Solar Energy and Solar Water Heaters", N.B.R.I., Pretoria, 1976.

14. Zarem A.M. and Erway D.D. "Introduction to the Utilization of Solar Energy", McGraw Hill, U.S.A., 1976.

15. Klein S.A., Beckman W.A. and Duffie J.A. " A design procedure for solar heating systems", Solar Energy 18, 113-127.

16. Seale R.L. and Sierka K.A. "Energy needs and the environment", University of Arizona Press, Arizone, 1973.

17. Fuller B. and Metcalfe J. "Inventory of world reserve human trends and needs". Document 1, phase 1.

18. McHale J. "World design science decade '65 - 75'" phase IV document 6, 1967.

19. "Energy Primer", Portola Institute, 1974.

20. Halacy D.S. Jr. "The coming age of solar energy". Harper & Row U.S.A., 1973.

21. Holman J.P. "Heat Transfer", McGraw Hill, Tokyo, 1972.

22. Simon F.F. "Flat plate solar collector performance evaluation with a solar simulator as a basis for collector selection and performance prediction", Solar Energy 18, 451 - 466.

23. "The Stockholm Conference: Only One Earth", Friends of the Earth, London, 1973.

24. Jordan R.C. and Ibele W.E. "Mechanical Energy from Solar Heat", World Symposium on Applied Solar Energy, Arizona,1955.

25./...

25. Threlkeld J.L. "Thermal Environmental Engineering", Prentice-Hall Inc. U.S.A. 1962.

26. Whillier A. "Prospects for the engineering utilization of solar energy in South Africa", S.A. Mech.Eng. Oct. 1956.

27. Whillier A. "The Utilization of Solar Energy in South Africa", The South African Institute of Mechanical Engineers, April 1953, pp 261-266.

28. Brinkworth B.J. "Solar Energy for Man", Compton Press, Cardiff 1972.

29. Rankine A.D. and Chooters W.W.S. "Combined Convective and Radiative Heat losses from Flat Plate Solar Air Heaters", Solar Energy 12, 517, 1969.

30. Klein S.A. "Calculation of flat plate collector coefficients", Solar Energy 17, 1975.

31. Hyde F.J. "Thermistors" Butterworth & Co. Ltd., London, 1971.